University of Twente

EEMCS / Electrical Engineering
Control Engineering

Dual stage actuation in linear drive systems

Gerdo Jong

M.Sc. Thesis

Supervisors
dr.ir. T.J.A. de Vries
prof.ir. H.M.J.R. Soemers
ir. R. Radzim

January 2005

Report nr. 001CE2005
Control Engineering
EE-Math-CS
University of Twente
P.O. Box 217
7500 AE Enschede
The Netherlands

Summary

The aim of this research was to contribute to the transfer of knowledge and experience of research in HDD dual-stage actuation to dual-stage actuation in linear drive systems. As a case study, application of dual-stage actuation to the Fast Component Mounter (FCM) is considered.

Dual-stage actuation is the combination of a first-stage actuator, which has a relative large stroke and small bandwidth, with a second-stage actuator, which has a relative small stroke and large bandwidth. The combination of these two actuators can result in a larger bandwidth, compared to using only the first-stage actuator. In literature, it is reported that the principle of dual-stage actuation is applied to increase the bandwidth of HDDs. As a result, the response time of positioning the read/write head can be decreased and at the same time, the accuracy of positioning the read/write head can be increased.

In applying dual-stage actuation to HDDs, decoupled operation of the two actuators is assumed. Consequently, it is shown that two controllers for each of the actuators can be independently designed using SISO-design methodologies. During this research, the topic of decoupling has been investigated. It has been shown that decoupling occurs only if the load mass to the second-stage actuator is very small. Hence, the SISO-design methodologies from literature cannot be applied directly to the coupled system. In that case, the dual-stage actuated system becomes unstable. Therefore, a tuning procedure is presented to tune the controller parameters of the decoupled designed controllers, such that the coupled system is stabilized.

Furthermore, attention is paid to the sensory system, which is required for effective dual-stage operation. Since in HDDs the position of the read/write head is measured, the sensory system need not be adapted for effectively including a second-stage actuator. However, in case of the FCM, the position of the end-effector is not measured. For both the coupled and decoupled model it is investigated which changes to the sensory system should be made, in order to increase the bandwidth of the dual-stage actuated FCM.

Finally, for both models, it was shown how much the sensitivity bandwidth and the closed-loop bandwidth can be increased by including a piezo-actuator as second-stage actuator. In this analysis, also the load mass to the second-stage actuator is varied, in order to evaluate the achievable bandwidth.

Preface

Currently, it is exactly one week before The Day. Graduation comes closer every day. After exactly 6.5 years I finish my study Electrical Engineering. This is a perfect moment to look back, to finish things and to look into the next phase of life.

At this point, I would like to mention that in the case one talks about ”looking back”, one mainly focusses on the last period of time. Therefore, I mainly look back at this period of time in which I worked on my MSc project. Starting in a warm summer, in which most working days ended in the swimming pool. Followed by a rainy autumn, in which especially a couple of news items are remembered. Especially, the day on which Theo van Gogh was murdered, as well as the day on which everybody in this country had its eyes on the *Laakkwartier* in The Hague are remembered in this respect. Finally, winter came and brought me, exactly one day before Christmas, a solution to one of my final problems. In my opinion, although I was working on dual-stage actuation in linear motion systems, the world did not stop turning. And it will turn in the same manner as I present my findings to you.

However, at this moment I have to finish things; finish studying, finish writing this report. And at the same time I have the opportunity to start new things; starting my new job, starting a different life. But, I cannot start with that before I state my appreciation for those of you who helped me, either in carrying out this MSc project or in keeping the good spirit while I was working on this project.

First of all, I would like to thank Theo (de Vries) for giving me this interesting assignment, for giving me the freedom to work on the parts I was most interested in. But thank you also for putting me with both feet on the ground, while I was presenting my results to you. I hope that my work provides a basis for you to work further on this research topic. Furthermore, I would like to thank prof. Soemers for assisting in this research as well. Your experience with the design of the FCM and its practical sensor configurations was of importance for the quality of my work. Last but not least, I want to thank Richard (Radzim). At first for your linguistical corrections; I hope that the systematic error I made did not bore you. But secondly and more importantly, I appreciate the time you took and the enthusiasm you had in discussing various topics of my work.

Finally, I come to thank those who kept the good working spirit in the *afstudeerdershok*. Those of you, with whom it was coffee time at 10.15 and 15.00, and lunch time at 12.30. Those of you, who made a competition of saying *gezondheid* upon someone’s sneezing. Those of you, who also knew all songs and ads on the radio by heart. Those of you, who were so kind as to be interested in listening to my explanation of the problems associated with dual-stage actuation in linear motion systems. Should I mention names? I don’t think so!

And there is another person who deserves my appreciation, but I neither name here; she just knows that I am grateful.

Gerdo Jong,
Enschede, January 2005

Contents

Chapter 1

Introduction and Problem definition

1.1 Introduction

In several industrial applications, linear drive systems are used for positioning purposes, e.g. the displacement of silicium wafers in a lithography process or component placement in an electronic assembly process. Common linear drive systems consist of either linear motors, see figure 1.1a, or spindle drive systems, see figure 1.1b. Current industrial research aims to improve the accuracy of these systems. In lithographic stepper stages the required accuracy of the x-y-table is 20 [nm] or less. In component placement the aim is to increase the throughput of the system preferably with an increase of the accuracy of the system.

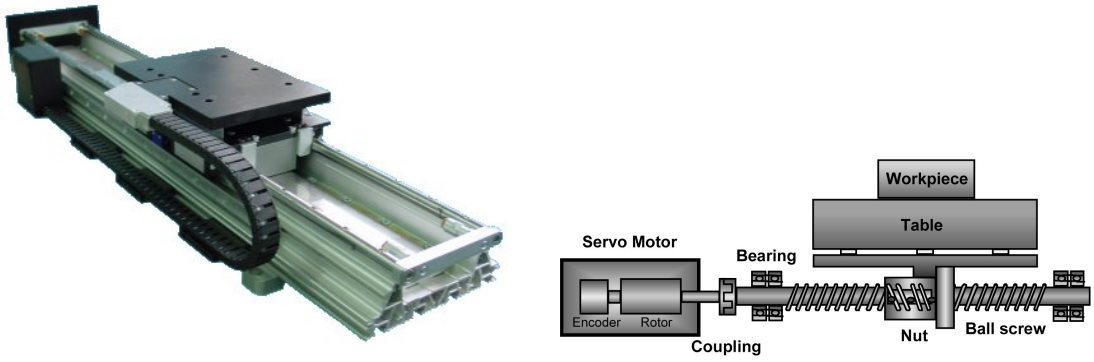

a) b)

Figure 1.1: a) Example of a linear motor for industrial positioning purposes and b) example of the application of a spindle drive system in positioning a table.

Further improvement of the drive mechanisms and consequently of the overall accuracy might be a possibility to achieve these requirements. However, this will be either at the cost of the response time of the system or the costs associated with the application will increase significantly, in order to design and fabricate the mechanics such that the required accuracy can be achieved. In order to prevent these scenarios, an alternative solution is sought. Analogous challanges are found in the field of hard disk drives (HDDs), and there it has been shown that dual-stage actuation may offer a solution.

1.2 Problem definition

The aim of this research is to contribute to the transfer of knowledge and experiences of research in HDD dual-stage actuation to dual-stage actuation in linear drive systems. It should be investigated which possibilities and

conditions apply to incorporating a second-stage actuator in an industrial application. Therefore, as a case study, the application of dual-stage actuation to the Fast Component Mounter (FCM) (Assembleon, 2004) is considered. In this application the focus is both on the plant model of the dual-stage actuated (DSA) system, as well as on the location and number of position sensors, which are required for the control system to function. Optimization of the controllers is not the primary aim.

Therefore the problem definition of this research comes down to answering the following questions:

- can theory of dual-stage actuated HDDs be directly used in general DSA systems and in the FCM in particular?
- which changes need to be made to a single-stage actuated system in general, and the FCM in particular, if a second stage is included?
- which benefits may be expected from implementing a second-stage actuator?
- what are the main disadvantages of implementing a second-stage actuator?

1.3 Outline

The outline of this report is as follows.

In chapter 2, the findings of the literature research are presented and related to the case study. From the latter analysis, the main research topics emerge. It is concluded, that both the coupling between the two stages and the required sensory system should be investigated.

In chapter 3, a model of the Placement Module of the FCM is derived. This model serves as the model of the first-stage actuator. In chapter 4, the piezo-actuator is modelled and a controller for this actuator is derived. This model serves as the model of the second-stage actuator. In chapter 5, it is investigated under which circumstances decoupling between the two stages occurs. The previously derived models serve as the basis for this analysis.

In chapter 6, the focus is on the sensory systems. For both the coupled and the decoupled model, possible sensor configurations are presented. For each sensor configuration are the closed-loop transfer and sensitivity function derived. Subsequently, the resulting closed-loop and sensitivity bandwidths are determined.

Finally, in chapter 7 conclusions of this research are drawn. Furthermore, recommendations for further research are presented as well.

Chapter 2

Dual Stage Actuation in Hard Disk Drives

2.1 Introduction

Increasing the capacity of hard disk drives (HDDs) using existing magnetic storage technology hits the super-paramagnetic limit within a couple of years. At this limit, the media grain becomes so tiny that the medium is not able to retain information stably, due to thermal decay (Wu et al., 2003). The current approach to increase the capacity of HDDs is to increase the track density (the number of tracks-per-inch in radial direction) rather than the linear density, i.e. the amount of bits-per-inch along the track (Wu et al., 2003). The HDD industry is targeting at an areal density of one terabit per square inch. Consequently, the track density increases to 500.000 [TPI] and results in a track width of 50 [nm] (Horowitz et al., 2004). Since the required accuracy of the positioning system is equal to $\frac{1}{10}$ of the trackwidth, nanometer-level precision of the servo system is required.

Furthermore, in order to increase the data-rate, the rotational velocity has also been increased; nowadays rotational speeds of 10.000 [RPM] are common. This results in disturbance signals with relative high frequencies, for example due to eccentricity of the disc. The required accuracy of the high-capacity disk drives results in an increase of the required bandwidth of the servo controller (Sasaki et al., 1998). However, according to Suthasun et al. (2004) in single-stage actuated HDDs a servo-bandwidth of 1 kHz can hardly be achieved. Sasaki et al. (1998) call for a servo-bandwidth of 3-4 kHz when the HDD rotates at 10.000 [RPM].

The call for more precision and a higher response speed, thus requires an increase in HDD servo-bandwidth. This has lead to the development of DSA HDDs, where apart from the conventional single actuator a second actuator is placed near the read-write head.

From literature it becomes clear that the main problem of dual-stage actuation lies in finding a suitable controller structure that is able to generate separate control signals for both the voice coil motor (VCM) and the second-stage actuator from one position measurement (Wu et al., 2003).

This chapter gives an overview of the main topics found in literature on DSA HDDs. First, in section 2.2 attention is paid to the single-stage actuated HDD. From this section the problems in single-stage actuated HDDs become apparent. Then in section 2.3 three principles for implementing a second-stage actuator in HDDs are presented. Followed in section 2.4 by a short discussion on the models that are used to describe the frequency response of both actuators. Next, in section 2.5 two approaches to designing controllers for the dual-stage actuated (DSA) system are discussed. It was found that researchers have applied both MIMO design methodologies, as well as decoupled or sequential SISO design methodologies in order to control the DSA-system. The latter methodologies are discussed in detail. Finally, in section 2.6 the findings of the literature research are related to the application. From this discussion, analogies and differences between literature and the application become clear and from this, the main research topics become apparent.

2.2 Single-stage actuated HDDs

Before going into detail on dual-stage actuation, first the problems associated with single-stage actuated HDDs are discussed in more detail. This discussion is illustrated by figure 2.1 in which a schematic overview of a HDD with

a single-stage actuator is shown.

The positioning of the read-write head over the disk surface is done by sweeping the arm over the disk by actuating the voice coil motor (VCM). The arm consists of a pivot around which it rotates, an E-block and a suspension which are designed to suspend the read-write head. The suspension is shaped such that it is able to transfer the lateral force from the E-block to the slider, in which the read-write head is positioned. But it also provides a downward force, which is required to balance the lift generated by the flying slider and to preserve a certain distance to the disk itself. The slider is used to physically support the head and hold it in the correct position relative to the disc as the head floats over its surface. Such a slider is necessary since the read/write heads are too small to be used without attaching them to a larger unit; this is the function the slider fulfills.

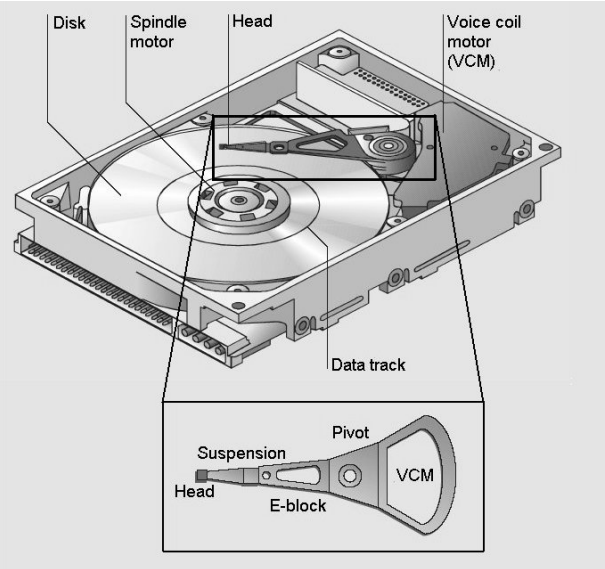

Figure 2.1: Schematic overview of a HDD. In the lower part of the figure the single-stage VCM actuator is shown. This figure is adapted from a figure in Horowitz et al. (2004).

When the actuator in figure 2.1 is used in practice, multiple mechanical resonance modes of the pivot, the E-block and the suspension between the VCM and the head are observed. Furthermore, nonlinear friction of the pivot bearing puts limits on the servo precision (Horowitz et al., 2004). Also, the large inertia of the VCM limits the achievable bandwidth (Suthasun et al., 2004).

In Kobayashi and Horowitz (2001) alternatives for increasing the bandwidth of single-stage actuated HDDs are given. First the use of robust control systems for controlling the mechanical resonance modes is suggested. Also the use of multi-sensing control systems, which use an accelerometer or strain gauge as a vibration sensor have been presented. However, dual-stage actuation has shown to be a relatively simple and effective way to overcome the limitations of single-stage actuated HDDs.

2.3 Dual-stage actuated HDDs

In the previous section the limitations of the single-stage actuated HDDs have become clear. In this section attention is paid to implementing a dual-stage actuator in HDDs. A clear advantage of using dual-stage actuation in HDDs is that only one additional actuator and some modifications of the control system are required. Dual-stage actuation in HDDs can be categorized in three groups: (Horowitz et al., 2004; Wu et al., 2003)

Actuated suspension : In this case the suspension is redesigned, such that it contains a piezo-electric actuator, which is used to position the slider and magnetic head. A possible implementation of this type is shown in figure 2.2. For track-following, the two piezo-actuators are driven such that one actuator stretches, while

the other contracts. Since the suspension is located relatively far from the read/write head, by means of mechanical amplification the displacement range of the piezo-actuators is increased (Niu et al., 2000). A major drawback of this approach is according to both Horowitz et al. (2004) and Niu et al. (2000) that the system is still susceptible to instabilities due to the excitation of one of the suspension resonance modes. According to Kim and Lee (2004) this type of dual-stage actuators is one of the two types which is considered mostly in industry.

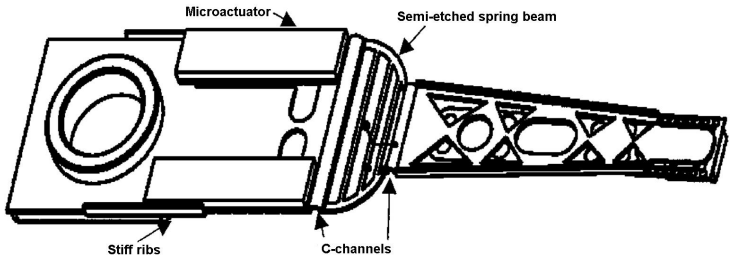

Figure 2.2: Schematic drawing of the actuated suspension (Niu et al., 2000).

Actuated slider : In this case a micro-actuator is placed between the slider and suspension to position the slider and consequently the magnetic head. An example of this approach is shown in figure 2.3. In this example, the beam parts consist of stacked piezoelectric layers, which are actuated in opposing directions. As a result, the slider bends and the moveable part, to which the read/write head is attached, is displaced (Soeno et al., 1999). An advantage of this approach over the previous one is that this system is able to suppress the mechanical resonance modes of the suspension. However, a redesign of the suspension is necessary in order to retain flying stability of the slider (Horowitz et al., 2004; Niu et al., 2000). Kim and Lee (2004) state that this is the second type of dual-stage actuators which is considered most in industry.

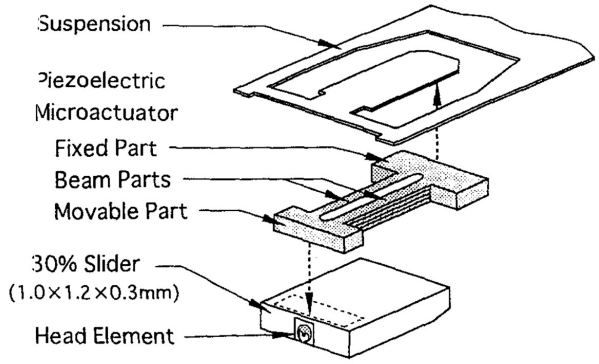

Figure 2.3: Schematic drawing of the actuated slider (Soeno et al., 1999)

Actuated head : In this principle it is necessary to redesign the slider in order to incorporate the micro-actuator in the slider block. As a result, the read/write head can be actuated with respect to the rest of the slider body. An example of this principle is shown in figure 2.4. It can easily be seen that the driving principle of this second-stage actuator is comparable with the previous two approaches. The main advantage of this approach is that in this case the lowest mass should be displaced by the second-stage actuator, which normally results in the largest achievable bandwidth (Soeno et al., 1999). Furthermore, the second-stage actuators can be very light, such that the slider weight is increased only slightly. As a result, the slider suspension does not need to be redesigned (Horowitz et al., 2004). This approach has also the advantage of bypassing the suspension and

does therefore not excite one of the suspension resonance modes. Although researchers have implemented this type of dual-stage actuation in HDDs (Horowitz et al., 2004; Fujita et al., 1999), according to Kim and Lee (2004) this type of dual-stage actuators is not considered much in industry.

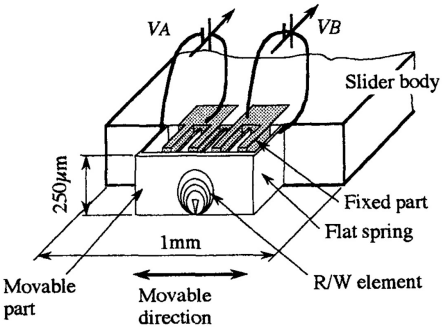

Figure 2.4: Schematic drawing of the actuated head (Fujita et al., 1999).

It can be concluded that mostly piezoelectric micro-actuators are used, since these actuators do not interfere with the magnetic field of the read/write head as electromagnetic actuators would do. It should also be mentioned that by implementation of the second-stage the measurement system has not been adapted since the read/write head of the HDD serves as the single positional sensor of the system.

2.4 Modelling dual-stage actuated HDDs

For both the design of servo-controllers and assessing the appropriateness of the designed servo-controllers, models of both actuators in the DSA system are required. In literature models for DSA HDDs are mainly obtained by means of system identification. Mostly, models for the first and second actuator are obtained separately under the assumption that there is no mechanical coupling between the two actuators. Consequently, the output position of the system is regarded as a summation of the displacement of the VCM and the micro-actuator; throughout this research this modelling approach is denoted as the *decoupled model*.

In general, the transfer function from the VCM input current to the VCM to the position of the read/write head of a single-stage actuated HDD consists of a double-integrator model for low frequencies, followed by one or more resonances. A typical magnitude plot is shown in figure 2.5a.

Considering the frequency response of the micro-actuator, it can be concluded that the plant transfer function from the applied voltage to the displacement shows a constant gain over a large frequency range up to the first resonance frequency. As example, in figure 2.5b a typical response of a piezo-actuator is given. Furthermore, concerning the the plant model of the micro-actuator, in the model the saturation of the second-stage actuator should be taken into account (Guo. et al., 2003), since this causes stability problems in the control system.

2.5 Controllers for dual-stage actuated HDDs

In Horowitz et al. (2004) an overview of controllers for DSA HDDs is given. The controller types can roughly be divided into two groups. The first group is based on decoupled or sequential SISO design. The second group is based on optimal design methodologies such as LQG/LTR, H_∞ and μ-synthesis. In this latter approach, the controllers for both stages are obtained simultaneously.

2.5.1 SISO design methodologies

In literature, four approaches to transform the dual-stage control problem into two decoupled or sequential SISO control problem have been proposed (Horowitz et al., 2004). These approaches are displayed in figure 2.6 and are

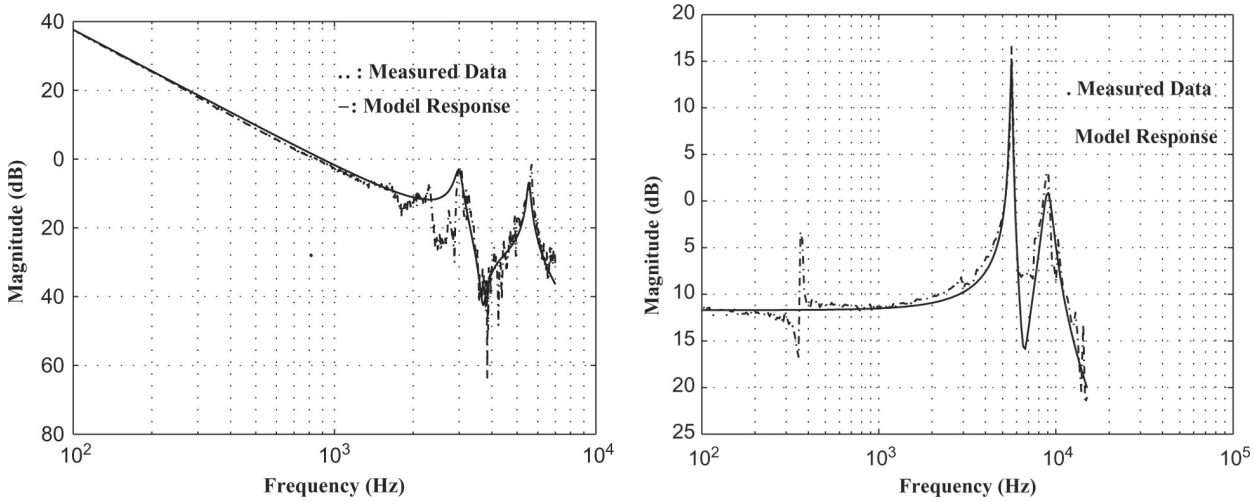

Figure 2.5: Typical Bode magnitude plots of a) the plant transfer function from the applied current to the resulting position of a single-stage actuated HDD and b) the plant transfer function from the applied voltage to the output position of the piezo-actuator (Suthasun et al., 2004).

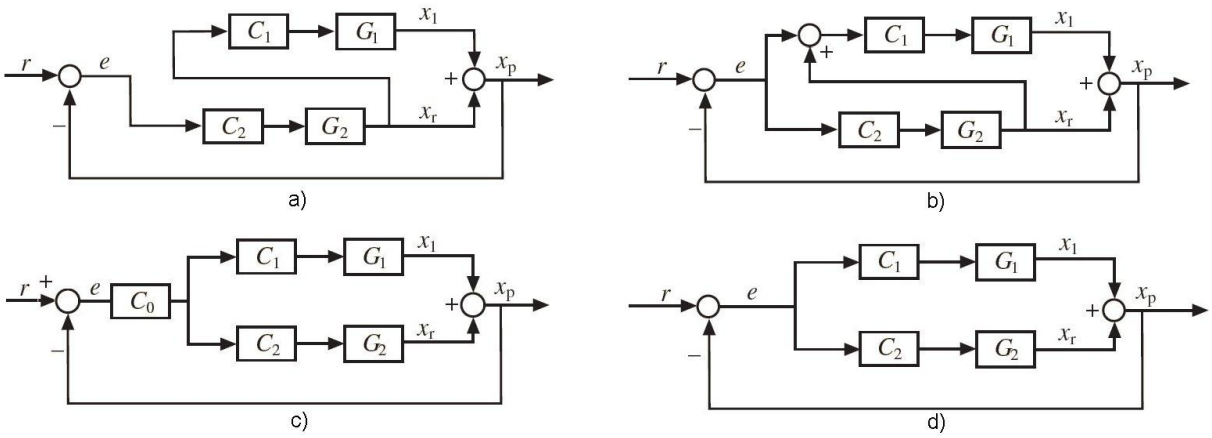

Figure 2.6: Four possible SISO control structures that result from transformations on the actual system. In all figures, G_1 comprises the VCM and G_2 the second-stage actuator. In this figure the following SISO design methodologies are shown: a) master-slave design, b) decoupled control design, c) PQ control design and d) parallel control design.

discussed in more detail in the course of this section.

Master-slave control approach : As can be seen in figure 2.6a, in this approach the positional error, $x_p - r$, is fed to the controller C_2 of the second-stage actuator. The resulting displacement of this second-stage actuator, x_r, is fed as a signal to the input of C_1 of the VCM controller, which as a result follows the second-stage actuator in order to prevent saturation (Horowitz et al., 2004).

Decoupled control approach : Figure 2.6b shows the decoupled control approach as it was presented by Mori et al. (1991). In contrast with the first approach, the positional error, $x_p - r$, is fed to both the controller of the VCM and the second-stage actuator. Furthermore, the output of the second-stage, x_r, is added to the positional error applied to the VCM controller, such that this error signal equals the positional error of the

VCM. In Li and Horowitz (2001) an important property of this system for controller design is given; they have shown that the sensitivity function of the DSA system is a multiplication of the sensitivity functions of the independent control loops.

PQ control approach : This approach to controlling a dual-stage actuator is presented in Schroeck et al. (2001), a block diagram is given in figure 2.6c. The first step in this design methodology is to define a new SISO-system $P = \frac{G_1}{G_2}$. Then a controller $Q = \frac{C_1}{C_2}$ is designed to parameterize the relative contribution of both actuators. The controller Q determines the cross-over frequency and phase margin of the SISO system PQ. The controller Q is designed such that the output of the SISO-system is dominated in the high frequency range by the second-stage actuator and by the VCM in the low frequency range.

In the second step a third controller C_0 is designed, such that both the gain and phase margin and the error rejection requirements of the overall control system are satisfied.

A drawback of this approach is that there is no guarantee on the stability of the VCM feedback loop. This is especially a problem when the second-stage actuator is not activated (Numasato and Tomizuka, 2003).

Parallel control approach : This approach is presented in Semba et al. (1999) and is shown in figure 2.6d. The two controllers in this approach are designed by two design constraints and by sequential loop closing. The design contraints are such that for high frequencies the open loop frequency response equals that of the second-stage actuator. Whereas for low frequencies the controller C_1 is designed to satisfy the low frequency constraint and overall stability requirements.

2.5.2 MIMO design methodologies

Since the dual-stage actuator in HDD servo systems is a MIMO-system, it seems logical to use MIMO design tools. Methods that have been extensively discussed are LQG/LTR control, for example Suh et al. (2001), H_∞ and μ-synthesis, for example Semba et al. (1999); Herrmann and Guo (2004). From these references it became clear that using these techniques to design controllers for the DSA system have important drawbacks. First, the required computational capabilities for implementation exceed the practically available capacity and the required accuracy of modelling the disturbances can hardly be achieved.

However, the robustness analysis that can be performed by using these techniques can be of importantance, since resonance frequencies of PZT-elements tend to variate 15% as a result of the fabrication process (Horowitz et al., 2004). When this is not taken into account in the controller design, the controller performance degrades.

Apart from these optimal control approaches, also approaches like *sliding mode control* (Lee et al., 2000), *neural networks* (Sasaki et al., 1998) and *mode switching control* (Numasato and Tomizuka, 2003) have been presented in literature.

2.6 Conclusions for dual-stage application in the FCM

In the previous sections, results from the literature research on DSA HDDs are presented. From this research we have gained insight into the four elements that make up a DSA system:

1. dual-stage plant model
2. second-stage actuator model
3. sensor configuration
4. controller structure

In this section, it is discussed how these elements are related between DSA HDDs and the FCM.

Concerning the plant model of the DSA system, in literature on DSA HDDs, except for some exceptions, decoupling of the first and second-stage is assumed. However, in this case the authors have assumed that the two stages do not influence each other. In order to investigate whether this assumption is realistic, in chapter 5, models of both the first and second-stage are used to determined transfer functions of both the coupled and decoupled

model. Subsequently, it is determined for which values of the second-stage parameters c_{13} and m_3 decoupling occurs. Furthermore, in chapter 6 it is shown that it is not necessary to have a decoupled system in order to use similar SISO design methodologies as in section 2.5.1.

Furthermore, in case of DSA HDDs, the measurement setup needs not to be adapted; the measurement setup of the single-stage actuated system measures the position of the read/write head. It is not necessary to change this implementation after including a second-stage actuator. However, in the case of the single-stage actuated FCM we do not have a measurement of the end-effector position. Instead, the position of the first-stage actuator is measured and used for feedback (Coelingh, 2000). Therefore, in chapter 6 possible position sensor configurations are given for implementation in the DSA FCM. Subsequently, these sensor configurations are evaluated in terms of the closed-loop bandwidth as well as the sensitivity function.

With respect to the controller structure that is found in literature on DSA HDDs, it was already concluded that this can be roughly split into sequential or decoupled SISO design methodologies and MIMO design methodologies. Furthermore, it is revealed that the MIMO design methodologies have certain major drawbacks. The first being that the required computational capabilities for implementation exceed that of what is practically available. Secondly, these methods require accurate modelling of disturbances which can hardly be achieved. The SISO design methodologies are insightful and relatively simple to implement. It is desired to implement the controllers for the DSA system as one of the given SISO design methodologies. Therefore, in chapter 6 the decoupled control approach and the parallel control approach are applied to the decoupled model of the DSA FCM. These controller structures have the advantage of being easy to implement, ensure stability of both stages and are expected to result in the largest bandwidth of the DSA system compared to the other two SISO design methodologies in section 2.5.1.

Finally, concerning the type of second-stage actuation in DSA HDDs it is found in literature on DSA HDDs, that mainly piezo-electric actuators are used. However, depending on the way in which the second-stage actuator is implemented in the HDD the possible actuator type differs. It is seen, that in case of the actuated head implementation either a piezo-actuator or an electrostatic actuator is used. The main reason is that these actuation principles do not interfere with the magnetic field which should be picked up by the read/write head. It should be mentioned that this implementation has an important advantage; since in this case the smallest mass should be displaced by the second-stage actuator, the largest bandwidth results. For the FCM a comparable solution is suggested. In this case, (part of) the end-effector should be actuated by the second-stage actuator, in order to displace the smallest mass. In case of dual-stage actuation in the FCM, compared to the topic of magnetic interference in the HDD case, it is of less importance which actuation principle is used, as long as the actuator has a sufficient stroke and relatively large bandwidth. Using this as starting point, then it can be concluded that piezo-actuators or electromagnetic actuators are most suitable for implementation as second-stage actuators in the FCM. During this research only the implementation of a piezo-actuator as a second-stage actuator is considered.

Chapter 3

Modelling the FCM's Placement Module

3.1 Introduction

In the previous chapter an overview of literature on dual-stage actuated (DSA) systems is given. By modelling the single-stage actuated HDD, it became clear that the resonance between the actuator and the read/write head limits the achievable bandwidth of this system. In this chapter a model of the single-stage actuated Placement Module (PM) of the Fast Component Mounter (FCM) (Assembleon, 2004) is derived.

The FCM is a machine which is used for assembly operations; it is used to place electric components on a Printed Circuit Board (PCB). Regarding the capacity of the machine, the FCM is capable of placing up to 100.000 components per hour. In order to achieve this capacity, a maximum of 16 PM modules are placed in parallel. An impression of the FCM is shown in figure 3.1.

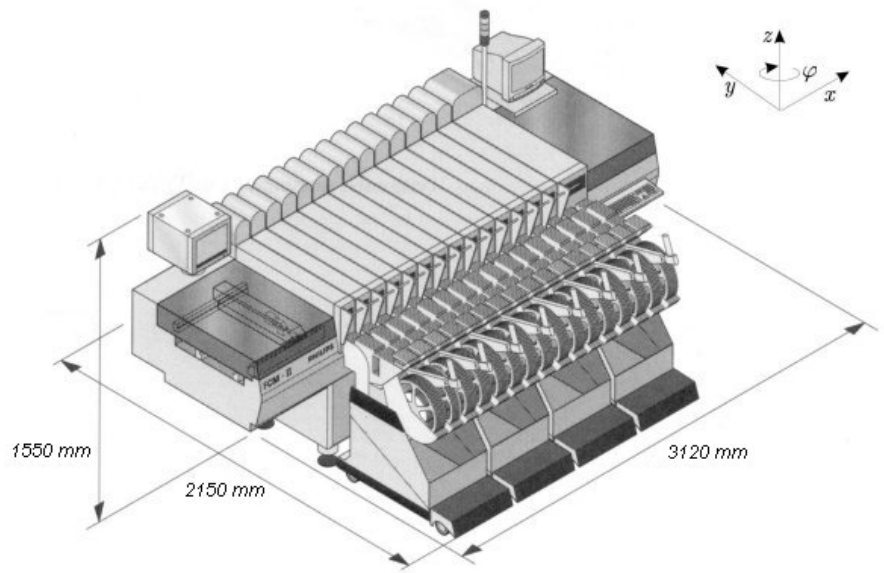

Figure 3.1: Impression of the FCM as it was originally designed by Philips (Coelingh, 2000).

The PM module, which is considered in this report, is a servo-controlled pick-and-place robot. The main drive of a PM module consists of an actuator, which drives a spindle-drive via a gear-belt. The direction of motion of this main drive is in y-direction. The spindle-drive subsequently drives a carriage, on which the pipette, or end-effector, is attached. The motion of this pipette is in z-direction, such that it can move up and down to pick and place the

components on the PCB. The carriage can also perform a small stroke motion in the x-direction. An impression of the PM module is shown in figure 3.2. It should be mentioned that (the improvement of) the motion of the pipette in y-direction is considered in this report.

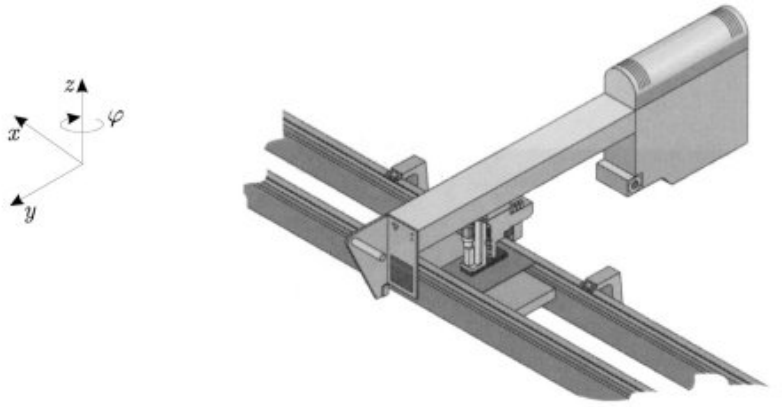

Figure 3.2: Impression of the PM module. The FCM consists of up to 16 of these modules placed in parallel.(Coelingh, 2000)

The aim of modelling the PM is to investigate whether the achievable bandwidth of the PM is also limited by a resonance. If that is the case, then it is useful to investigate the application of dual-stage actuation to the PM. In section 3.2 a model of the PM and the model parameters are derived. In section 3.3 conclusions on the resulting model are drawn.

3.2 Modelling the Placement Module

In figure 3.3, a schematic diagram of the placement module of the FCM is given. A motor drives a set of pulleys by means of a timing belt. The lower pulley is connected directly to a spindle. When the spindle rotates, the carriage is displaced via a ball screw. To this carriage a pipette, or end-effector, is attached, which is used for picking up electronic components and placing them on the PCB. It should finally be noted that a linear guiding is used to fix the position and the orientation of the carriage in z-direction (Coelingh, 2000).

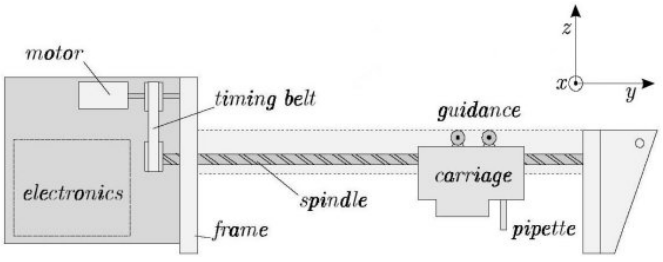

Figure 3.3: Schematic diagram of the placement module of the FCM (Coelingh, 2000).

Using the bondgraph model from Coelingh (2000), an iconic model of the FCM's placement module is obtained, see figure 3.4. It can be seen that in this model the displacement of the end-effector is a summation of the movements of the frame and the spindle drive, assuming that frame vibrations remain small and hence superposition because of linearity applies.

The model in figure 3.4 will be simplified for three reasons. First, applying model reduction to this model will result in a fourth order model, which is much more simple to analyze compared to the model in figure 3.4. In the

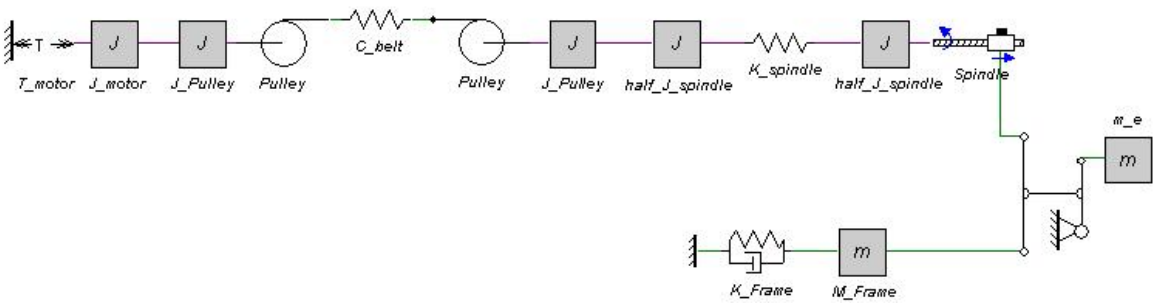

Figure 3.4: Iconic diagram of the PM module.

resulting model, the performance limiting resonance becomes apparent. Secondly, reducing the model to a fourth-order system makes it possible to use the assessment method from Coelingh (2000) for designing controllers to this model. Finally, for the sake of our research aim, we motivate the simplification from the desire to obtain analogy to the HDD case, rather than from actual system properties.

In the HDD case, the end-effector is connected to the motor mass by means of a flexible suspension. Therefore, the stiffness of the frame of the FCM is assumed to be infinite. Using the superposition principle as before, the frame resonances can be seen as an output. Then a model simplification is carried out on the remaining model by removing the transformation ratio's of the spindle and both pulleys, as well as combining dependent inertias. The result is shown in figure 3.5.

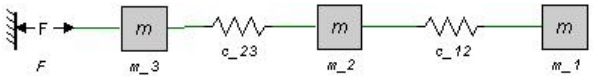

Figure 3.5: Simplified model from figure 3.4 after removing the transmission ratio's and combining the inertias.

After the first model reduction, the new numerical values of the model parameters should be calculated. First, we define the transmission ratio i of the spindle with pitch p as

$$i = \frac{p}{2\pi} \text{ [m/rad]} \tag{3.1}$$

and the transmission ratio of the pulleys as r [m]. Using these definitions and the parameters from Coelingh (2000), the parameters of the sixth order model are calculated as

$$\begin{aligned} m_3 &= \frac{J_{motor} + J_{pulley}}{i^2} = 3.33 \text{ [kg]} \\ c_{23} &= \frac{c_{belt} r^{-2}}{i^2} = 4.6 \cdot 10^7 \text{ [N/m]} \\ m_2 &= \frac{J_{pulley} + \frac{1}{2} J_{spindle}}{i^2} = 1.66 \text{ [kg]} \\ c_{12} &= \frac{k_{spindle}}{i^2} = 4.0 \cdot 10^7 \text{ [N/m]} \\ m_1 &= \frac{\frac{1}{2} J_{spindle}}{i^2} + m_e = 1.54 + 2.3 = 3.84 \text{ [kg]} \end{aligned} \tag{3.2}$$

This model can be further reduced by using the intuitive model reduction approach (Van Lochem, 1997). This approach uses the diagram in figure 3.6 in order to determine which of the elements m_2, c_{12} or c_{23} can be removed from the model, such that the resonance frequency of the reduced order model differs at maximum 4% from the sixth-order model.

For this approach two ratios should be calculated:

$$\frac{m_1}{m_2} = 2.3 \tag{3.3}$$

$$\frac{c_{12}}{c_{23}} = 0.87 \tag{3.4}$$

These numerical values are plotted as the dotted lines in figure 3.6. It can be concluded that leaving out m_2 results in a fourth order model with the smallest deviation in resonance frequency from the sixth order model. Leaving out this mass means that the springs c_{12} and c_{23} should be combined to one spring. The resulting stiffness of this spring equals

$$c = \frac{c_{12} \cdot c_{23}}{c_{12} + c_{23}} = 21.4 \cdot 10^6 \text{ [N/m]} \tag{3.5}$$

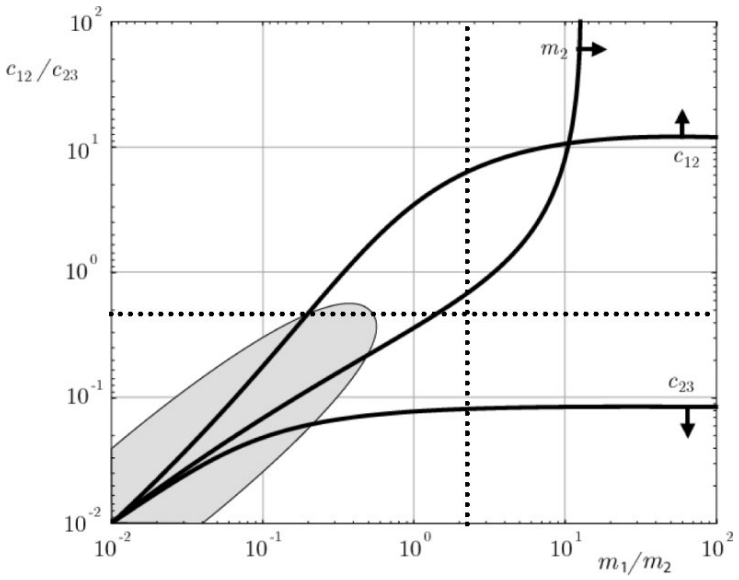

Figure 3.6: The 4% error boundaries in resonance frequency when the indicated parameter is removed from the sixth order system (Van Lochem, 1997).

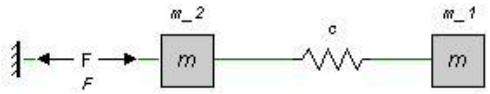

Figure 3.7: Reduced-order model after the intuitive model reduction approach is carried out.

The parameters of the resulting fourth order model in figure 3.7 are summarized as

$$\begin{aligned} m_2 &= 3.33 \text{ [kg]} \\ c &= 21.4 \cdot 10^6 \text{ [N/m]} \\ m_1 &= 3.84 \text{ [kg]} \end{aligned}$$

In the remainder of this report, the stiffness c between m_1 and m_2 is denoted as c_{12}.

3.3 Conclusions

The aim in modelling the PM module was to check whether the model of the single-stage actuated PM is analogous to that of the HDD. From chapter 2 it is known that the transfer function of the VCMs input current to the position of the read/write head can be seen as a double integrator plus at least one lightly damped resonance mode. The plant transfer function from the force F to the output position x_1 of m_1 of the plant in figure 3.7 is given as:

$$P(s) = \frac{x_1}{F} = \frac{c_{12}}{s^2\big(m_1 m_2 s^2 + (m_1 + m_2)c_{12}\big)} \text{ [m/N]} \tag{3.6}$$

By substituting the model parameters, the magnitude plot of the plant transfer function is shown in figure 3.8a. It can easily be seen that this plant transfer function has double integrator behavior ($\frac{1}{s^2}$), as well as a resonance due to the pole-pair in the second part of the denominator. Furthermore, in figure 3.8a also the sixth order plant transfer function from figure 3.5 is shown. This transfer is characterized by the two resonances. It can also be seen that the lowest resonance frequency of the two models are very close to each other, figure 3.8b zooms in on the frequency range around these lowest resonances. From that figure can be concluded that due to the model order reduction the resonance frequency is only shifted slightly.

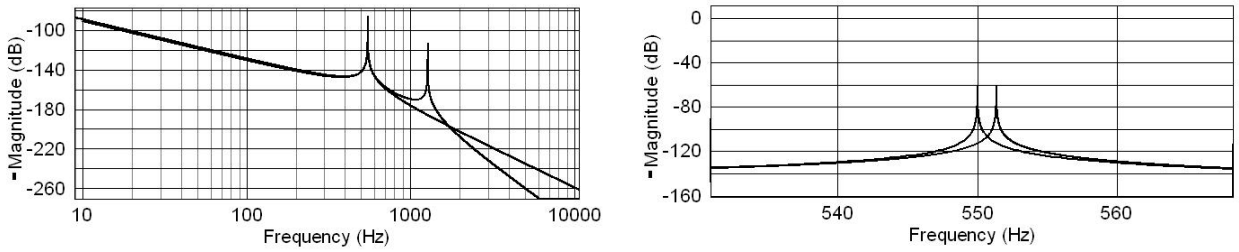

a) b)

Figure 3.8: a) Magnitude plot of both the the sixth order model from figure 3.5 and the fourth order model from figure 3.7. The first transfer function is characterized by two resonance peaks; the first peak coincides with the fourth order model. b) Zooming in on the frequency range around the first two resonances of both the sixth and the fourth order model. The highest resonance originates from the fourth order model. From this plot it can be concluded that the model reduction results in a small increase in resonance frequency.

A final conclusion that can be drawn from the previous analysis is that the frequency response of the FCM model is similar to that of the single-stage actuated HDD. The resonance that is observed between the actuator and the output position of the PM limits the bandwidth of this single-stage actuated system. In order to increase the bandwidth of this system the possibilities to implement a second-stage actuator in this system are investigated in the remainder of this report.

Chapter 4

Piezo-actuator

4.1 Introduction

In the previous chapter a model of the Placement Module (PM) of the Fast Component Mounter is derived. In this chapter a model of a piezo-actuator is derived. These two models are used in the next chapter to analyze the model of the dual-stage actuated PM. In that chapter it will be investigated under which circumstances the decoupled model from literature research applies. In that case, the relatively simple and insightful SISO controller design methods from section 2.5.1 can be applied.

From literature research became clear that piezo-actuators are most suitable for dual-stage actuated (DSA) HDDs. Therefore, in case of the PM, piezo-actuators are used as a starting point for designing and analyzing a DSA PM. In case of HDDs, the main advantage of the piezo-actuator is found in the fact that magnetic interference with the read/write head is absent. However, piezo-actuator have more advantages which make them interesting to implement as second-stage actuators. The main advantage is that this actuation principle has proven to combine a short stroke with a high bandwidth. Furthermore, piezo-actuators have the advantage of being able to perform nanometer and sub-nanometer steps at high frequency with high repeatability, because they realize their motion through solid state crystal effects (PI-Tutorial, 2004). However, the problem in obtaining these resolutions lies in the required sensors; in order to achieve sub-nanometer resolution, sensors with the same resolution are required. This problem is especially relevant for large bandwidth applications (Salapaka et al., 2002). Furthermore, PZTs can be designed to move heavy loads or can be made to move lighter loads at frequencies of several tens of kHz. Thereby, PZTs require very little power in static operation, this simplifies the power supply needs. Finally, PZTs require no maintenance because they are solid state. Disadvantages of using piezo-actuators are mainly restricted to open-loop behavior. In this case piezo-actuators exhibit non-linearities such as hysteresis, creep and drift. However, closing the servo-loop by measuring the displacement of the actuator results in a cancellation of these effects (PI-Tutorial, 2004; Salapaka et al., 2002).

In this chapter, first in section 4.2 a model of a piezo actuator is developed. Then in section 4.3 the topic of bidirectional operation is briefly discussed. In this section the model is adapted to incorporate this behavior. Next, in section 4.4 the controller structure for the piezo-actuator is presented. Subsequently, rules for determining the controller settings are presented. Finally, in section 4.5 the influence of a load mass on the achievable bandwidth of the controlled system is discussed.

4.2 Modelling the piezo-actuator

It is generally known that a piezo-actuator can be modelled in two analoguous ways. One way is to put a position actuator in series with a spring and an equivalent mass, the other way is a force actuator in parallel with a spring. Furthermore, in modelling the piezo-actuator it should be taken into account that the voltage that can be applied to the actuator is limited. Therefore a signal limiter is included in the model to limit the applied voltage u to u'. Finally, the conversion from voltage to displacement or force should be included in the respective models. For the model that uses a force actuator, as is shown in figure 4.1a, the force F that is applied by the force actuator, is

obtained by multiplying the voltage to force conversion factor $d_{U,F}$ with the voltage u'. Thus $F = d_{U,F} \cdot u'$, where $d_{U,F}$ is calculated as

$$d_{U,F} = \frac{F_{block}}{U_{max}} \text{ [N/V]} \tag{4.1}$$

Both the blocking force F_{block} and the maximum operating voltage U_{max} are given for a certain actuator. In the model that uses the position actuator the conversion from voltage u' to displacement x that is applied by the position actuator, can be calculated by rewriting the relation for the spring force and using $F = d_{U,F} \cdot u'$:

$$x = \frac{F}{c} = \frac{d_{U,F} u'}{c} = d_{U,x} \cdot u' \text{ [m]} \tag{4.2}$$

The resulting models are shown in figure 4.1. It should be mentioned that only the displacement of the piezo-actuator in reaction to a supply voltage is considered in the model and not its charge-generating behavior upon application of a load force.

Calculating the transfer functions of these two models results in the plant transfer function from the applied voltage u' to the output position $x_{m_{eff}}$

$$P_{MA}(s) = \frac{x_{m_{eff}}}{u'} = d_{U,x} \frac{\omega_r^2}{s^2 + \omega_r^2} = \frac{1}{c} \frac{F_{block}}{U_{max}} \frac{\omega_r^2}{s^2 + \omega_r^2} \text{ [m/V]} \tag{4.3}$$

where ω_r is given as

$$\omega_r = \sqrt{\frac{c}{m_{eff}}} \text{ [rad/s]} \tag{4.4}$$

with c the stiffness of the actuator and m_{eff} is the effective mass of the piezo-actuator. This mass is about $\frac{1}{3}$ of the mass of the ceramic stack plus any installed end pieces (PI-Tutorial, 2004). In the following, m_{eff} is calculated from the given resonance frequency ω_r by using (4.4). It should be noted that equation (4.3) represents the plant transfer function from the controller output u to the position $x_{m_{eff}}$ as long as $0 \leq u \leq u'$.

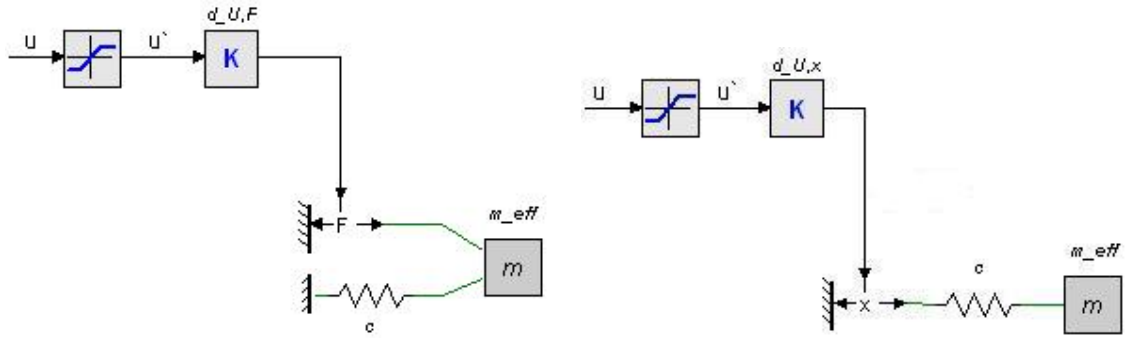

Figure 4.1: Model of the piezo-actuator a) in which the displacement of the actuator is caused by application of a force on the effective mass and b) the displacement of the piezo-actuator is a result of a position actuator.

From equation (4.3) it can be concluded that the resulting model of the piezo-actuator has an undamped resonance frequency. In practice this resonance frequency will be slightly damped by the structure of the actuator and its mounting. In the following simulations it is assumed that the resonance frequency of the piezo-actuator is damped, with relative damping $\zeta \approx 0.01$. Consequently, the transfer function of the piezo-actuator from equation (4.3) becomes

$$P_{MA}(s) = \frac{1}{c} \frac{F_{block}}{U_{max}} \frac{\omega_r^2}{s^2 + 2\zeta\omega_r + w_r^2} \text{ [m/V]} \tag{4.5}$$

4.3 Bidirectional operation

In general, piezo-actuators cannot be used for generating pull forces. However, in a DSA system, the piezo-actuator should be able to compensate for both positive and negative positional errors. Consequently, the piezo-actuator should be able to apply both a push and pull force, preferably with the same maximum magnitude.

Methods for generating the pull force of the piezo-actuator consist of preloading the piezo-element with a push force. Since the aim of this research is to contribute to the concepts of dual-stage actuation, it is not important yet to decide which of the possible implementations should be selected. Practical limitations are of interest in further research, when the concept of dual-stage actuation in linear motion systems has been proven successful.

Bidirectional operation of the piezo-actuator is implemented in the model of section 4.2 as follows. The model itself is not adjusted, but it is assumed that the piezo-actuator is able to generate displacements in the range $[-\frac{1}{2}x_{max}; \frac{1}{2}x_{max}]$, when a voltage in the range $[-\frac{1}{2}U_{max}; \frac{1}{2}U_{max}]$ is applied.

4.4 Controlling the actuator displacement

In this section a controller for the piezo-actuator as second-stage actuator is developed. In the design of this controller it is assumed that the output position $x_{m_{eff}}$ is measured by means of a position sensor. In figure 4.2 can be seen how the controller is placed in series with the actuator model from figure 4.1b. It will be shown in this section that the controller parameters can easily be derived from the parameters of the piezo-actuator model from section 4.2.

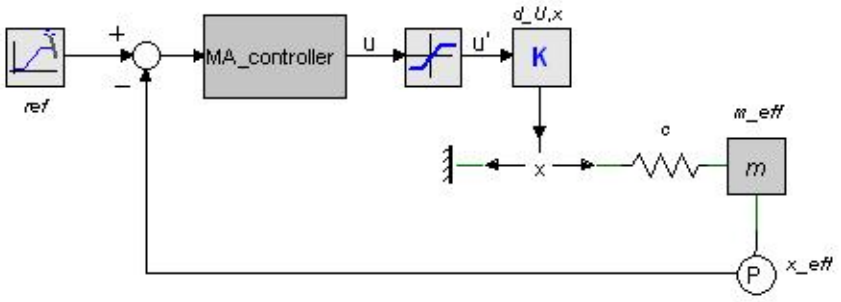

Figure 4.2: Schematic drawing of the closed-loop piezo-actuator. In this section it is assumed that the output position of the actuator is measured.

A common approach to control the displacement of a piezo-actuator is to use a PI-controller in series with a low-pass filter (see for example Van Dijk (2003)), this controller is henceforth denoted as PI+ controller. Apart from the PI+ controller also an anti-windup scheme (Aström and Hägglund, 1995) is implemented in the controller. The resulting controller structure is shown in figure 4.3. The anti-windup scheme is implemented in order to prevent saturation of the actuator by keeping the integrator output to a proper value when the actuator saturates. Saturation occurs when the positional error of the DSA system becomes larger than the displacement range of the piezo-actuator. It is necessary to implement this scheme since otherwise desaturation of the actuator can take a long time and the second-stage actuator is implemented for fast responses.

The implementation of the anti-windup scheme is as follows. The output voltage of the controller is measured and compared with the maximum and minimum operating voltage. When these limits are exceeded, a feedback loop is activated which makes sure that the integral action of the parallel PI-controller is kept to a proper value. The difference between the output and input of the voltage limiter is divided by a time constant τ_a to control this process. The result of this division is added to the input of the integrator in the PI-controller. As a consequence, the controller can immediately undertake action when the error changes to values within the displacement range. It can be concluded that the anti-windup scheme is set only by the parameter τ_a. As a rule of thumb, $\tau_a \leq \tau_i$ is chosen equal to τ_i (Aström and Hägglund, 1995).

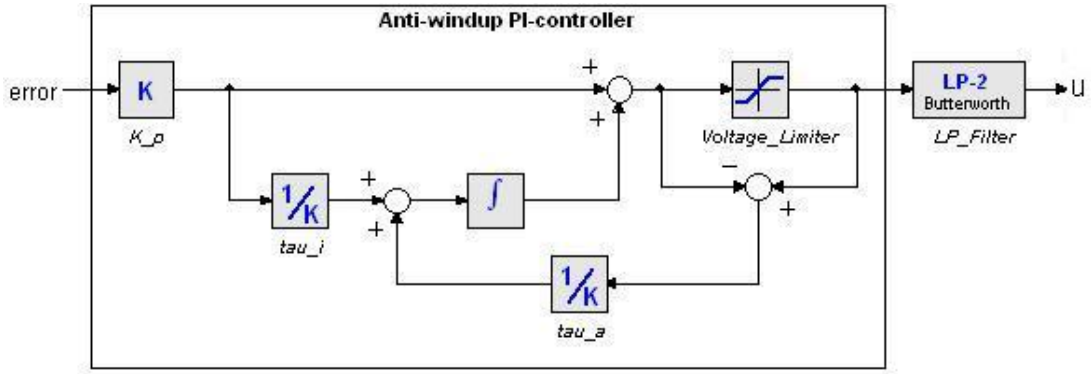

Figure 4.3: Implementation of the PI+ controller for the micro-actuator in 20sim.

Regarding the controller settings of the PI+ controller, from Van Dijk (2003) rules of thumb for determining the settings of a PI+ controller are known. In this case, the transfer function of the PI+ controller from the applied error to the controller output at the output of the low-pass filter is given as

$$H_{PI+}(s) = \frac{k_i}{s} \frac{\omega_{LP}^2}{s^2 + 2\zeta_{LP}\omega_{LP} + \omega_{LP}^2} \text{ [V/m]} \tag{4.6}$$

However, the previous transfer function of this PI+ controller differs with the implementation of a parallel PI-controller as shown in figure 4.3. The latter transfer function (without anti-windup) is

$$H_{PI,parallel}(s) = \left(k_p + \frac{k_p}{s\tau_i}\right) \frac{\omega_{LP}^2}{s^2 + 2\zeta_{LP}\omega_{LP} + \omega_{LP}^2} \text{ [V/m]} \tag{4.7}$$

It can thus be concluded that the controller parameters k_p and τ_i should be chosen such that the first terms in (4.6) and (4.7) equal each other, thus

$$\frac{k_i}{s} = k_p + \frac{k_p}{s\tau_i} \tag{4.8}$$

In order to make the I-action of the parallel PI controller dominant and using the fact that in practice $k_i \gg 1$, k_p is chosen equal to 1 and consequently $\tau_i = \frac{1}{k_i}$.

It can thus be concluded that the PI+ controller is set by two parameters; the cut-off frequency of the low-pass filter (f_{LP}) and the proportional gain of the PI-controller (k_i). The rules of thumb for the controller settings are (Van Dijk, 2003)

$$f_c < \frac{1}{4}\frac{1}{2\pi}\omega_r^{'} \text{ [Hz]} \tag{4.9}$$

$$f_{LP} = 2.5 f_c \text{ [Hz]} \tag{4.10}$$

$$k_i = f_c c \tag{4.11}$$

where f_c is the gain cross over frequency of the controlled piezo and $\omega_r^{'}$ is the resonance frequency of the loaded piezo-actuator. This latter parameter of the piezo-actuator is treated in the next section, where also these rules of thumb are applied to two piezo-actuators. For these actuators the controller settings are determined for varying load mass, such that certain open-loop stability margins are satisfied.

4.5 Controller properties for varying load mass

From equation (4.9), it became clear that the PI+ controller settings are based on the resonance frequency of the piezo-actuator. In the previous it has already been shown how the resonance frequency of the unloaded piezo-actuator can be calculated, see equation (4.4). However, the resonance frequency of the actuator changes, when

$\mathbf{f_{res}^{'}}$ **[Hz]**	$\mathbf{m_3}$ **[kg]** P-885.10	$\mathbf{m_3}$ **[kg]** P-888.20	$\mathbf{f_{LP}}$**[Hz]**	$\tau_\mathbf{i}$	**GM [dB]**	**PM** [°]	**BW [Hz]**
1000	2.92	8.94	625	$4.0 \cdot 10^{-11}$	6.2	52.0	246
2000	0.73	2.24	1250	$2.0 \cdot 10^{-11}$	6.2	52.0	492
2463	0.48	1.47	1500	$1.6 \cdot 10^{-11}$	6.5	52.4	656
3557	0.23	0.71	2223	$1.1 \cdot 10^{-11}$	6.1	50.8	887
5000	0.12	0.36	3125	$8.0 \cdot 10^{-12}$	6.2	51.9	1230
13275	$16 \cdot 10^{-3}$	$5.0 \cdot 10^{-2}$	8296	$3.0 \cdot 10^{-12}$	6.2	51.7	3275

Table 4.1: Parameters of the MA-actuator and controller for two piezo-actuators (PI P-885.10 and P-888.20)

loaded with a mass m_{load}, as it will be in the application. The resonance frequency of the loaded piezo-actuator is calculated as

$$\omega_r^{'} = \sqrt{\frac{c}{m_{eff} + m_{load}}} = \sqrt{\frac{c}{m_3}} \text{ [rad/s]} \tag{4.12}$$

where m_{eff} the effective mass of the actuator and m_{load} the applied load mass. In the right hand side of this equation we have defined, that in the remainder of this report the loaded actuated piezo-actuator is denoted as m_3; $m_3 = m_{eff} + m_{load}$.

In this section, the PI+ controller settings for PI's P-885.10 and P888.20 piezo-actuators (PI-datasheets, 2004) are determined for various values of m_{load}. These two piezo-actuator are chosen for two reasons. First, as is shown in appendix A, the maximum displacement of both actuators is in the same order of magnitude. Consequently, the influence of other parameters, especially the stiffness of the actuator, on the performance of the DSA system can be investigated. Secondly, during the research it became clear that the larger the stiffness of the actuator is, the larger the load mass on the piezo-actuator can be while retaining the same bandwidth of the controlled system. But also the larger the stiffness of the piezo-actuator, the larger the bandwidth of the second-stage actuator is for the same load mass. Therefore, two actuators are chosen which have a considerably large stiffness, hence, their maximum displacement is relatively small.

Subsequently, for various values of m_{load} both the open-loop stability margins, as well as the bandwidth of the closed-loop are determined. As before, it is assumed that the output position of the piezo-actuator is measured. The bandwidth of the closed-loop controlled piezo-actuator is determined by plotting the sensitivity function of the controlled piezo-actuator and determine the lowest frequency at which the sensitivity function crosses the 0dB line from below. The sensitivity function is defined as

$$S(s) = \frac{x_{out}}{\delta} = \frac{x_{m_{eff}} + \delta}{\delta} \tag{4.13}$$

where δ is an output position disturbance. The sensitivity function $S(s)$ is symbolically derived in appendix C.2. For determining the bandwidth of the closed-loop system, the sensitivity function is determined using 20sim.

In order to determine the loaded resonance frequency and consequently the controller settings, the parameters of both micro-actuators are given in appendix A. The controller settings at each value for m_{load} are determined using the rules of thumb from section 4.4. Consequently, τ_i is adjusted in order to obtain a gain margin (GM) which is minimally equal to 6 [dB]. For both piezo-actuators the resulting controller settings, open-loop stability margins and bandwidth are given in table 4.1. It should be noted that this analysis is carried out under the assumption that the actuator is not in saturation; in this case the controller is given by equation (4.7). As an example, the open-loop frequency response of P-885.10 loaded with a mass of 0.12 [kg] is shown in figure 4.4a. Furthermore, in figure 4.4b the sensitivity function of the same actuator and load mass combination is shown.

It should be mentioned that direct application of the rules of thumb from section 4.4 results in an open-loop response with a gain margin greater than 6 [dB]. In order to maximize the bandwidth of the second-stage actuator and yet retain a stable system as well, τ_i should be adjusted (manually) such that GM is almost equal to 6 [dB].

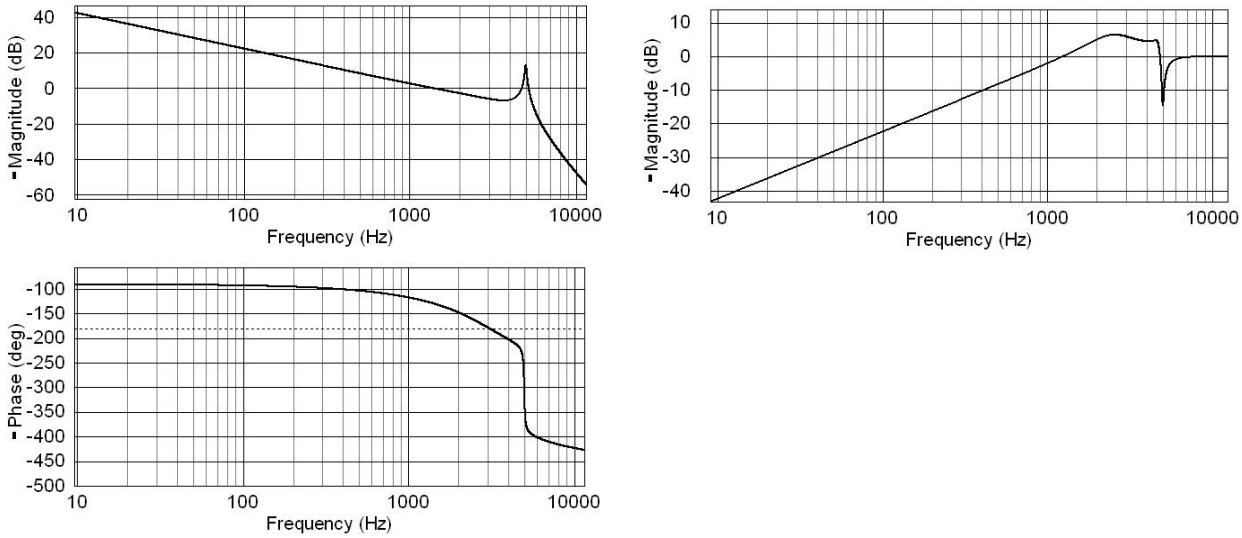

a) b)

Figure 4.4: a) Open-loop frequency response from x_{ref} to x_3 of the controlled piezo-actuator P885.10 loaded with a mass of 0.12 [kg] and b) plot of the accompanying sensitivity function.

4.6 Conclusions

From table 4.1 it can be concluded that in general the bandwidth of the closed-loop system is $\frac{1}{4}$ of the resonance frequency of the loaded actuator. This observation is of practical interest; from literature research it has become clear that using the decoupled model assumption, the bandwidth of the DSA system is in practice almost equal to the bandwidth of the second-stage actuator. When designing a DSA system, the desired bandwidth of the DSA system should be quantified and can be translated into a value of the loaded resonance frequency of the piezo-actuator. This is one of the first steps in the design procedure of DSA systems.

Chapter 5

Dual-stage plant model analysis

5.1 Introduction

It has been pointed out in chapter 2 that in literature on dual-stage actuated HDDs, the DSA system is modelled as two parallel systems. The output of the DSA system is a summation of the output of both the first and the second stage system. Consequently, the relatively simple SISO controller design techniques sketched in section 2.5.1 can easily be used to design controllers for this system. In the previous two chapters, we have derived the models of both the first-stage and the second-stage actuators. In this chapter we analyze the interation between the two stages.

In practice, the second-stage actuator is attached to the first-stage. When the second stage is actuated, it will exert a force both on the second-stage mass, as well as on the first-stage. The interconnection of the two systems is shown in figure 5.1a. It can thus be concluded that the second-stage influences the dynamics of the first-stage. To what extent this influence stretches, is depending on the parameters of both stages, as will be shown in the coming sections. This analysis is carried out by considering two cases. First in section 5.2 the case in which the second-stage actuator influences the first-stage is discussed. Then in section 5.3 the connection between these systems is assumed to be negligible, in that case the system is decoupled as is shown in figure 5.1b. For both cases the partial plant transfer functions from the inputs $F_{in}, x_{2^{nd}}$ to the output position x_3 are calculated:

$$\left.\frac{x_{out}}{x_{2^{nd}}}\right|_{F_{in}=0} \tag{5.1}$$

$$\left.\frac{x_{out}}{F_{in}}\right|_{x_{2^{nd}}=0} \tag{5.2}$$

In the course of this chapter, in case of the coupled system it is assumed that in the design of the dual-stage actuated (DSA) system, mass can be distributed from the first-stage to the second-stage, however the total mass remains constant. In this case it is thus assumed that

$$m_{ce} = m_{1,c} + m_3 \text{ [kg} \tag{5.3}$$

where m_{ce} is the total mass of carriage and end-effector, its numerical value is in case of the FCM equal to 3.84 [kg]. Furthermore, in case of the decoupled system, the first-stage actuator should displace all masses in the system. Therefore the numerical value for $m_{1,d}$ can be calculated as

$$m_{1,d} = m_{1,c} + m_3 \text{ [kg} \tag{5.4}$$

where m_3 is defined in chapter 4 as the summation of m_{eff} of the piezo-actuator and m_{load} the load mass to the actuator.

After having determined the partial transfer functions of both the coupled and the decoupled model, in section 5.4 the coefficients of these partial transfer functions are compared with each other. Also, the poles and zeros of both models are compared, such that the maximum value for m_3 for which decoupling occurs can be calculated.

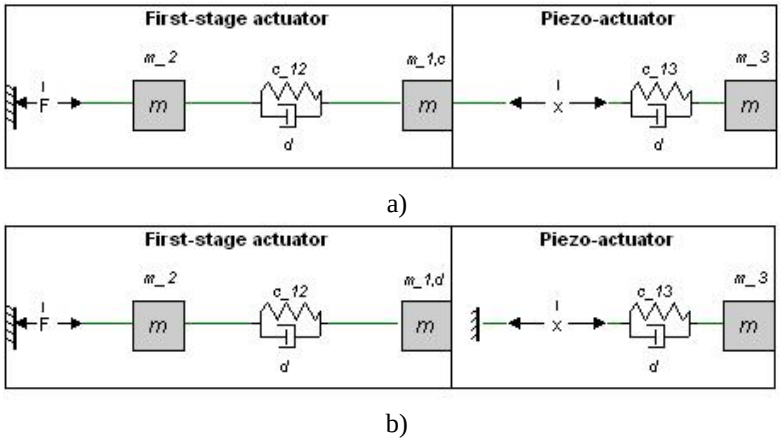

Figure 5.1: Schematic drawing of a) coupled DSA system, the first-stage is influenced by the second-stage actuator and b) decoupled DSA system in which the first-stage is not influenced by the second-stage actuator. In both models damping is added to both stages. In the analysis, this damping is first assumed to be absent and is added later in this chapter. Note that the position of m_2 is denoted by x_2, the position of $m_{1,c}$ and $m_{1,d}$ as x_1 and finally, the position of m_3 as x_3.

From that maximum value for m_3 and the pole-zero analysis, also a minimum value for the stiffness of the piezo-actuator is derived in the same section. Finally, in section 5.5 conclusions on the performed analysis and the results are drawn.

It should be noted that in this chapter, in order to simplify the analysis, the gain $d_{U,x}$ which is present in the piezo-actuator model, is not taken into account. Including this gain would only shift the input signal to this system. Since in this chapter the partial transfer functions of the coupled and decoupled model are determined, the analysis is not influenced by omitting $d_{U,x}$.

5.2 Partial plant transfer functions of coupled model

In this section the partial plant transfer functions from the inputs F_{in}, $x_{2^{nd}}$ to the output position of the coupled system, x_3, is presented. This system is shown in figure 5.1a. The approach to determine x_3 as a function of the two inputs is to calculate subsequently the position of each of the three masses. These positions are calculated from the resulting force acting on the respective masses. First x_2 is determined, followed by x_1 and finally x_3. Details of this calculation are given in appendix B.1.

The output position of the coupled system without damping is in this case given by x_3. A relation to calculate this position is also calculated in appendix B.1. From that relation for x_3 the partial plant transfer functions can be calculated. First, the plant transfer function from F_{in} to x_3 is given by

$$P_{1,c} = \frac{x_3}{F_{in}} = \frac{d_0}{a_6 s^6 + a_4 s^4 + a_2 s^2} \text{ [m/N]} \tag{5.5}$$

And the partial transfer function from $x_{2^{nd}}$ to x_3 is calculated as

$$P_{2,c} = \frac{x_3}{x_{2^{nd}}} = \frac{b_4 s^4 + b_2 s^2}{a_6 s^6 + a_4 s^4 + a_2 s^2} \tag{5.6}$$

For both transfer functions, the coefficients are calculated as

$$\begin{aligned} a_6 &= m_{1,c} m_2 m_3 \\ a_4 &= (m_{1,c} + m_2)\, m_3 c_{12} + (m_{1,c} + m_3)\, m_2 c_{13} \\ a_2 &= c_{12} c_{13}\, (m_{1,c} + m_2 + m_3) \end{aligned} \tag{5.7}$$

$$\begin{aligned} b_4 &= m_{1,c} m_2 c_{13} \\ b_2 &= c_{12} c_{13} \left(m_{1,c} + m_2 \right) \\ d_0 &= c_{12} c_{13} \end{aligned}$$

In section 5.4, these transfer functions are compared with the partial transfer functions of the decoupled model.

5.3 Partial plant transfer functions of decoupled model

In this section the partial plant transfer functions from the inputs F_{in}, $x_{2^{nd}}$ to output position of the decoupled system, x_{out}, is presented. The system is shown in figure 5.1b. In this case, x_{out} is given as

$$x_{out} = x_1 + x_3 \text{ [m]} \tag{5.8}$$

It was already stated in the introduction to this chapter that in case of the decoupled system, it is assumed that $m_{1,d} = m_{1,c} + m_3$, where m_3 is the load mass to the second-stage actuator.

The plant transfer function of this model is obtain by partly reusing the results from the previous section. Details of calculating x_{out} in case damping is not considered are given in appendix B.2. From that relation for x_{out}, the partial transfer functions can be calculated. First, the plant transfer function from F_{in} to x_{out} is given by

$$P_{1,d} = \frac{x_{out}}{F_{in}} = \frac{d_2 s^2 + d_0}{a_6 s^6 + a_4 s^4 + a_2 s^2} \text{ [m/N]} \tag{5.9}$$

And the partial transfer function from $x_{2^{nd}}$ to x_{out} is calculated as

$$P_{2,d} = \frac{x_{out}}{x_{2^{nd}}} = \frac{b_4 s^4 + b_2 s^2}{a_6 s^6 + a_4 s^4 + a_2 s^2} \tag{5.10}$$

For both transfer functions, the coefficients are calculated as

$$\begin{aligned} a_6 &= m_{1,c} m_2 m_3 + m_3^2 m_2 \\ a_4 &= \left(m_{1,c} + m_2 \right) m_3 c_{12} + \left(m_{1,c} + m_3 \right) m_2 c_{13} + m_3^2 c_{12} \\ a_2 &= c_{12} c_{13} \left(m_{1,c} + m_2 + m_3 \right) \\ b_4 &= m_{1,c} m_2 c_{13} + m_2 m_3 c_{13} \\ b_2 &= c_{12} c_{13} \left(m_{1,c} + m_2 + m_3 \right) \\ d_2 &= m_3 c_{12} \\ d_0 &= c_{12} c_{13} \end{aligned} \tag{5.11}$$

In the next section, these transfer functions are compared with the partial transfer functions of the coupled model.

5.4 Comparing the transfer functions

In the previous two sections, partial transfer functions of two modelling approaches of DSA systems are derived. The question is under which circumstances the decoupled model results in a similar frequency response as the coupled model. In that case can via a relatively simple approach controllers for the DSA system be designed.

First the coefficients in equations (5.5) and (5.6) are compared with the coefficients in equations (5.9) and (5.10). It is evaluated under which circumstances both approaches yield similar coefficients. This analysis is given in section 5.4.1. Next, in section 5.4.2 an approach to determine from the poles and zeros of both models a maximum value for m_3 and a minimum value for c_{13}, in order for decoupling to occur, is sketched.

5.4.1 Comparing coefficients

Comparing the mentioned equations reveals that the coefficients a_6, a_4, b_4 and b_2 differ between the two approaches. It will be shown that the value of m_3 is the main factor for the coefficients to become similar. Furthermore, it will turn out that the maximum value for m_3 under which similarity is obtained is related to both $m_{1,c}$ and m_2. Finally, it should be noted that in the decoupled model a new coefficient d_2 is introduced. As a result, a zero pair is introduced in the partial transfer function from F_{in} to x_{out}. The influence this zero pair has on the similarity of the two models is further discussed in section 5.4.2.

In analyzing the limitations for m_3, first a_6 is considered. In this term $m_3^2 m_2$ is introduced in the decoupled model. In order to be able to neglect this term, its value should be much smaller than the remainder of a_6, thus

$$m_3^2 m_2 \ll m_{1,c} m_2 m_3 \rightarrow m_3 \ll m_{1,c} \tag{5.12}$$

Furthermore, it is concluded that in the decoupled model in a_4 the term $m_3^2 c_{12}$ is introduced. Following the same line of reasoning as before, this term should also become much smaller than the remaining terms of this coefficient. Thus

$$m_3^2 c_{12} \ll (m_2 m_3 + m_{1,c} m_3)\, c_{12} + (m_{1,c} m_2 + m_2 m_3)\, c_{13} \tag{5.13}$$

Now from the fact that $c_{12}, c_{13} > 0$, $m_i > 0$, it follows immediately that if equation (5.12) is satisfied, then equation (5.13) is also met.

Now continuing with the coefficients in the numerator of the plant transfer function, it was concluded that in b_4 the term $m_2 m_3 c_{13}$ is introduced. This term should become much smaller than $m_{1,c} m_2 c_{13}$, thus

$$m_2 m_3 c_{13} \ll m_{1,c} m_2 c_{13} \rightarrow m_3 \ll m_{1,c} \tag{5.14}$$

which puts the same restriction on m_3 as (5.12). Finally the difference in b_2 between the two models is analyzed. It can be concluded that in the decoupled model the term $m_3 c_{12} c_{13}$ is introduced, thus

$$m_3 c_{12} c_{13} \ll c_{12} c_{13} (m_{1,c} + m_2) \rightarrow m_3 \ll m_{1,c} + m_2 \tag{5.15}$$

which also results in the same restriction as (5.12).

It can thus be concluded that in order to use the decoupled model, $m_3 \ll m_{1,c}$ should be satisfied. However, it should be made explicit how much smaller m_3 should be compared with $m_{1,c}$. This is worked out in the next section. In this section it is also analyzed what the stiffness of the micro-actuator should minimally be in order for the two models to become similar.

5.4.2 Pole-zero analysis

A second means to compare the models is to compare the poles and zeros of the two models with each other. In the previous section it was already concluded that in the decoupled model a zero pair was introduced in the term for F_{in}. It will be shown in this section, that this zero pair puts limitations on the value of c_{13}, for a known value of m_3. However, before the limitation on c_{13} is determined, first the maximum value for m_3 for using the decoupled model is determined.

Decoupled model

First, the poles and zeros of the plant transfer function in the decoupled model are determined. From these poles and zeros the frequency response of the system can be determined. Furthermore, the poles and zeros of the decoupled model are compared with the coupled model and it is then investigated under which circumstances these yield the same numerical values. The poles and zeros of the partial plant transfer functions (5.9) and (5.10) are given in appendix B.2.

From these poles and zeros it can easily be concluded that the zero pair that is introduced in the decoupled model, $z_{5,6}$, cancels $p_{5,6}$. This can explained as follows. The pole pair $p_{5,6}$ represents the resonance frequency of the loaded actuator. In the transfer function of the decoupled model, the plant transfer function is a summation of the output of the two subsystems. Thus resonances of the second-stage actuator are not observed in the frequency response of the first-stage actuator and vice versa. This is exactly what the zero pair does, it cancels exactly the

Case 1		
$m_{1,c}$	3.82	[kg]
m_2	3.33	[kg]
m_3	$16 \cdot 10^{-3}$	[kg]
c_{12}	$21.4 \cdot 10^6$	[N/m]
c_{13}	$115 \cdot 10^6$	[N/m]

Table 5.1: Model parameters of the FCM and the second-stage actuator for the decoupled model.

Case 1			Case 2		
m_3	0.23	[kg]	m_3	$16 \cdot 10^{-3}$	[kg]
$m_{1,c}$	3.61	[kg]	$m_{1,c}$	3.82	[kg]
m_2	3.33	[kg]	m_2	3.33	[kg]
c_{12}	$21.4 \cdot 10^6$	[N/m]	c_{12}	$21.4 \cdot 10^6$	[N/m]
c_{13}	$115 \cdot 10^6$	[N/m]	c_{13}	$115 \cdot 10^6$	[N/m]

Table 5.2: Model parameters of the FCM and the second-stage actuator for two simulation cases of the coupled model.

resonance frequency of the second-stage actuator in the transfer function of the first-stage actuator. The same line of reasoning can be applied to $z_{3,4}$ and $p_{3,4}$, but then it should be concluded that the resonance of the second-stage remains.

Using the model parameters of the FCM, Bode plots of the partial transfer functions (5.9) and (5.10) of the decoupled model can be drawn. The magnitude plots of both partial transfer functions are given in figure 5.2. The model parameters for this case are given in table 5.1. From this table it can be concluded that the numerical value for m_3 is chosen equal to $16 \cdot 10^{-3}$ [kg]; it will turn out later in this section that for this value of m_3 both models are comparable.

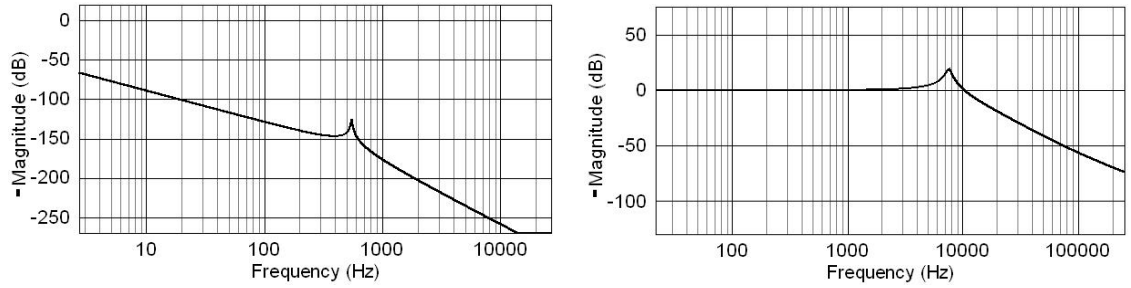

Figure 5.2: Magnitude plots of the partial transfer functions using the decoupled model and the FCM model parameters a) from F_{in} to x_{out} and b) from $x_{2^{nd}}$ to x_{out}. Note the difference in scales between the two figures.

Coupled model without damping

In contrast to the poles and zeros of the decoupled model, the poles and zeros of the coupled model cannot be given as insightful relations. The poles and zeros of the coupled model are given in terms of the coefficients in the partial plant transfer functions (5.5) and (5.6) in appendix B.1. However, since these relations are not insightful, the poles and zeros of the coupled model are analyzed using the FCM model parameters. In order to analyze the effect of the second-stage parameters on the poles and zeros of the plant model, the numerical values for m_3 and c_{13} are varied. It should be kept in mind that $m_{1,c} = m_{ce} - m_3 = 3.84 - m_3$.

First, the transfer function from $x_{2^{nd}}$ to x_3 is investigated for the parameters for case 1 in table 5.2. The

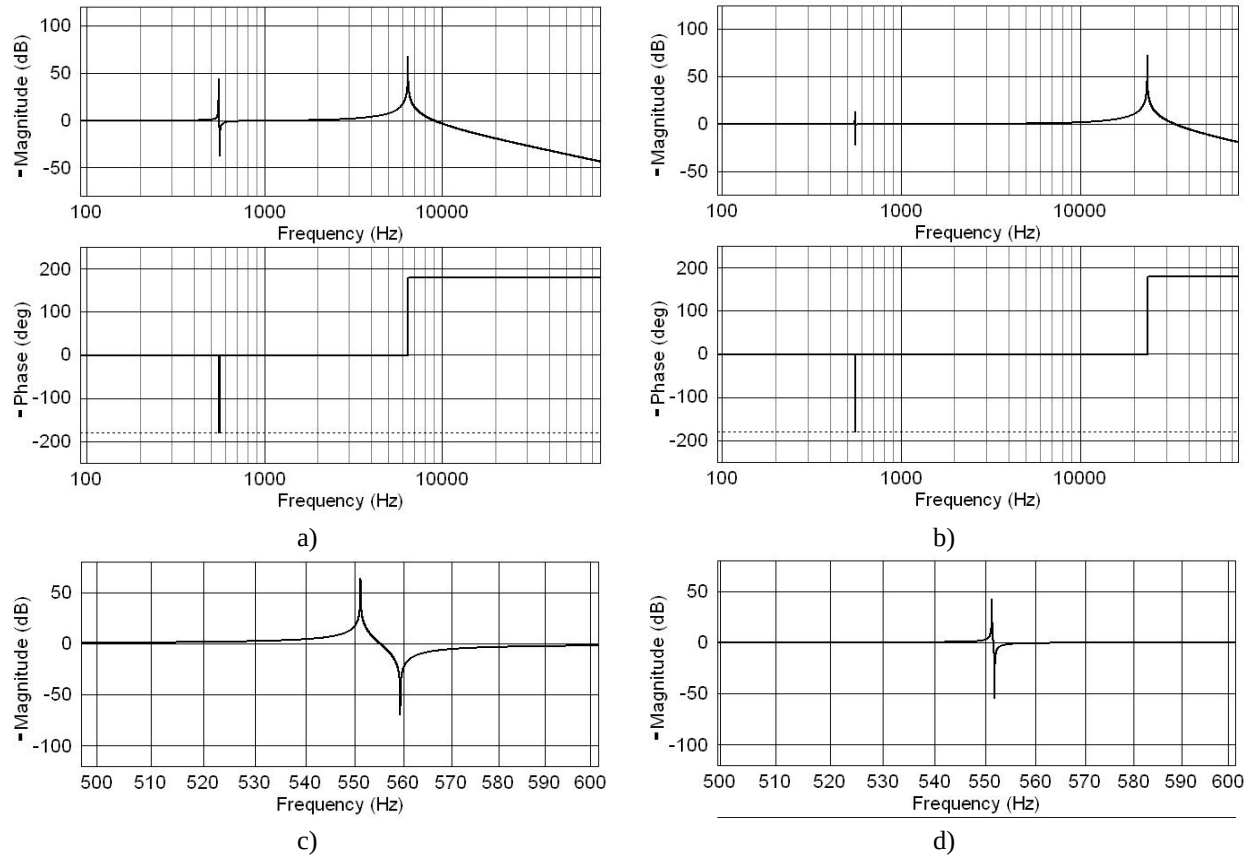

Figure 5.3: Bode plots of the transfer from $x_{2^{nd}}$ to x_3 in the coupled model for a) $m_3 = 0.230$ [kg] with lowest resonance frequency 542 [Hz], anti-resonance frequency 559.4 [Hz], b) $m_3 = 16 \cdot 10^{-3}$ [kg] with lowest resonance frequency 550.7 [Hz], anti-resonance frequency 551.8 [Hz], c) zoom in on the resonance and anti-resonance frequencies of the magnitude plot in figure a) and finally, d) zoom in on the resonance and anti-resonance frequencies of of the magnitude plot in figure b). In case of decoupling, figures a) and b) should resemble figure 5.2b.

resulting Bode plot of this transfer is shown in figure 5.3a. Then the same transfer function is drawn, using the parameters for case 2 in table 5.2. In this latter case, the mass m_3 is reduced to $16 \cdot 10^{-3}$ [kg]. The resulting Bode plot is shown in figure 5.3b. Furthermore, figures 5.3c and d zoom in on the frequency range around the resonance and anti-resonance frequencies in order to see how these change for varying values of m_3. From these figures can be concluded that for decreasing values of m_3 the anti-resonance and resonance shift towards each other. As a result, for very small values of m_3, the resonance and anti-resonance are very close to each other. When there is no damping in the system, the resonance and anti-resonance cancel each other when $m_3 = 0$. Consequently, the frequency response of the coupled and decoupled system to $x_{2^{nd}}$ are identical, as was desired. However, in this specific case damping is assumed to be absent, which is clearly not the case in practice. In the following will be shown that adding relative damping to the poles and zeros of the system results in larger values of m_3 for the responses to be comparable.

Coupled model with damping

First, a rule of thumb is given in order to determine whether damped pole-zero pairs cancel each other. This rule of thumb assumes that the pole-zero pairs are damped with the same relative damping ζ. In that case, it is defined that the pole-zero pairs cancel each other, when the maximum gain at the resonance and anti-resonance frequency deviate 5 % or $\pm$ 0.43 [dB] from the gain at low frequencies. It is shown in figure 5.4, that in this case the maximum phase deviation is $5.5°$. For the case in which the relative damping, ζ, is equal to 0.01, a frequency response is

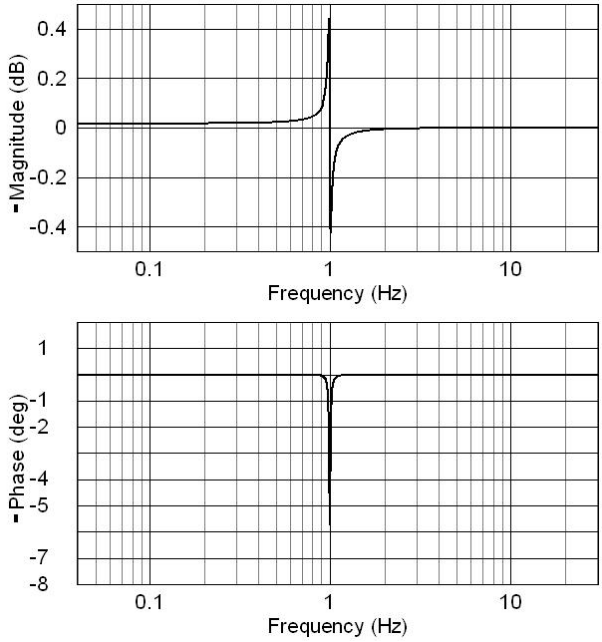

Figure 5.4: Frequency response of a RA-system with relative damping ζ equal to 0.01. In this case the pole-zero pairs cancel each other according to the given rule of thumb. The resonance frequency in this case is equal to 1.0 [Hz], the anti-resonance is 1.001 [Hz].

given in figure 5.4. In that case the resonance frequency is 1.0 [Hz] and the anti-resonance is found at 1.001 [Hz]. It can be concluded that in this case the response remains within the above limitations. For three values of ζ, $\zeta = 0.01, 0.02, 0.05$, it is determined how far the imaginary part of the zero-pair (anti-resonance) can be placed with respect to the imaginary part of the pole-pair (resonance) in order to remain within the given limitations. It is revealed that

$$\Im(z) = \left(1 + \frac{1}{10}\zeta\right) \cdot \Im(p) \tag{5.16}$$

where z comprises the zero-pair, p the pole-pair, ζ the relative damping and $\Im(\cdot)$ calculates the imaginary part of the expression between the brackets. Consequently, a relation can be derived, which gives the maximum value for m_3 for a certain value of ζ and the model parameters. From section 5.4.1 it is already known, that the decoupled model is valid if $m_3 \ll m_{1,c}$. Furthermore, it is seen that for small values of m_3 the lowest resonance frequency of the coupled model is equal to the lowest resonance frequency of the decoupled model. Using this observation, $m_{3,max}$ can be solved from the following relation

$$\Im(z_{3,4,coupled}) = \left(1 + \frac{1}{10}\zeta\right) \Im(p_{3,4,decoupled}) \tag{5.17}$$

where $\Im(p_{3,4,decoupled})$ is the imaginary part of the pole-pair that gives rise to the lowest resonance frequency of the decoupled model and $\Im(z_{3,4,coupled})$ the imaginary part of the zero-pair that gives rise to the lowest anti-resonance frequency of the coupled model. Expressions for $p_{3,4,decoupled}$ and $z_{3,4,coupled}$ are given in appendix B.

Solving equation (5.17) for m_3 results in the desired relation for determining the maximum value of m_3, for which the decoupled model can be used for the quantified maximum deviations:

$$m_{3,max} = \frac{m_{1,d}\left(\zeta^2 + 20\zeta\right)}{\zeta^2 + 20\zeta + 100\frac{m_2}{m}} \text{ [kg]} \tag{5.18}$$

where m is the total mass to be displaced by the first-stage actuator, i.e. $m = m_{1,d} + m_2$. From equation (5.18), it can easily be concluded that in case $\zeta = 0$, $m_{3,max} = 0$ as was indicated before.

Apart from the previous approximated approach to determine $m_{3,max}$, also the exact solution is determined. In this case $m_{3,max}$ is calculated from writing out (compare with equation (5.17)

$$\Im(z_{3,4,coupled}) = \left(1 + \frac{1}{10}\zeta\right) \Im(p_{3,4,coupled}) \tag{5.19}$$

and solve for m_3. It has turned out that in this case c_{13}, the stiffness of the piezo-actuator, should be known in order to obtain a numerical value for $m_{3,max}$. This is a disadvantage of this approach, since a minimum value for c_{13} is given hereafter. However, using the stiffness of the two piezo-actuators given in appendix A, numerical values for $m_{3,max}$ are determined using both the exact and approximated solution. Subsequently, the results of both solutions are compared with each other. It is revealed, that differences between the numerical values for $m_{3,max}$ using either of the two solutions are in the order of $1 \cdot 10^{-4}$ and less. From this analysis it can therefore be concluded, that the approximated solution for determining $m_{3,max}$ in equation (5.18) results in a sufficiently accurate calculation of $m_{3,max}$, independent of the value of c_{13}.

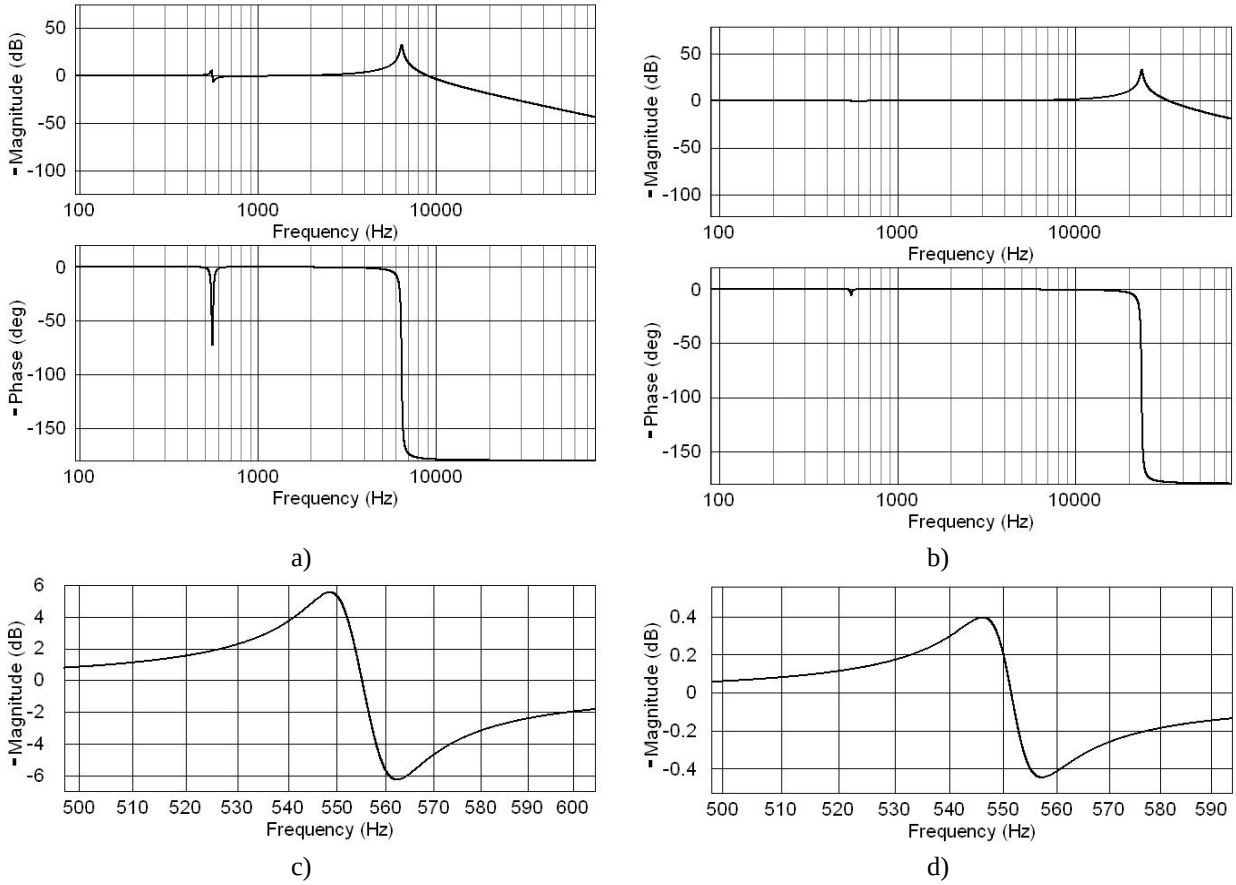

Figure 5.5: Bode plots of the transfer from $x_{2^{nd}}$ to x_3 in the coupled model when all poles and zeros are lightly damped (1%), for a) $m_3 = 0.230$ [kg], b) $m_3 = 16 \cdot 10^{-3}$ [kg], c) zooming in on the frequency range around the resonance and anti-resonance frequencies of the magnitude plot in figure a) and finally d) zooming in on the frequency range around the resonance and anti-resonance frequencies in the magnitude plot of figure b). Note the difference in scales between the latter two figures.

Finally, substituting the model parameters of the FCM in equation (5.18), the maximum value for m_3 is determined. For the current case, where $\zeta = 0.01$, it is calculated that in case $m_3 < 16 \cdot 10^{-3}$ [kg] decoupling occurs and consequently, the decoupled model of the DSA system can be used for controller design. This conclusion is

supported by plotting the magnitude plots of the transfer from $x_{2^{nd}}$ to x_3, while damping is added to the model. This is done for the model parameters from table 5.2. The resulting Bode plots are shown in figure 5.5. Especially zooming in on the frequency range around the resonance and anti-resonance frequencies show the difference in magnitude response for the two values of m_3.

Comparing figures 5.5c and d leads to the conclusion that in this case, when damping is added to the system, the resonance and anti-resonance in the lower frequency range almost cancel each other when $m_3 = 16 \cdot 10^{-3}$ [kg]. In this case the low-frequency gain is equal to -0.0 [dB], the maximum resonance magnitude equals 0.4 [dB], whereas the magnitude of the anti-resonance equals -0.42 [dB]. The transfer function differs thus not more than 5% from its initial value. Finally, also the phase of the transfer function is analyzed. The plant transfer function of the piezo-actuator has a phase almost equal to zero before it drops to -180° around the resonance frequency. When $m_3 = 16 \cdot 10^{-3}$ [kg], the phase has a minimum value of -4°, compared to -16° when $m_3 = 0.23$ [kg]. It can be concluded that in case $m_3 = 16 \cdot 10^{-3}$ [kg], or smaller, decoupling of the two stages occurs.

Minimum required stiffness of micro-actuator

As was already stated in the introduction to this section, a limitation on the value of c_{13}, in order to be able to use the decoupled model, can be drawn from the maximum value for m_3. Whereas this maximum value for m_3 was drawn from making the transfer $\frac{x_3}{x_{2^{nd}}}$ equal to $\frac{x_{out}}{x_{2^{nd}}}$, deriving the minimum value for c_{13} focusses on making the remaining partial transfer functions equal to each other.

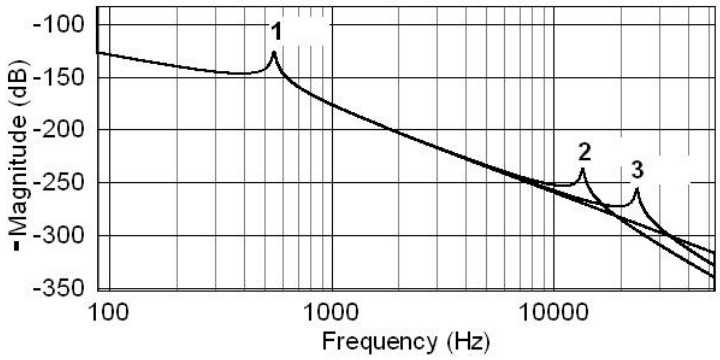

Figure 5.6: Magnitude plot of 1) the decoupled model with transfer function $\frac{x_{out}}{F_{in}}$. Furthermore, the coupled model with transfer function $\frac{x_3}{F_{in}}$ is denoted as 2) with $c_{13} = 115 \cdot 10^6$ [N/m] and as 3) with $c_{13} = 353 \cdot 10^6$ [N/m]. In all cases $x_{2^{nd}} = 0$ and in the latter two cases $m_3 = 16 \cdot 10^{-3}$ [kg].

First, the magnitude of the transfer function $\frac{x_{out}}{F_{in}}$ of the decoupled model is plotted, using the model parameters from table 5.2. This transfer function is in figure 5.6 indicated with '1'. It can be seen that this resonance is independent of m_3. Consequently, the magnitude plot of the transfer function $\frac{x_3}{F_{in}}$ for the model parameters for case 2 in table 5.2 is shown in figure 5.6 and is marked with '2'. It can be seen that in this case, the first resonance frequency of the decoupled model coincides with the first resonance frequency of the coupled model. Also, the existence of a second resonance is observed in the high frequency range.

Finally, from the previous parameters, only the stiffness c_{13} of the piezo-actuator is increased, in order to visualize the effect on the transfer function. In this case, the value for c_{13} is increased from $115 \cdot 10^6$ [N/m] to $353 \cdot 10^6$ [N/m], according to appendix A. The resulting transfer function is shown in figure 5.6 and is marked with '3'. It can again be concluded that the first resonance coincides with that of the coupled model. However, due to the higher stiffness of the piezo-actuator, the second resonance is at a higher frequency.

From the above, it can be concluded that the stiffer the piezo-actuator is, the further the second-resonance frequency is separated from the first resonance. As a consequence, the frequency response of the decoupled model resembles the response of the coupled model better. As a rule of thumb, it is suggested that the stiffness of the piezo-actuator in combination with the load mass should be such that the second resonance is at least 10 times

higher in frequency than the first resonance. In this case, it can be concluded that the frequency response of both models is similar.

5.5 Conclusions

Previously, it has been determined for which values of the second-stage parameters c_{13} and m_3 the frequency responses of the coupled and decoupled model are similar. It turned out that it was necessary to assume damping in the model of the first-stage actuator in order to come up with a non-zero value for the maximum value of m_3 for which decoupling occurs. For that case a definition was introduced that defines constraints on the maximum deviation for the maximum and minimum gain of the resonance frequency and the anti-resonance frequency respectively. Using this definition, $m_{3,max}$ can be calculated by equation (5.18). Using that value for $m_{3,max}$, the influence of the micro-actuator's stiffness on the frequency response was investigated. It was seen that in this case a resonance in the transfer from F_{in} to x_3 was introduced. As a rule of thumb, it was stated that this resonance should be 10x higher in frequency than the resonance of the first-stage actuator, in order for the frequency response of the coupled and the decoupled model to be similar.

Application of the FCM parameters has shown to result in a relatively small value for $m_{3,max}$. In practice, it is not likely, that a location in the PM of the FCM can be found, where a mass of $16 \cdot 10^{-3}$ [kg] can be displaced and to which a second-stage actuator can be rigidly attached. It is therefore not possible to assume decoupling in the DSA FCM. However, it is interesting to check whether the controller settings that are derived based on the decoupled model result in a stable controlled system of the coupled model. This analysis is amongst others worked out in the next chapter.

Chapter 6

Evaluating bandwidth for various sensor locations

6.1 Introduction

In the previous chapters, models of both actuators and a controller for the piezo-actuator are developed. Furthermore, in the previous chapter attention was paid to the topic of decoupling the two stages. It was shown in that chapter, that under certain circumstances the system can be assumed to be decoupled. However, using the model parameters of the FCM, it was concluded that the second-stage actuator should displace a very small mass only in order for decoupling to occur.

In this chapter, for both the decoupled and coupled model, regardless of the previous findings, sensor configurations are determined. Subsequently, these sensor configurations are evaluated in terms of *closed-loop bandwidth* and *sensitivity bandwidth*. In this case, *closed-loop bandwidth* is defined as the lowest frequency at which the magnitude of the closed-loop transfer crosses the -3dB line from above. Using this definition of bandwidth, it can be determined up to which frequency the output of the system is able to follow the applied reference signal. Furthermore, *sensitivity bandwidth* is defined as the lowest frequency at which the magnitude of the sensitivity function crosses the 0dB line from below. Using this definition of bandwidth, it can be determined up to which frequency output disturbances can be suppressed by the controller.

However, before these bandwidths are determined, first the stability and stability margins of the closed-loop system are determined. It is chosen to evaluate stability using the closed-loop transfer of the system, since for controlling the first-stage actuator the PD-controller from Coelingh (2000) is used. One of the inputs to this controller is a measurement of the velocity of the first actuator. According to Coelingh (2000), a disadvantage of this controller type is that it cannot be described by a single loop transfer function. Consequently, we motivate for determining the stability of the closed-loop system by evaluating (Skogestad and Postlethwaite, 1996)

$$M_s = max|S(s)| \leq 6 \text{ [dB]} \tag{6.1}$$

$$M_t = max|T(s)| \leq 2 \text{ [dB]} \tag{6.2}$$

where $S(s)$ is the sensitivity function and $T(s)$ the closed-loop transfer function. According to these definitions, in case M_s is known, the stability margins of the closed-loop system are guaranteed as (Skogestad and Postlethwaite, 1996)

$$GM = \frac{M_s}{M_s - 1} \text{ [dB]} \tag{6.3}$$

$$PM = 2 \arcsin\left(\frac{1}{2M_s}\right) \text{ [rad]} \tag{6.4}$$

In case M_t is known, the stability margins are guaranteed as (Skogestad and Postlethwaite, 1996)

$$GM = 1 + \frac{1}{M_t} \text{ [dB]} \tag{6.5}$$

$$PM = 2\arcsin\left(\frac{1}{M_t}\right) \text{ [rad]} \tag{6.6}$$

In these relations, GM denotes the gain margin and PM the phase margin. The definitions of stability given in equations (6.1) and (6.2) are especially of interest in section 6.4. In this section, the SISO-controllers designed on basis of the decoupled models are applied to the coupled model. Subsequently, it is investigated under which circumstances this results in a stable system that also satisfies the stability margins (6.1) and (6.2). After having stabilized the closed-loop system, both the closed-loop bandwidth and the sensitivity bandwidth are determined.

Furthermore, in this chapter it is assumed that the bandwidth of the sensors does not put limitations on the bandwidth that can be achieved by the DSA system. Also, the amplitude of the signals applied to the second-stage controller, is such that the output voltage of the controller does not exceed the maximum operating voltage of the piezo-actuator. Hence, linear analysis of the second-stage controller can be applied in determining the relevant transfer functions. Finally, as in the previous section, the gain $d_{U,x}$ of the piezo-actuator model is not drawn explicitly in the coming figures, but is assumed to be present in the submodel *MA-controller*.

First, in section 6.2 both definitions of bandwidth are applied to the single-stage actuated system. The results are used for benchmarking; in section 6.3 the bandwidth of two controller designs using the decoupled model is derived. A similar analysis is carried out in section 6.4 where the bandwidth of the system resulting from designs using the coupled model is determined, after having stabilized the closed-loop system. Finally, in section 6.5 conclusions on the developed and analyzed sensor configurations are drawn.

6.2 Single-stage actuation

From the introduction to this chapter, it has become clear that in order to judge the bandwidth increase of the DSA system, the bandwidth of the single-stage actuated system should be known. For the single-stage actuated system, the bandwidth is determined for the sensor configuration shown in figure 6.1a. This analysis is worked out in section 6.2.1. Furthermore, in figure 6.1b can be seen that a second sensor configuration for controlling the first-stage of the FCM is possible. In section 6.2.2, it is briefly discussed that this setup is not suitable for the DSA FCM.

6.2.1 Measure end-effector position and actuator velocity

For controlling the first-stage actuator, the PD-controller structure from Coelingh (2000) is used. This structure is shown in figure 6.2. This PD-controller is the implementation of submodel *PD-controller* in figure 6.1. It can be seen that the proportional gain K_p is applied to the *positional error*, i.e. the difference between the measured position and the reference position. Furthermore, the derivative gain K_d is applied to the measured *velocity* of the first actuator, i.e. $\dot{x}_2$ is measured. The PD-controller is thus set by the parameters K_p and K_d. These parameters are calculated as (Coelingh, 2000)

$$K_p = (m_1 + m_2) \cdot (\Omega_p \omega_{ar})^2 \tag{6.7}$$
$$K_d = (m_1 + m_2) \cdot \Omega_d \omega_r \tag{6.8}$$

where Ω_p and Ω_d are the optimal controller settings from Coelingh (2000) and ω_{ar}, ω_r are respectively the anti-resonance and resonance frequency of the plant. The optimal controller settings vary between the various *concepts* that are given in Coelingh (2000). The concepts are characterized by the type of frequency response that results of the combination of the plant model and sensor configuration. For the combination in figure 6.1 it can be concluded from Coelingh (2000) that concept AR-R applies.

For this concept, optimal controller settings Ω_p and Ω_d are given in the same reference. It should however be checked whether these optimal controller settings can be directly applied or not; the optimal controller settings are valid for certain values of the so-called frequency ratio ρ. According to Coelingh (2000) ρ is calculated as

$$\rho = \left(\frac{\omega_{ar}}{\omega_r}\right)^2 \tag{6.9}$$

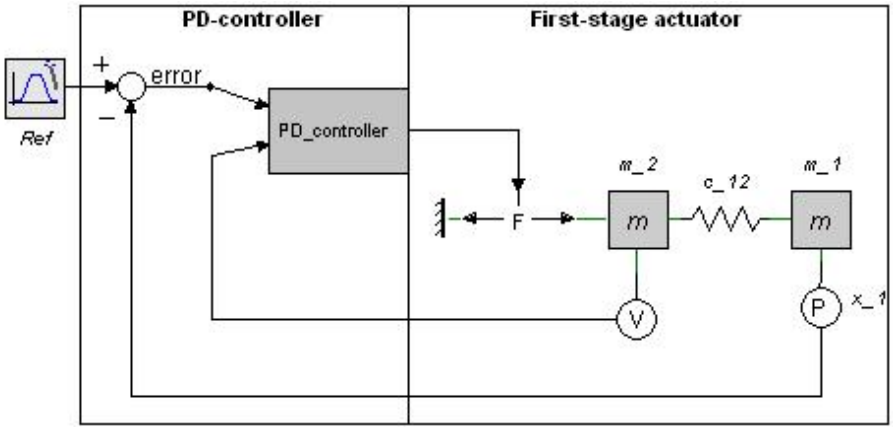

a)

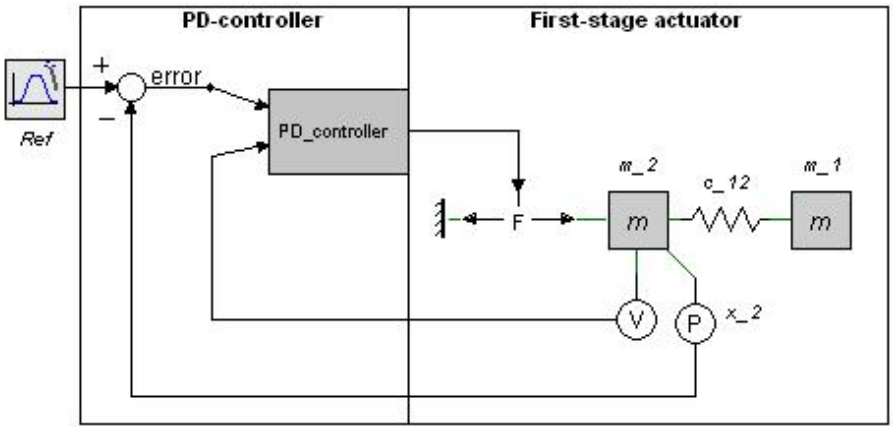

b)

Figure 6.1: Sensor configuration for controlling the output position of the first-stage actuator by a) measuring x_1 and $\dot{x}_2$, b) measuring x_2 and $\dot{x}_2$. The latter approach is not suitable for implementation in a DSA system.

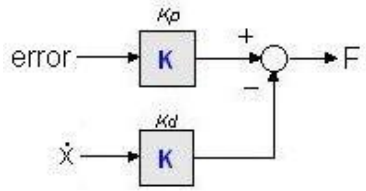

Figure 6.2: PD-controller structure for the first-stage actuator (Coelingh, 2000).

where ω_{ar} and ω_r are calculated as

$$\omega_{ar} = \sqrt{\frac{c_{12}}{m_1}} \text{ [rad/s]} \tag{6.10}$$

$$\omega_r = \sqrt{\frac{c_{12}}{m_1} + \frac{c_{12}}{m_2}} \text{ [rad/s]} \tag{6.11}$$

Now using the numerical values of the plant model from chapter 3, it revealed that $\omega_{ar} = 3464$ [rad/s] and $\omega_r = 2360$ [rad/s]. Subsequently, the frequency ratio is determined to be 0.46. Comparing this with Coelingh (2000) leads to the conclusion that the optimal controller settings can be directly applied. Consequently, the

controller gains are calculated as

$$K_p = 1.44 \cdot 10^7 \tag{6.12}$$
$$K_d = 1.19 \cdot 10^4 \tag{6.13}$$

It should be clear at this point, that we are now considering a single-stage actuated system with a resonance frequency of 551 [Hz]. In the following, we determine the bandwidth of this single-stage actuated system, such that we can determine the bandwidth increase, in case of dual-stage actuation, thereafter.

First, the closed-loop transfer function from the reference position x_{ref} to the output position x_1 of this sensor configuration is calculated. This closed-loop transfer function is calculated as

$$H(s) = \frac{x_1}{x_{ref}} = \frac{c_{12}K_p}{m_1 m_2 s^4 + m_1 K_d s^3 + (m_1 + m_2)\, c_{12} s^2 + c_{12} K_d s + c_{12} K_p} \tag{6.14}$$

Substituting the model parameters from chapter 3 and the controller parameters from equation (6.12) and (6.13), a Bode plot of this closed-loop transfer is obtained. This plot is shown in figure 6.3a. From this plot it can be concluded that the -3dB point of the closed-loop transfer is found at 471 [Hz].

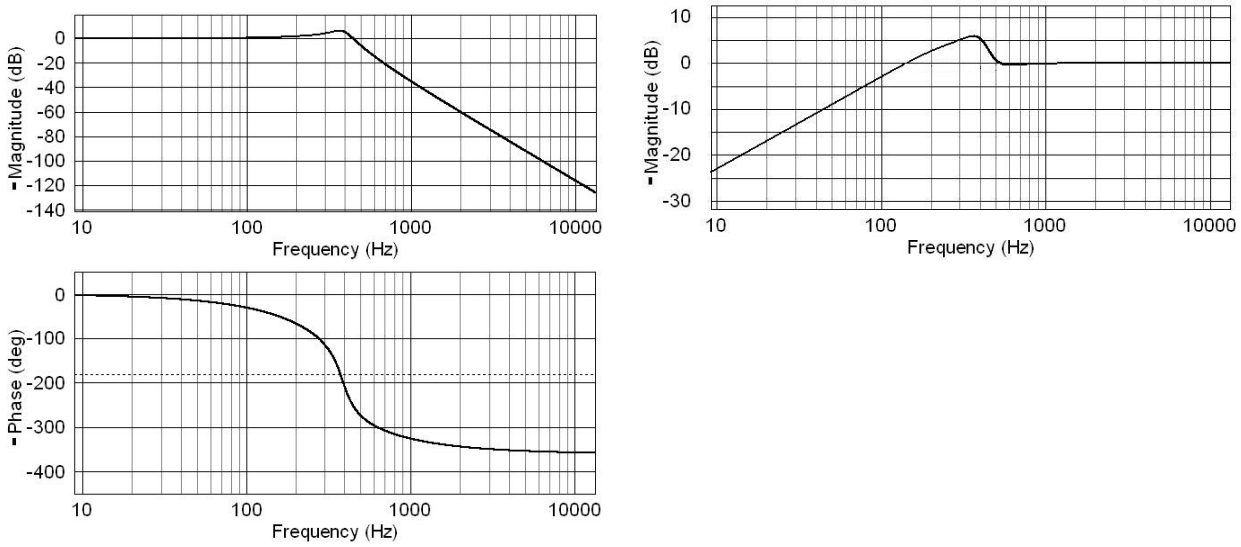

a) b)

Figure 6.3: a) Bode plot of the closed-loop transfer function from equation (6.14) and b) plot of the sensitivity function from equation (6.16).

Subsequently, the sensitivity function of this system is determined. This analysis is performed while $x_{ref} = 0$. The sensitivity function is defined as

$$S(s) = \frac{x_1 + \delta}{\delta} \tag{6.15}$$

where δ is an output position disturbance, which is measured by the position sensor. Consequently, the signal $-(x_1 + \delta)$ is fed to the proportional gain K_p. In appendix C.1, the sensitivity function of this sensor configuration is derived. The resulting sensitivity function is given by

$$S(s) = \frac{m_1 m_2 s^4 + m_1 K_d s^3 + (m_1 + m_2)\, c_{12} s^2 + c_{12} K_d s}{m_1 m_2 s^4 + m_1 K_d s^3 + (m_1 + m_2)\, c_{12} s^2 + c_{12} K_d s + c_{12} K_p} \tag{6.16}$$

Using the model parameters and the controller settings as before, a plot of the sensitivity function can be obtained. It should be noted that in order to obtain $max|S(s)| \leq 6$ [dB], the proportional gain K_p is manually tuned to $1.0 \cdot 10^7$. In this case, $max|S(s)| = 5.9$ [dB]. Consequently, the stability margins, as defined in the introduction to this chapter, are satisfied. The resulting sensitivity plot is shown in figure 6.3b. From this plot it can be concluded that the 0dB line is crossed from below at 140 [Hz].

6.2.2 Measure actuator position and velocity

According to Coelingh (2000), a second sensor configuration can be used for controlling the single-stage actuated FCM. In this sensor configuration, both the position x_2 and the velocity $\dot{x}_2$ of the first actuator are measured. This sensor configuration is shown in figure 6.1b. From this figure it can easily be concluded that this sensor configuration does not give information about the carriage position m_1. However, in order to apply relevant error signals to the micro-actuator controller in case of dual-stage actuation, this position should be known. It is therefore concluded, that this sensor configuration is not suitable for dual-stage actuation.

6.3 Sensor configurations using the decoupled model

In this section, three sensor configurations that use the decoupled model from chapter 5 are presented and their closed-loop transfer and sensitivity function are determined. During the research, it has turned out that two of the three suggested sensor configurations resulted in the decoupled control structure. This structure was originally presented in chapter 2 and is for convenience redrawn in figure 6.4b. These sensor configurations are presented in section 6.3.2. Furthermore, of the three suggested sensor configurations, one setup resulted in the parallel control structure. As for the decoupled controller, for convenience this structure is redrawn in figure 6.4a. This latter sensor configuration is first presented in section 6.3.1. Subsequently, in this section the mentioned transfer functions of this sensor configuration are determined.

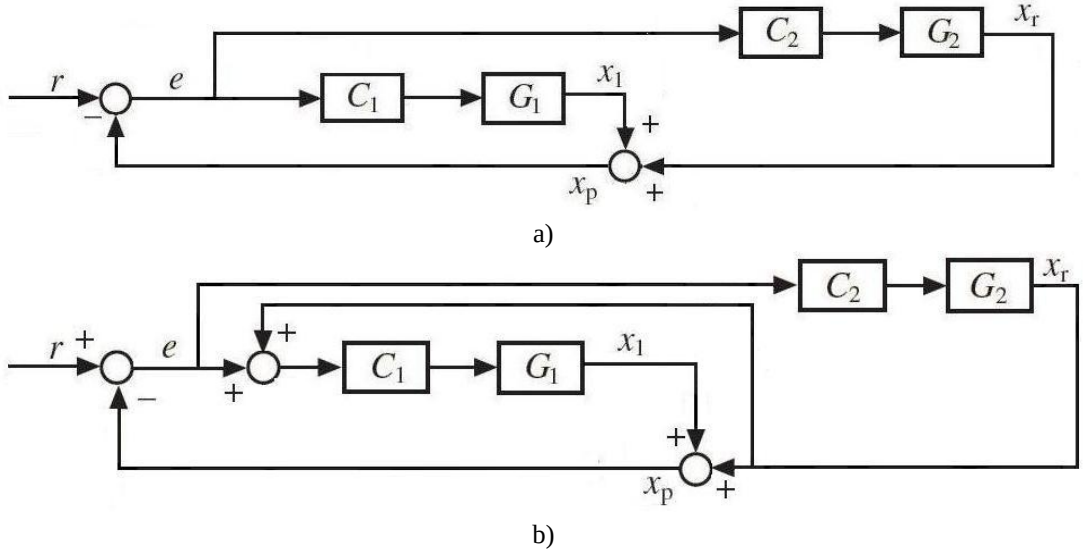

Figure 6.4: Schematic diagram of a) the parallel controlled DSA system and b) the decoupled controlled DSA system. In both figures the decoupled model from chapter 5 is used.

6.3.1 Sensor configuration resulting in parallel control approach

The first sensor configuration that is analyzed for implementation of the DSA system is shown in figure 6.5. In this sensor configuration, the output position of the system is measured. This measurement is used as feedback signal for both the controller of the first-stage and the second-stage actuator. Comparing this figure with figure 6.4a reveals immediately that this sensor configuration is comparable with the parallel control approach.

In practice, the output position of the DSA system can be measured using a laser triangulation system or a camera system. Furthermore, assuming that the movements of the PM are 1 dimensional, summing the measurement of carriage position and piezo-actuator displacement also results in a measurement of th end-effector position. In this case, the position of the carriage can for example be measured by means of a laser triangulation system, a

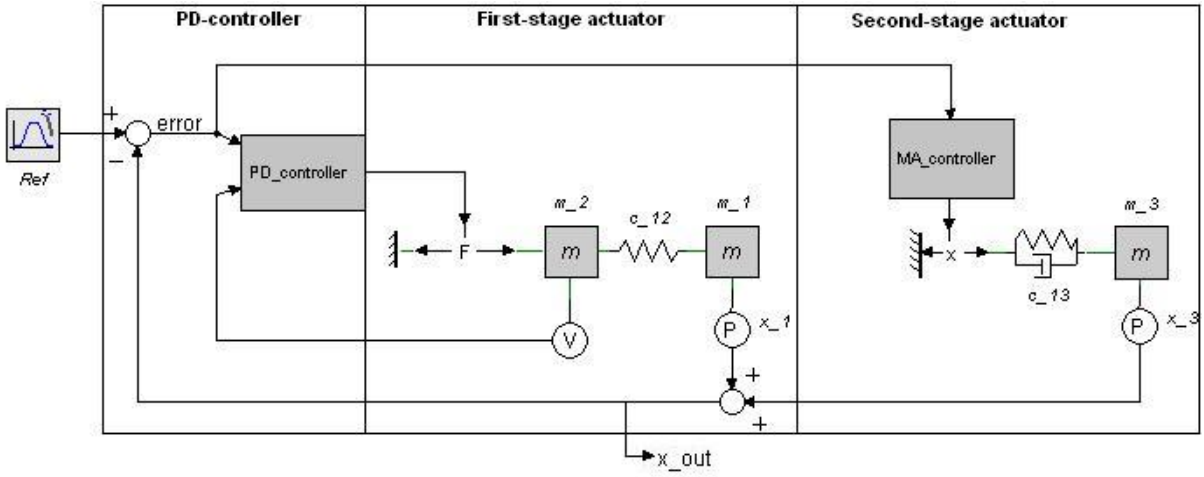

Figure 6.5: Model implementation of the parallel controlled DSA system with end-effector position measurement. This position is obtained by adding the absolute positions of m_1 and m_3 with respect to the respective fixed worlds to each other.

more common approach is to use an optical encoder. The displacement of the piezo-actuator can be measured by means of a capacitative position sensor.

In the following, first the sensitivity function of this sensor configuration is defined and calculated. Then, the closed-loop transfer function is determined. Finally, using the parameters of the FCM model and the derived controller settings, these functions are plotted and the respective bandwidths are determined.

Sensitivity function

In this case, since the output position of the DSA system is measured, the sensitivity function of the DSA system is defined as

$$S(s) = \frac{x_{out} + \delta}{\delta} = \frac{x_1 + x_3 + \delta}{\delta} \tag{6.17}$$

where δ is an output positional disturbance. Using the model presented in figure 6.5, the sensitivity function of this sensor configuration is derived in section D.2. Finally, in equation (D.14) the resulting sensitivity function is given. Due to its complexity this function is not reproduced here.

Closed-loop transfer function

The closed-loop transfer function of the sensor configuration in figure 6.5 is defined as the transfer from the reference position x_{ref} to the output position $x_{out} = x_1 + x_3$, with both feedback loops closed. This closed-loop transfer function is derived in section D.1. The obtained transfer function is given in equation (D.6). Due to its complexity, it is not reproduced here.

Bandwidth

After having derived the closed-loop transfer function and the sensitivity function of this sensor configuration, using the FCM model parameters and the derived controller settings these functions are plotted. In this case, the FCM model parameters for which decoupling of the two stages occurs are used. These model parameters are found as 'Case 2' in table 5.2. Furthermore, the controller settings for the first-stage actuator are given by equations (6.12) and (6.13). Finally, the controller for the second-stage actuator is set according to the parameters in table 4.1, for piezo-actuator P-885.10 and $m_3 = 16 \cdot 10^{-3}$ [kg]. It should be mentioned, that the proportional gain of the second-stage controller is manually adjusted in order to make $max|S(s)| \leq 6$ [dB], such that the controlled

system satisfies the phase and gain margin as stated in the introduction to this chapter. It turned out that increasing τ_i to $3.2 \cdot 10^{-12}$ resulted in $max|S(s)| = 5.9$ [dB].

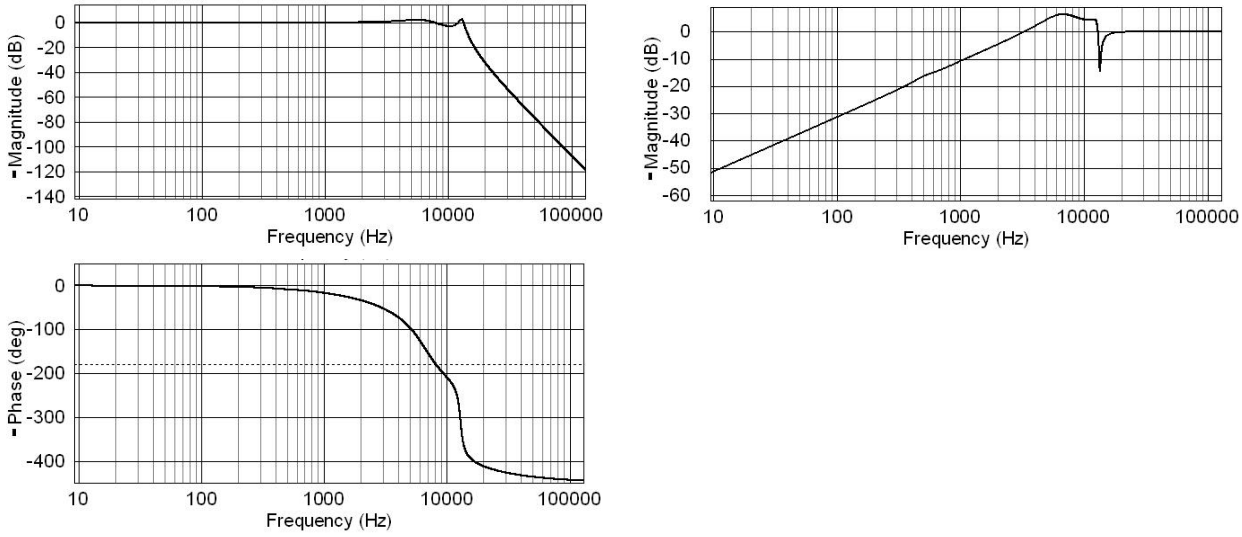

a) b)

Figure 6.6: a) Bode plot of the closed-loop transfer function from equation (E.9) and b) plot of the sensitivity function from equation (D.14) using the model parameters of the FCM and the respective controller settings. Note that in this case τ_i of the second-stage controller is manually adjusted in order to satisfy the stability margins as stated in the introduction to this chapter.

The resulting closed-loop transfer function is plotted in figure 6.6a, whereas the resulting sensitivity function is plotted in figure 6.6b. From these figures it can be concluded that the lowest frequency at which the sensitivity function crosses the 0dB line from below is found at 3155 [Hz]. Furthermore, it is observed that the lowest frequency at which the closed-loop transfer function crosses the -3dB line from above is found at 9049 [Hz].

6.3.2 Sensor configurations resulting in the decoupled control approach

As was already stated in the introduction to this section, two of the three suggested measurements setups in the decoupled model of the DSA FCM result in a decoupled controller. These sensor configurations are shown in figure 6.7. The main difference between the two sensor configurations is found in the position that is measured and used as feedback signal to the first-stage controller.

In figure 6.7a, measurement of the end-effector position is assumed. In this case, the end-effector position is measured and used as feedback signal to the first-stage controller. In practice, the end-effector position can either be measured using a laser triangulation system or camera system. However, under the assumption that movements of the PM are 1 dimensional, summing the measurement of carriage position and piezo-actuator displacement. In that case, the position of the carriage can for example be measured by means of a laser triangulation system. However, a more common approach is to use an optical encoder. The displacement of the piezo-actuator can be measured by means of a capacitative position sensor.

Furthermore, in figure 6.7b it is assumed the position of the carriage is measured and this measurement is used as feedback signal to the first-stage controller. Thereby, it is necessary to measure the piezo-actuator displacement as well, in order to decouple both controllers. This is shown in the following. In this case the previously mentioned sensors for measuring the respective positions apply.

From the previous it can be concluded that for both implementations two sensors are required for implementation of the sensor configuration. In the following of this section, it is first shown that the closed-loop transfer function from the reference position x_{ref} to the output position x_{out}, is for both sensor configurations in figure 6.7 equal to the closed-loop transfer of the model in figure 6.4b. Consequently, the sensitivity function and closed-

loop transfer functions of this controller design approach are presented. Finally, using the FCM parameters and the derived controller settings, the bandwidth of this controller design is determined.

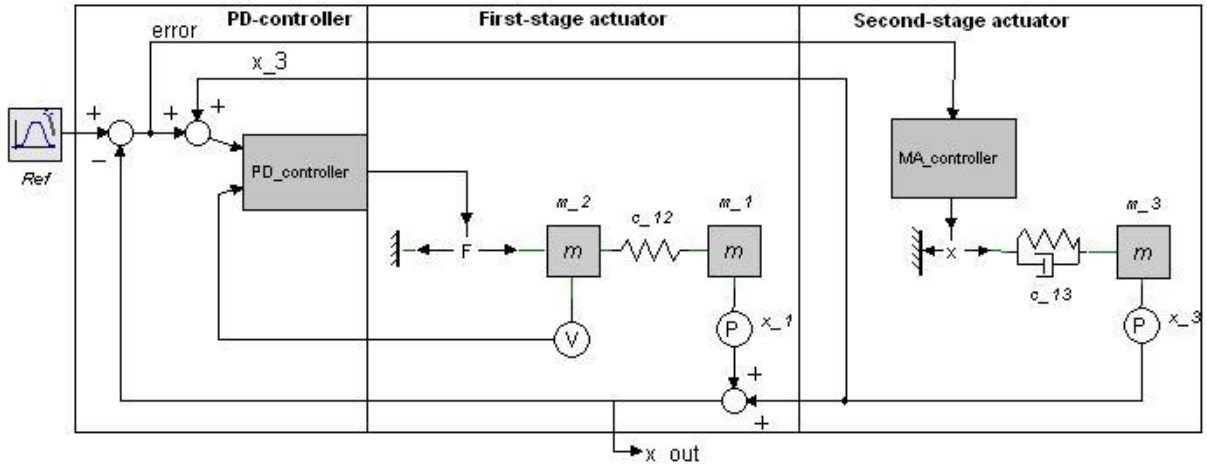

a)

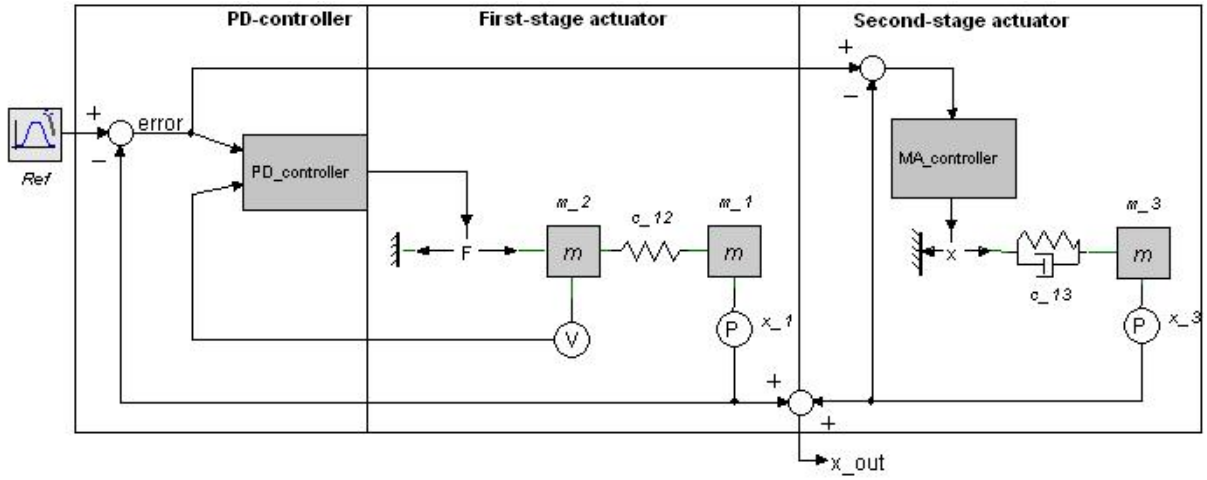

b)

Figure 6.7: Model implementation of a) the decoupled controlled approach DSA system, with end-effector position measurement and b) the decoupled controlled approach DSA system with carriage position measurement. In a) the end-effector position is obtained by adding the absolute positions of both m_1 and m_3 with respect to the respective fixed worlds to each other.

Analyzing closed-loop transfer functions

In analyzing the closed-loop transfer function of the sensor configurations, the controllers of the first-stage and the second-stage actuators in figure 6.7 are respectively denoted as C_1 and C_2, as in figure 6.4b. Furthermore, the plant model of the first-stage is denoted as G_1 and that of the second-stage as G_2.

First, from figure 6.4b it can be concluded that $x_{out} = x_1 + x_r$. Furthermore, the positions x_1 and x_r can be calculated as

$$x_1 = C_1G_1 \cdot (e + x_r) \tag{6.18}$$

$$x_r = C_2G_2 \cdot e \tag{6.19}$$

The first of these equations can be rewritten by substitution of the second equation as

$$x_1 = (C_1G_1 + C_1C_2G_1G_2) \cdot e \tag{6.20}$$

In case the closed-loop frequency response is analyzed, the error e is calculated as $x_{ref} - x_{out}$. Substituting this in the previous relations and solve for x_{out} yields the closed-loop transfer function as

$$H(s) = \frac{x_{out}}{x_{ref}} = \frac{C_1G_1 + C_2G_2 + C_1C_2G_1G_2}{1 + C_1G_1 + C_2G_2 + C_1C_2G_1G_2} \tag{6.21}$$

Now, for the model in figure 6.7a it can easily be seen that this sensor configuration has the same structure as the one in figure 6.4b. The output position of this system is a summation of x_1 and x_3, the positions of the first and second-stage respectively. Furthermore, a measurement of the position x_3 is added to the positional error that is applied to the controller of the first-stage.

It is somewhat more difficult to see the same analogy in the sensor configuration of figure 6.7b. Therefore, the closed-loop transfer function is calculated. As before, it is seen that $x_{out} = x_1 + x_3$. In this case,

$$x_1 = C_1G_1e \tag{6.22}$$

$$x_3 = C_2G_2 \cdot (e - x_3) \tag{6.23}$$

first x_3 should be solved from the latter equation, in order to end-up with a relation for x_3 that can be substituted in the relation for x_{out}. Consequently, the relation $e = x_{ref} - x_1$ should be substituted in both relations in order to obtain the relation for x_{out}. As a consequence, the first relation should then be solved for x_1. Performing these operations yields

$$x_1 = \frac{C_1G_1}{1 + C_1G_1} \cdot x_{ref} \tag{6.24}$$

$$x_3 = \frac{C_2G_2}{1 + C_2G_2} \cdot (x_{ref} - x_1) \tag{6.25}$$

Finally, substituting the relation for x_1 in the relation for x_3, x_{out} is obtained and consequently, the closed-loop transfer is found as

$$H(s) = \frac{x_{out}}{x_{ref}} = \frac{C_1G_1 + C_2G_2 + C_1G_1C_2G_2}{1 + C_1G_1 + C_2G_2 + C_1G_1C_2G_2} \tag{6.26}$$

It can easily be concluded that this closed-loop transfer is equal to the one presented in equation (6.21). Therefore, in figure 6.7 two sensor configurations that result in a decoupled controller are presented. As a consequence, the property that the sensitivity function of this DSA system can be calculated by multiplying the sensitivity functions of the independent control loops can be used in the course of this section.

Sensitivity function

Since from the literature it is known that in case of decoupled control the sensitivity function of the DSA system can be obtained by multiplication of the sensitivity functions of the independent control loops, in appendices C.1 and C.2 the sensitivity functions of both the first and second-stage control loops are derived. The resulting sensitivity functions are given in equations (C.6) and (C.8). Since the decoupled modelling approach is used, in the sensitivity function (C.6), m_1 should be replaced with $m_{1,d}$, as defined in chapter 5.

Since from the partial sensitivity functions it can directly be concluded how parameter variation affects the partial sensitivity function and as a results affects the overall sensitivity function, the overall sensitivity function of the DSA system is not worked out.

Closed-loop transfer function

After having determined the sensitivity function of the decoupled controller approach, the closed-loop transfer function of this approach is determined. It should be noted, that in this case the loop from measuring $\dot{x}_2$ to the PD-controller is taken into account.

In appendix E, the closed-loop transfer function from reference position x_{ref} to output position x_{out} of the sensor configurations in figure 6.7 is derived. It should be noted that for both sensor configurations the same closed-loop transfer results, hence only one derivation is given. The resulting transfer function is given in equation (E.9). Due to its complexity it is not reproduced here.

Bandwidth

In the previous, both the sensitivity function and the closed-loop transfer function are derived in terms of the parameters of the decoupled model. In the previous chapter it has been shown for which parameters of the FCM model decoupling between the two stages occurs. These model parameters are given as 'Case 2' in table 5.1 and are used in this section to plot the sensitivity function and the closed-loop transfer function of this control approach. Furthermore, the numerical values for K_p and K_d from equations (6.7) and (6.8) are used for setting the PD-controller of the first-stage actuator. Finally, the controller for the piezo-actuator is set using the parameters from table 4.1 for PI actuator P885.10 and $m_3 = 16 \cdot 10^{-3}$ [kg]. It should be mentioned that as for the parallel controlled system, the proportional gain of the second-stage controller should be increased to $3.2 \cdot 10^{-12}$ in order to make $max|S(s)| \leq 6$ [dB]. In this case, $max|S(s)| = 5.9$ [dB] and the controlled system satisfies the phase and gain margin as stated in the introduction to this chapter.

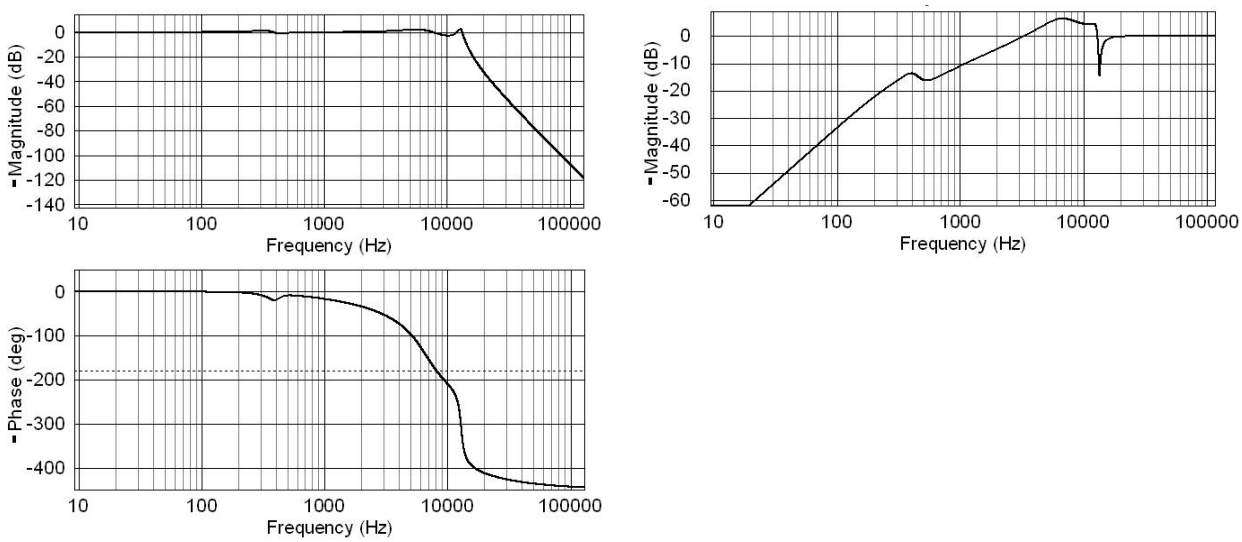

a) b)

Figure 6.8: a) Bode plot of the closed-loop transfer function from equation (E.9) and b) plot of the sensitivity function that results from multiplying equation (C.6) with (C.8) and using the model parameters of the FCM and the respective controller settings. Note that in this case τ_i of the second-stage controller is manually adjusted in order to satisfy the stability margins as stated in the introduction to this chapter.

The closed-loop transfer function is plotted in figure 6.8a. From this plot it can be concluded that the -3dB line is crossed for the first time at 9050 [Hz]. Subsequently, in figure 6.8b the sensitivity function of this controller design is plotted. From this figure it can be concluded that the sensitivity function crosses the 0dB line from below for the first time at 3155 [Hz].

6.4 Sensor configurations using the coupled model

Previously, three sensor configurations have been presented which use the decoupled model of the DSA system as a starting point. In chapter 5 we have concluded that in the case that decoupling occurs, m_3 becomes so small that practical implementation in the FCM is not likely to be possible. As a consequence, it can be concluded that controllers for the DSA system should be designed using MIMO design tools. However, since it is attractive to implement the previously derived, relatively simple controllers to control the DSA system, it is investigated under which circumstances these controllers can be applied to the coupled model and result in a stable controlled system.

For the coupled model, two sensor configurations have been found. The first is shown in figure 6.9. This sensor configuration measures the position of the end-effector and uses this measurement as feedback signal to both the first-stage and second-stage controllers. The idea behind this implementation is similar to the parallel

control approach of the decoupled system. Further details on this sensor configuration are given in section 6.4.1.

The second sensor configuration is given in figure 6.11. It can be seen that in this case the carriage position is measured and used as feedback to the first stage actuator. Furthermore, the displacement of the piezo-actuator is measured and this measurement is used together with the carriage position measurement as input to the second-stage controller. The idea behind this implementation is similar to the decoupled control approach of the decoupled system. Details on this sensor configuration are given in section 6.4.2.

6.4.1 Measure end-effector position

In this section, for the sensor configuration in figure 6.9, it is investigated under which circumstances the controllers can be separately designed, such that the controlled system satisfies the stability margins as stated in the introduction to this chapter. This is done by first calculating the poles of the closed-loop transfer of this system. It is checked whether these are located in the left half plane of the pole-zero plot. If that is the case, then the system is stable. Subsequently, the maximum value of the closed-loop transfer function of the system is determined and it is checked whether this value is smaller than 2 [dB]. If that is the case, the stability margins as defined in the introduction to this chapter are satisfied.

First, the implementation of this sensor configuration is discussed. From figure 6.9, it can be seen that the position of the end-effector is measured and used as feedback signal to both controllers. In practice, the measurement system can be implemented by means of a laser triangulation system or camera system. Furthermore, by measuring both the position of the carriage and the relative displacement of m_3 with respect to $m_{1,c}$ and summing these, the position of the end-effector can also be obtained. However, this implementation can only be considered in case the movements of the system are 1-dimensional. In this case, the position of the carriage can be measured by means of an optical encoder, whereas the displacement of the piezo-actuator can be measured by means of a capacitative displacement sensor.

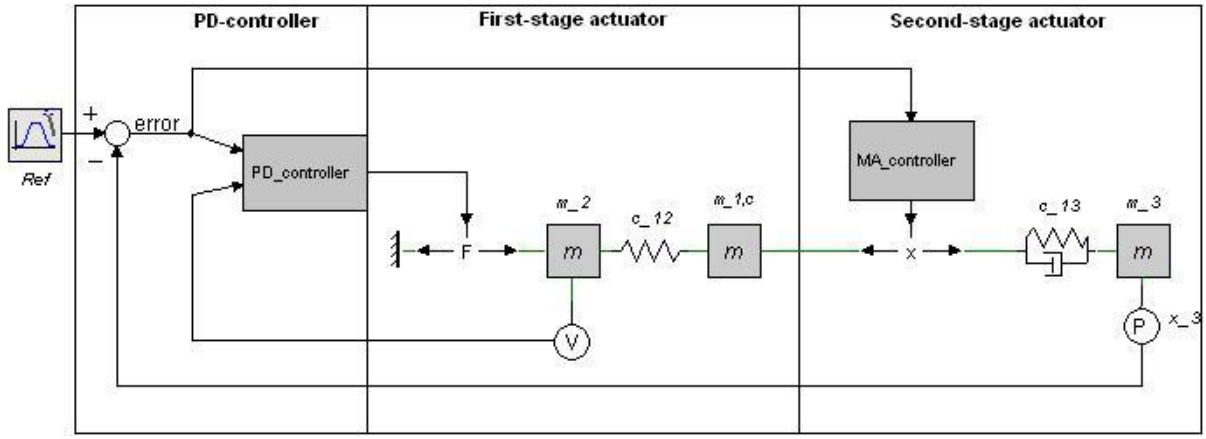

Figure 6.9: Sensor configuration using the coupled model and measuring the position of the end-effector.

Stability

In order to analyze the stability of the system in figure 6.9, for various values of m_3, first the closed-loop transfer function from the reference position x_{ref} to the output of the system $x_{out} = x_3$ is derived in section F.1. From this calculation, the resulting closed-loop transfer function is given in equation (F.7). Furthermore, the sensitivity function of the sensor configuration in figure 6.9 is defined as

$$S(s) = \frac{x_3 + \delta}{\delta} \tag{6.27}$$

where δ is an output positional disturbance that is measured by the sensory system. In section F.2 the sensitivity function of this system is derived. The resulting sensitivity function is given in equation (F.14). Due to their complexity, the closed-loop transfer and the sensitivity function are not reproduced here.

From chapter 5, we know that in case $m_3 = 16 \cdot 10^{-3}$ [kg] decoupling occurs. It is first investigated whether for this value of m_3 the closed-loop transfer and sensitivity function of the coupled model satisfy the stability margins as defined in the introduction to this chapter. Substituting this value for m_3 and the accompanying controller settings in the closed-loop transfer function, reveals that in this case, the closed-loop poles are located in the left half plane of the pole-zero plot. Furthermore, the maximum value of the closed-loop transfer function is 2.4 [dB]; this maximum value is found in the frequency range in which the piezo-actuator operates. Thus increasing τ_i to $4 \cdot 10^{-12}$, which in effect lowers the time-constant of the PI-controller, reduces this peak. The tuning procedure for this case is illustrated in figure 6.10a. It is observed that in this case the maximum value of the closed-loop transfer is equal to 1.8 [dB]. Consequently, the system satisfies the stability margins.

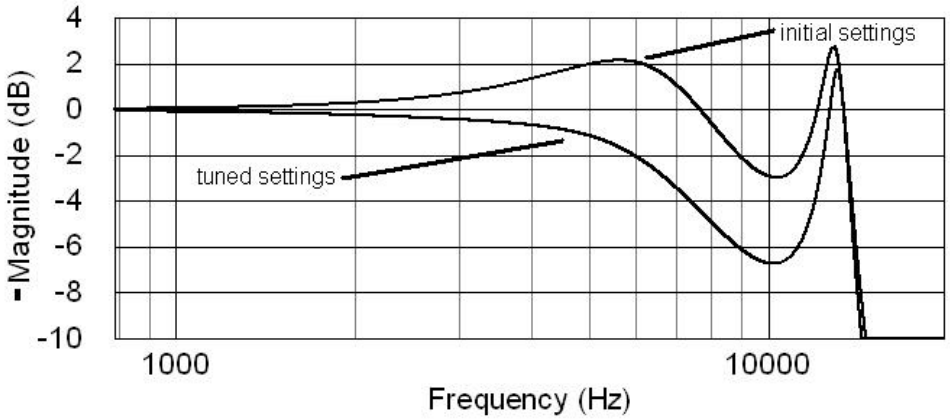

a)

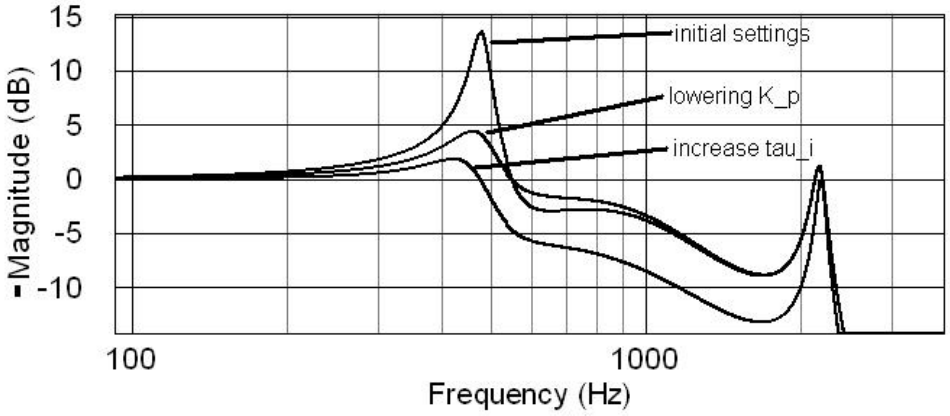

b)

Figure 6.10: Magnitude plots of the closed-loop transfer in case of a) $m_3 = 16 \cdot 10^{-3}$ [kg] and b) $m_3 = 0.73$ [kg]. In figure a), the stability margins are satisfied by increasing τ_i only, since the instability might be caused by the second-stage actuator. In figure b), first K_p is decreased in order to decrease the maximum value of $T(s)$, subsequently τ_i is increased in order to satisfy the stability margins and to maintain a large bandwidth.

Next, m_3 is increased to 0.73 [kg] and the accompanying controller settings for the second-stage controller from table 4.1 are substituted in the closed-loop transfer function. Subsequently, the closed-loop transfer function is plotted, see figure 6.10b. From this plot, the maximum value is determined to be equal to 13.6 [dB]. It is thus concluded that in this case the stability margins are not satisfied. It should be noted that in this case the maximum value of the closed-loop transfer is found in the frequency range in which the first-stage actuator operates. Furthermore, since increasing m_3 results in decreasing $m_{1,c}$, the resonance and anti-resonance frequency of the first-stage actuator shift. This observation gave rise to investigate the closed-loop stability and the stability margins by manually tuning the controller parameters K_p, K_d. Eventually, fine-tuning can be done by increasing τ_i.

$\mathbf{m_3}$ [kg]	$\mathbf{K_p}$	$\tau_\mathbf{i}$	$\mathbf{max}\|\mathbf{T(s)}\|$ [dB]	$\mathbf{f}_{\|\mathbf{T(s)}\|=-\mathbf{3}}$ [dB] [Hz]	$\mathbf{f}_{\|\mathbf{S(s)}\|=\mathbf{0}}$ [dB] [Hz]
$16 \cdot 10^{-3}$	$1.0 \cdot 10^7$	$4.0 \cdot 10^{-12}$	1.8	6707	2800
0.23	$1.0 \cdot 10^7$	$1.3 \cdot 10^{-11}$	2.0	1963	760
0.48	$0.8 \cdot 10^6$	$1.8 \cdot 10^{-11}$	2.0	1227	433
0.73	$0.6 \cdot 10^6$	$2.0 \cdot 10^{-11}$	2.0	516	326

Table 6.1: Controller settings for varying values of m_3 using a measurement of the end-effector position. Using these controller settings, the stability margins given in the introduction to this section are obtained. In the latter two columns the resulting bandwidth of the closed-loop transfer function and the sensitivity function are given.

It first revealed, that changes in K_d, even after changing K_p, resulted in instability. From this, it was concluded that only small variations in the magnitude of K_d are possible. Changes in K_d are therefore not considered. However, lowering the magnitude of K_p resulted in a lower maximum value of the closed-loop transfer, as can be seen in figure 6.10b.

The tuning procedure for stabilizing the system for various values of m_3 is as follows: *If for a given value of m_3 the maximum value of the closed-loop transfer is located in the frequency range of the first-stage actuator, then the magnitude of K_p is lowered as long as $max|T(s)| > 2$ [dB] and lowering K_p results in a significant decrease of $max|T(s)|$. In case $max|T(s)|$ does not decrease significantly and still $max|T(s)| > 2$ [dB], the stability margins can be satisfied by increasing τ_i.* It should be noted that the system can also be stabilized by only increasing τ_i. However, τ_i largely determines the bandwidth of the second-stage actuator and increasing τ_i results in a smaller bandwidth. Since the bandwidth of the DSA system is determined by the bandwidth of the second-stage actuator, this method is not preferable.

The above given tuning procedure is applied to the model in figure 4.1 and using three values of m_3. The resulting values for K_p, τ_i and $max|T(s)|$, as well as the bandwidth of the system from the sensitivity function and the closed-loop transfer function are given in table 6.1

Conclusions

From the previous it has become clear that the independently designed SISO controllers for the first-stage and second-stage actuator should in case of implementation be manually tuned. Consequently, a stable closed-loop system with poles in the left half plane of the pole-zero plot and a maximum value of the closed-loop transfer smaller than 2 [dB] can be obtained.

Furthermore, it has also been shown that the value for m_3 for which decoupling occurs, is not necessarily a limit on the value of m_3 in order to use the separately designed controllers. In the previous examples, it has been shown that even in case $m_3 = 0.73$ [kg] the resulting bandwidth is larger than in case of the single-stage actuated system. Further increasing the numerical value of m_3 and stabilizing the system seems possible, however the resulting increase of bandwidth is limited.

6.4.2 Measure carriage position

Another possible sensor configuration for controlling the DSA system, while assuming the coupled model, is given by figure 6.11. This configuration measures both the position of the carriage and the displacement of the piezo-actuator. In this case, the carriage position is used as feedback to the first-stage controller. The displacement of the piezo-actuator is used together with the carriage position measurement, as input to the second-stage controller. The idea behind this implementation is drawn from the decoupled controller design approach sketched in section 2.5.1.

However, a main difference between implementing this sensor configuration in the coupled and the decoupled model is found in the sensitivity function. In case of the decoupled model, the sensitivity function is found as a multiplication of the sensitivity functions of the independent control loops. However, in case of the coupled model, the sensitivity function should be determined per feedback loop. Using figure 6.11 and assume that $x_{ref} = 0$, it can easily be seen that an output disturbance δ_1, which is measured by position sensor x_1, is only compensated for

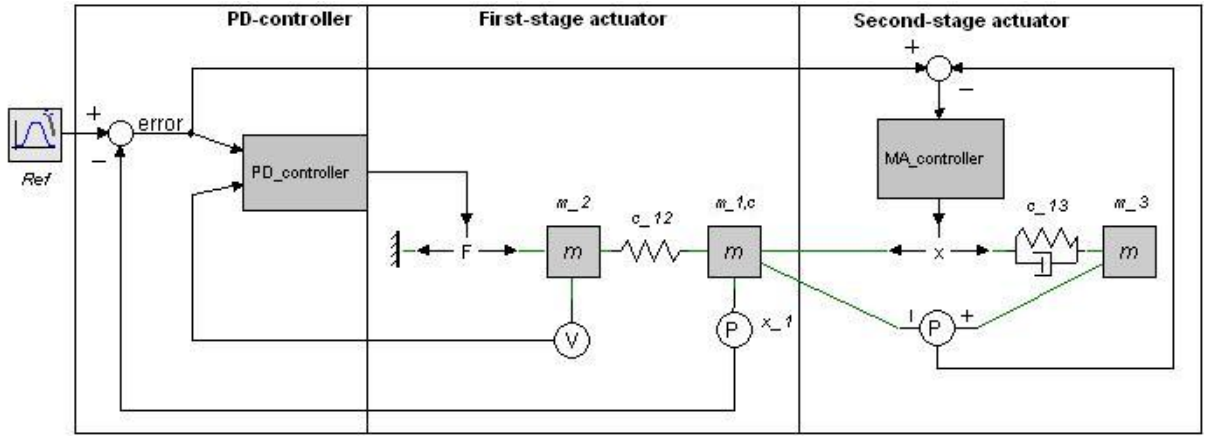

Figure 6.11: Sensor configuration using the coupled model and measuring both the position of the carriage and the displacement of the piezo-actuator.

by the first-stage controller. As a result, in the position x_3, the output position of the DSA system, the disturbance δ_1 is directly observed. From this analysis it can be concluded that this sensor configuration does not increase the sensitivity bandwidth of the DSA system. In fact, the sensitivity bandwidth can be approximated by that of the single-stage actuated system.

Stability

For reasons of completeness, the closed-loop transfer function of the system in figure 6.11 is derived in section G.1. The resulting closed-loop transfer is given in equation (G.7). It was already concluded that in this case the sensitivity function should pe determined per feedback loop. In this case, two feedback loops are relevant. First, the loop in which the from carriage position $x_{1,c}$ is measured. Secondly, the loop in which the displacement of the second-stage actuator is measured, i.e. $x_3 - x_{1,c}$. However, of the latter feedback loop, we already now the sensitivity function, since this was already determined in chapter 4. It is also known that the sensitivity bandwidth of the second-stage actuator is larger than that of the single-stage actuated system. Therefore, the sensitivity bandwidth of the carriage position measurement determines ultimately the sensitivity bandwidth of the DSA system. This sensitivity function is defined as

$$S(s) = \frac{x_1 + \delta_1}{\delta_1} \tag{6.28}$$

This sensitivity function is derived in section G.2. The resulting sensitivity function is given in equation (G.14) As before, due to the complexity of both transfer functions, the transfer functions are not reproduced here.

Conclusions

For this sensor configuration, the same approach as in section 6.4.1 to stabilize the system is followed. The resulting controller settings and bandwidths are given in table 6.2. It can be concluded that although the resulting controller settings differ with the ones given in table 6.1, the resulting closed-loop bandwidth is the same. Furthermore, it should be noted that the sensitivity bandwidth is significantly smaller, due to the reasons given before.

Comparing this sensor configuration with the one given in section 6.4.1, it can be concluded that in order to enlarge the sensitivity bandwidth of the DSA system, it is necessary to measure the position of the end-effector. When this measurement is available, the second-stage actuator can be used to compensate for disturbances that are introduced by the movement of both the carriage and the end-effector movement; in this case both disturbances are observed.

$\mathbf{m_3}$ [kg]	$\mathbf{K_p}$	$\tau_\mathbf{i}$	$\max\|\mathbf{T(s)}\|$ [dB]	$\mathbf{f}_{\|\mathbf{T(s)}\|=-\mathbf{3}}$ [dB] [Hz]	$\mathbf{f}_{\|\mathbf{S(s)}\|=\mathbf{0}}$ [dB] [Hz]
$16 \cdot 10^{-3}$	$1 \cdot 10^{7}$	$4 \cdot 10^{-12}$	1.8	6707	137
0.23	$0.8 \cdot 10^{7}$	$1.1 \cdot 10^{-11}$	2.0	1966	124
0.48	$0.1 \cdot 10^{7}$	$1.8 \cdot 10^{-11}$	1.9	1227	40
0.73	$0.1 \cdot 10^{6}$	$2.8 \cdot 10^{-11}$	2.0	529	7

Table 6.2: Controller settings for varying values of m_3 using carriage position measurement. Using these controller settings, the stability margins given in the introduction to this section are obtained. In the latter two columns the resulting bandwidth of the closed-loop transfer function and the sensitivity function are given.

6.5 Conclusions

In this chapter, both the stability, closed-loop bandwidth and sensitivity bandwidth of both the coupled and decoupled model are determined for various sensor configurations. Four of the five presented sensor configurations increased both the sensitivity and the closed-loop bandwidth of the resulting DSA system. It should be noted that the results of this analysis are only valid for the case in which the second-stage actuator is not in saturation.

Considering the decoupled model first, it is concluded that the sensor configurations can be implemented by using two sensors at maximum. One sensor measures the position of the carriage and the other the displacement of the piezo-actuator. The alternative is to use one sensor which measures the position of the end-effector. Using the simplified FCM model, the presented controller parameters and a load mass $m_3 = 16 \cdot 10^{-3}$ [kg], such that decoupling occurs, it was shown that the closed-loop bandwidth can be increased to 9050 [Hz] and the sensitivity bandwidth to 3155 [Hz]. Compared to 471 [Hz] and 140 [Hz] respectively, in case of the single-stage actuated system. Note again, that a single-stage actuated system with a resonance frequency of 551 Hz is taken as starting point. Furthermore, between the two evaluated controller designs, we have not seen differences in closed-loop or sensitivity bandwidth.

It was already concluded in the previous chapter, that it is in practice not likely, that a location in the PM of the FCM can be found, where this mass can be displaced. The lesson that can be learnt from this example is however, that in case the decoupled model can be used, it is not necessary to measure the position of the end-effector in order to increase the sensitivity and closed-loop bandwidth. And consequently, the bandwidth of the DSA system can be approximated by the bandwidth of the second-stage actuator.

In case the parameters of the second-stage actuator are such, that decoupling of the two stages does not occur, it has been shown that the decoupled designed SISO-controllers for both stages can be used. However, the settings of this controller should be manually tuned in order to satisfy the stability margins of the closed-loop system, as defined in section 6.1. In section 6.4 it is described how the controller parameters are tuned in order to satisfy the stability margins. A main advantage of this method is that the bandwidth of the DSA system is preserved, while robustness is improved. Furthermore, it was concluded that of the two sensor configurations that were suggested for the coupled model, only one configuration increases both the sensitivity and the closed-loop bandwidth. In that case, the load mass to the second-stage actuator can be up to 0.73 [kg], while increasing both the closed-loop and sensitivity bandwidth. In fact, the bandwidth of the DSA system is somewhat smaller than given in table 4.1 for the piezo-actuator alone. Furthermore, comparing the sensor configurations for the coupled model leads to a general conclusion; in case of the coupled model, the position of the end-effector should be measured in order to increase both the sensitivity and closed-loop bandwidth. In case the DSA system performs a 1-dimensional motion, this position can be measured either via direct measurement of the end-effector position or by summing the carriage position and the piezo-actuator displacement.

Chapter 7

Conclusions and recommendations

7.1 Conclusions

Literature research

During this research, first a literature study on dual-stage actuation in HDDs was conducted. From that, it was concluded that dual-stage actuation in HDDs is considered as a means to increase the servo-bandwidth of the HDD, such that the demands in increasing response time and increasing accuracy at the same time can be met. It turned out, that the limiting factor in bandwidth is found in the mechanical resonances between the first-stage actuator and the read/write head. Furthermore, it is difficult to compensate for these mechanical resonances by means of improved mechanical design. Consequently, the solution is found in the application of a second actuator. This second actuator is characterized by a large bandwidth and short stroke, such that it is able to compensate for the high frequency disturbances. By modelling the FCM, it was concluded that in this application also a mechanical resonance is found, which puts limits on the achievable bandwidth.

Decoupled and coupled dual-stage actuated systems

Furthermore, from the literature research, it has become clear that for controlling the dual-stage actuated (DSA) HDD, decoupled SISO-design methodologies have been used. These methodologies have the advantage of being simple and insightful. The assumption underlying these methodologies is that the output of a DSA system is a summation of the displacement of the two stages.

In order to verify if this assumption holds for industrial applications like the FCM, models of both the first and second-stage actuator are developed. Subsequently, two DSA models were defined. One model was denoted as the *decoupled model*; in this case, the output of the DSA system was obtained by summing the output of both stages. The second model was denoted as the *coupled model*; in this case, interaction between the first and second-stage was present. The output of the system is given by the displacement of the second-stage actuator, which interacts with the carriage of the first-stage actuator.

Writing out the plant transfer functions of both models, it was concluded that in case of the coupled model, the Bode plot was different compared to the decoupled model. Actually, a resonance and an anti-resonance frequency were introduced in the plant transfer function from second-stage actuator input to second-stage actuator displacement. By assuming damping in the system, the mass of the second-stage for which decoupling occurs can be calculated. In order to be able to do so, a definition of decoupling was introduced, based on the Bode plot of the plant transfer. Application of this definition to the FCM model parameters, lead to the conclusion that decoupling occurs in case the load mass to the second-stage actuator is very small. From that, it was concluded that it is not likely that in practice a location in the FCM can be found, where that mass can be displaced and to which a second-stage actuator can be rigidly attached. Using the FCM model parameters, decoupling can thus not be assumed. However, this conclusion cannot be generalized.

Sensor configurations

From the literature research on DSA HDDs, it was furthermore concluded, that the sensory system of the HDD needed not be adapted in order to implement a second-stage actuator. This is due to the fact that in a single-stage actuated HDD, the position of the read/write head, i.e. the end-effector, is measured. However, in case of industrial applications in general and for the FCM in particular, this is not (always) the case. Therefore, for both the coupled and decoupled model, sensor configurations have been determined. Subsequently, for each configuration the closed-loop bandwidth and sensitivity bandwidth were determined.

Concerning the decoupled model, the main conclusion is that the sensitivity bandwidth and closed-loop bandwidth of the DSA system were approximated by those of the second-stage actuator. Furthermore, it turned out that measurement of the end-effector position is not necessary.

With respect to the coupled model, it was concluded that direct application of the decoupled designed controllers resulted in an unstable closed-loop system. By manually tuning the controllers, the system was stabilized and the stability margins satisfied. However, it was also concluded that in this case, in order to increase both the sensitivity and the closed-loop bandwidth of the DSA system, measurement of the end-effector position is required. This sensor configuration was used, in combination with the assumption of mass distribution between the two stages, to investigate the resulting bandwidth for various values of the load mass to the second-stage actuator. Furthermore, the first-stage was given by a fourth-order plant, with a resonance frequency of 551 [Hz]. From this, it appeared that assigning a load mass of up to 0.73 [kg] to the second-stage actuator, resulted in an increase of the sensitivity and the closed-loop bandwidth.

General conclusions

In general, it can be concluded that dual-stage actuation is an effective means to increase the sensitivity and closed-loop bandwidth of a system. Furthermore, in the case that decoupling between the first and second-stage occurs, only minor changes have to be made to the sensory system. Thereby, the presented SISO design methodologies can be directly applied.

However, in practice decoupling might be hard to achieve. In that case, more attention has to be paid to the development of suitable controllers. Furthermore, in the case that in the application the position of the end-effector is not measured, the sensory system should undergo major changes. This means that in the case of applying dual-stage actuation to the FCM, dual-stage actuation cannot be implemented without using an expensive sensory system to measure the end-effector position. However, for applications in which the end-effector position is already measured, dual-stage actuation can indeed be an inexpensive means to increase performance.

7.2 Recommendations

Previously, it was concluded that dual-stage actuation is an effective means to increase the system's bandwidth. However, in the analysis on dual-stage actuation in general and in the FCM in particular, some topics have not been discussed. Therefore, after having carried out this research, the following recommendations can be given.

2-D models

During this research, 1-dimensional motion was assumed. This assumption is justified for assessing the possibilities, advantages and disadvantages of dual-stage actuation. However, from literature on the FCM it is known that the motion of the end-effector is not 1-dimensional. In order to fully oversee the disadvantages of implementing a second-stage actuator to the FCM, it is recommended to included the second dimension of motion in the model. From that, conclusions on the suggested sensor configuration can be drawn. Consequently, it can be assessed whether or not the suggested sensor configuration can be implemented.

Other (micro-)actuators

During this research, only piezo-actuators have been used as a second-stage actuator. However, from literature on dual-stage actuated HDDs it appeared that also electrostatic and electromagnetic micro-actuators can be used for dual-stage actuation. It is recommended, that models be developed for these actuator types. Subsequently, it

is recommended to investigate for these actuator types, under which circumstances decoupling between the two stages occurs.

Controller design

During this research, it has been shown that using the coupled model in combination with the decoupled designed controllers, results in an unstable system. By means of manually tuning, the controller parameters became such that the system was stabilized. It is however recommended to formalize this tuning procedure and to investigate the possibilities to calculate the controller parameters of the DSA system in a comparable way as Coelingh (2000) did for a single-stage actuated system.

Furthermore, since the DSA system is MIMO in essence, it is recommended to investigate the possibilities of developing MIMO-controllers to the dual-stage actuated system. This is also of interest, since the resonance frequency of mass-produced piezo-actuators tend to variate in magnitude. In this case, MIMO-design tools can enhance robustness of the DSA system.

Practical setup

During this research, we performed an analytical investigation into the models, controller design and sensor configurations of a DSA system. From this research, we have concluded that in general, dual-stage actuation is an effective means to increase the system's bandwidth. However, the insight we gained in modelling and controlling dual-stage actuated system is meaningless, if we do not know what performance we can obtain in practice. It is therefore recommended to realize a practical setup, in which we can evaluate the response of the DSA system for various actuators, load masses and sensor configurations.

Appendix A

Parameters piezo-actuator

A.1 Parameters of P885.10 piezo-actuator

x_{max}	9	[μm]
U_{max}	120	[V]
F_{block}	900	[N]
c	$115 \cdot 10^6$	[N/m]
ω_r	$2\pi \cdot 135 \cdot 10^3$	[rad/s]
m_{eff}	$1.60 \cdot 10^{-4}$	[kg]
$d_{U,F}$	7.5	[N/V]
$d_{U,x}$	$6.5 \cdot 10^{-8}$	[m/V]

Table A.1: Parameters of the PI's P885.10 piezo-actuator (PI-datasheets, 2004).

A.2 Parameters of P888.20 piezo-actuator

x_{max}	11	[μm]
U_{max}	120	[V]
F_{block}	3600	[N]
c	$353 \cdot 10^6$	[N/m]
ω_r	$2\pi \cdot 110 \cdot 10^3$	[rad/s]
m_{eff}	$7.39 \cdot 10^{-4}$	[kg]
$d_{U,F}$	30	[N/V]
$d_{U,x}$	$8.5 \cdot 10^{-8}$	[m/V]

Table A.2: Parameters of the PI's P888.20 piezo-actuator (PI-datasheets, 2004).

Appendix B

Plant transfer function coupled and decoupled DSA-model

B.1 Coupled system

The position x_2 is calculated by solving the following relation for x_2

$$m_2 s^2 x_2 = F_{in} - F_{c_{12}} = F_{in} + c_{12}\left(x_1 - x_2\right) \tag{B.1}$$

This results in

$$x_2 = \frac{F_{in} + c_{12} x_1}{m_2 s^2 + c_{12}} \tag{B.2}$$

The same approach is followed for x_1. The position x_1 is calculated by solving the relation

$$m_{1,c} s^2 x_1 = F_{c_{12}} - F_{c_{13}} = -c_{12}(x_1 - x_2) + c_{13}(x_3 - (x_1 + x_{2^{nd}}) \tag{B.3}$$

substitution of (B.2) and solving for x_1 results in

$$x_1 = \frac{c_{12} F_i + \left(m_2 c_{13} s^2 + c_{12} c_{13}\right) x_3 - \left(m_2 c_{13} s^2 - c_{12} c_{13}\right) x_{2^{nd}}}{m_{1,c} m_2 s^4 + m_{1,c} c_{12} s^2 + \left(c_{12} m_2 + c_{13} m_2\right) s^2 + c_{12} c_{13}} \tag{B.4}$$

Finally the position x_3 is calculated by solving

$$m_3 s^2 x_3 = F_{c_{13}} = -c_{13}(x_3 - (x_1 + x_{2^{nd}})) \tag{B.5}$$

Substituting (B.4) and solving for x_3 results in

$$x_3 = \frac{\left(b_4 s^4 + b_2 s^2\right) x_{2^{nd}} + d_0 F_{in}}{a_6 s^6 + a_4 s^4 + a_2 s^2} \tag{B.6}$$

with

$$\begin{aligned} a_6 &= m_{1,c} m_2 m_3 \\ a_4 &= \left(m_2 m_3 + m_{1,c} m_3\right) c_{12} + \left(m_{1,c} m_2 + m_2 m_3\right) c_{13} \\ a_2 &= c_{12} c_{13}\left(m_{1,c} + m_2 + m_3\right) \\ b_4 &= c_{13} m_{1,c} m_2 \\ b_2 &= c_{13} c_{12}\left(m_{1,c} + m_2\right) \\ d_0 &= c_{12} c_{13} \end{aligned} \tag{B.7}$$

The poles and zeros of equation (B.6) can be calculated symbolically, by using some assumptions on the sign and relative magnitude of the coefficients. These assumptions follow from the coefficients above. The resulting assumptions are given as

$$\begin{aligned} a_6, a_4, a_2 &> 0 \\ a_2 &> a_6 \\ a_2 &> a_4 \\ a_4 &> a_6 \\ b_4, b_2 &> 0 \\ b_2 &> b_4 \end{aligned}$$

The poles and zeros have been determined using Maple. This results in

$$p_{1,2,coupled} = 0, 0 \tag{B.8}$$

$$p_{3,4,coupled} = \pm i\frac{1}{2}\frac{\sqrt{2\,a_6\left(a_4 - \sqrt{{a_4}^2 - 4\,a_6 a_2}\right)}}{a_6} \tag{B.9}$$

$$p_{5,6,coupled} = \pm i\frac{1}{2}\frac{\sqrt{2\,a_6\left(a_4 + \sqrt{{a_4}^2 - 4\,a_6 a_2}\right)}}{a_6} \tag{B.10}$$

$$z_{1,2,coupled} = 0, 0 \tag{B.11}$$

$$z_{3,4,coupled} = \pm i\sqrt{\frac{b_2}{b_4}} = \pm i\sqrt{\frac{c_{12}\left(m_{1,c} + m_2\right)}{m_{1,c}m_2}} \tag{B.12}$$

B.2 Decoupled system

In determining the position x_2, it can be concluded that, since the second-stage actuator does not exert a force directly on m_2, relation (B.2) is not changed.

It should be noted that in this case the numerical value for m_1 is changed

$$m_{1,d} = m_{1,c} + m_3 \tag{B.13}$$

This relation is substituted for m_1 in the coming relations. The position x_1 is determined by solving the relation

$$\left(m_{1,c} + m_3\right) s^2 x_1 = F_{c_{12}} = -c_{12}(x_1 - x_2) \tag{B.14}$$

by substituting (B.2) x_1 is solved as

$$x_1 = \frac{c_{12}F_{in}}{\left(m_{1,c} + m_3\right) m_2 s^4 + \left(\left(m_{1,c} + m_3\right) c_{12} + m_2 c_{12}\right) s^2} \tag{B.15}$$

The position x_3 in the decoupled system is easily calculated by recognizing that the plant transfer function of the piezo-actuator applies, thus

$$x_3 = \frac{c_{13}x_{nd}}{m_3 s^2 + c_{13}} \tag{B.16}$$

Finally x_{out} is determined by adding (B.14) and (B.16). This results in

$$x_{out} = \frac{\left(b_4 s^4 + b_2 s^2\right) x_{2^{nd}} + \left(d_2 s^2 + d_0\right) F_{in}}{a_6 s^6 + a_4 s^4 + a_2 s^2} \tag{B.17}$$

where the coefficients are calculated by:

$$\begin{aligned} a_6 &= m_{1,c}m_2m_3 + m_3^2 m_2 \\ a_4 &= \left(m_2m_3 + m_{1,c}m_3\right) c_{12} + \left(m_{1,c}m_2 + m_2m_3\right) c_{13} + m_3^2 c_{12} \end{aligned}$$

$$
\begin{aligned}
a_2 &= c_{12}c_{13}\left(m_{1,c}+m_2+m_3\right) \\
b_4 &= m_{1,c}m_2c_{13}+m_2m_3c_{13} \\
b_2 &= c_{12}c_{13}\left(m_{1,c}+m_2+m_3\right) \\
d_2 &= m_3c_{12} \\
d_0 &= c_{12}c_{13}
\end{aligned} \tag{B.18}
$$

As for the coupled model, the poles and zeros of equation (B.17) can be determined symbolically as

$$p_{1,2,decoupled} = 0,0 \tag{B.19}$$

$$p_{3,4,decoupled} = \pm i\frac{\sqrt{m_2\left(m_3+m_{1,c}\right)c_{12}\left(m_3+m_{1,c}+m_2\right)}}{m_{1,c}m_2+m_3m_2} \tag{B.20}$$

$$p_{5,6,decoupled} = \pm i\sqrt{\frac{c_{13}}{m_3}} \tag{B.21}$$

$$z_{1,2,decoupled} = 0,0 \tag{B.22}$$

$$z_{3,4,decoupled} = \pm i\frac{\sqrt{m_2\left(m_{1,c}+m_3\right)c_{12}\left(m_2+m_3+m_{1,c}\right)}}{m_{1,c}m_2+m_3m_2} \tag{B.23}$$

$$z_{5,6,decoupled} = \pm i\sqrt{\frac{c_{13}}{m_3}} \tag{B.24}$$

Appendix C

Single-stage transfer functions

C.1 Sensitivity function of concept AR-R

The sensitivity function of the single-stage actuated FCM is derived by determining the transfer function:

$$S(s) = \frac{x_{out}}{\delta} = \frac{x_1 + \delta}{\delta} \tag{C.1}$$

where x_1 is the output of the system and δ the output disturbance. In order to determine the sensitivity function S, the same line of reasoning as for determining the closed-loop transfer function of the single-stage actuated system is followed. For this analysis, the reference position x_{ref} is assumed to be 0. First, a relation for F_{in}, the input force to the FCM, is derived as

$$F_{in} = -K_p x_{out} - s x_2 K_d \tag{C.2}$$

Then, from the force balance on m_2, the position x_2 can be calculated as

$$x_2 = \frac{c_{12} x_1 - K_p x_{out}}{m_2 s^2 + s K_d + c_{12}} \tag{C.3}$$

Consequently, the same approach is followed to determine x_1 from the force balance on m_1. This results in

$$x_1 = -\frac{c_{12} K_p x_{out}}{s\left(m_1 s^3 m_2 + m_1 s^2 K_d + m_1 s c_{12} + c_{12} m_2 s + c_{12} K_d\right)} \tag{C.4}$$

Finally, by recognizing that

$$x_{out} = x_1 + \delta \tag{C.5}$$

x_{out} can be solved by substituting equation (C.4) in equation (C.5). By writing out the different terms, x_{out} can be written as a function of δ. From this relation, the sensitivity function is determined as

$$S_{FCM}(s) = \frac{m_1 m_2 s^4 + m_1 K_d s^3 + (m_1 + m_2)\, c_{12} s^2 + c_{12} K_d s}{m_1 m_2 s^4 + m_1 K_d s^3 + (m_1 + m_2)\, c_{12} s^2 + c_{12} K_d s + c_{12} K_p} \tag{C.6}$$

C.2 Piezo-actuator's sensitivity function

The sensitivity function of the controlled piezo-actuator can easily be derived. In contrast to the concept AR-R controlled first-stage actuator, the controlled piezo-actuator consists of only one feedback loop. Consequently, the sensitivity function S is defined as

$$S(s) = \frac{1}{1 + P(s)C(s)} \tag{C.7}$$

where $P(s)$ is the plant transfer function of the piezo-actuator and $C(s)$ the transfer function of the controller. From chapter 4 these transfer functions are known. This results eventually in the following sensitivity function

$$S_{MA}(s) = \frac{s\left(s^2 + 2\zeta_r\omega_r s + \omega_r^2\right)\left(s^2 + 2\zeta_{LP}\omega_{LP}s + \omega_{LP}^2\right)}{a_5 s^5 + a_4 s^4 + a_3 s^3 + a_2 s^2 + a_1 s + a_0} \tag{C.8}$$

where the coefficients of the denominator are given by

$$\begin{aligned}
a_5 &= 1 \\
a_4 &= 2\left(\zeta_{LP}\omega_{LP} + \zeta_r\omega_r\right) \\
a_3 &= \omega_{LP}^2 + 4\zeta_{LP}\omega_{LP}\zeta_r\omega_r + \omega_r^2 \\
a_2 &= 2\left(\zeta_r\omega_r\omega_{LP}^2 + \zeta_{LP}\omega_{LP}\omega_r^2\right) \\
a_1 &= \omega_r^2\omega_{LP}^2\left(1 + d_{U,x}\right) \\
a_0 &= \frac{\omega_r^2\omega_{LP}^2 d_{U,x}}{\tau_i}
\end{aligned}$$

Appendix D

Decoupled model: transfer functions for parallel controller

D.1 Closed-loop transfer using parallel controller

Deriving the closed-loop transfer function from the reference position x_{ref} to the output position $x_{out} = x_1 + x_3$ using the decoupled control approach starts with defining the error signals that are applied to the two controllers.

The error signal that is fed to both controllers is denoted as e and is given by

$$e = x_{ref} - x_{out} = x_{ref} - x_1 - x_3 \tag{D.1}$$

As before, relations that describe the positions x_1, x_2 and x_3 are derived by solving the force balances on each of the three masses. First the relation for the force of the first actuator F_{in} is given

$$F_{in} = K_p \left(x_{ref} - x_{out}\right) - K_d s x_2 \tag{D.2}$$

Consequently, the relation for x_2 is given by

$$x_2 = \frac{K_p x_{ref} - K_p x_{out} + c_{12} x_1}{m_2 s^2 + K_d s + c_{12}} \tag{D.3}$$

and for x_1 the following relation is obtained

$$x_1 = \frac{c_{12} K_p \left(x_{ref} - x_{out}\right)}{\left(m_{1,d} m_2 s^4 + m_{1,d} K_d s^3 + \left(m_{1,d} + c_{12} m_2\right) s^2 + c_{12} K_d s\right)} \tag{D.4}$$

Finally, the position x_3 is determined. It can easily be seen that in this case x_3 can be calculated as

$$x_3 = H_{PI,parallel}(s) d_{U,x} \frac{\omega_r^2}{s^2 + 2\zeta_r \omega_r s + \omega_r^2} \cdot e \tag{D.5}$$

where $H_{PI,parallel}$ is given by equation (4.7). Finally, a relation for x_{out} is found by substituting the respective relations in $x_{out} = x_1 + x_3$ and solve for x_{out}. From this relation the closed-loop transfer function of this system can be determined to be

$$H(s) = \frac{b_4 s^4 + b_3 s^3 + b_2 s^2 + b_1 s + b_0}{a_8 s^8 + a_7 s^7 + a_6 s^6 + a_5 s^5 + a_4 s^4 + a_3 s^3 + a_2 s^2 + a_1 s + a_0} \tag{D.6}$$

where the coefficients are given by

$$\begin{aligned}
b_4 &= m_{1,d} m_2 d_{U,x} \omega_r^2 \tau_i \omega_{LP}^2 + c_{12} K_p \tau_i \\
b_3 &= \left(\tau_i K_d + m_2\right) m_{1,d} d_{U,x} \omega_r^2 \omega_{LP}^2 + 2 K_p c_{12} \tau_i \left(\zeta_{LP} \omega_{LP} + \zeta_r \omega_r\right) \\
b_2 &= \left(K_p c_{12} \tau_i + \left(m_{1,d} + m_2\right) d_{U,x} \omega_r^2 \tau_i c_{12} + d_{U,x} \omega_r^2 m_{1,d} K_d\right) \omega_{LP}^2
\end{aligned}$$

$$
\begin{aligned}
& + 4c_{12}\zeta_r\omega_r K_p\tau_i\zeta_{LP}\omega_{LP} + c_{12}\omega_r^2 K_p\tau_i \\
b_1 &= \big(\left(m_{1,d}+m_2\right)d_{U,x}\omega_r^2 + \omega_r^2 d_{U,x}\tau_i K_d + 2\zeta_r\omega_r K_p\tau_i\big)c_{12}\omega_{LP}^2 \\
& + 2c_{12}\omega_r^2 K_p\tau_i\zeta_{LP}\omega_{LP} \\
b_0 &= \left(K_p\tau_i + d_{U,x}K_d\right)c_{12}\omega_r^2\omega_{LP}^2 \\
a_8 &= \tau_i m_{1,d}m_2 \\
a_7 &= 2m_{1,d}m_2\tau_i\zeta_{LP}\omega_{LP} + m_{1,d}\tau_i\left(2m_2\zeta_r\omega_r + K_d\right) \\
a_6 &= m_{1,d}m_2\tau_i\omega_{LP}^2 + \left(2m_2\zeta_r\omega_r + K_d\right)2m_{1,d}\tau_i\zeta_{LP}\omega_{LP} \\
& + \big(\left(m_{1,d}+m_2\right)c_{12} + \left(2K_d\zeta_r\omega_r + m_2\omega_r^2\right)m_{1,d}\big)\tau_i \\
a_5 &= \left(K_d + 2m_2\zeta_r\omega_r\right)m_{1,d}\tau_i\omega_{LP}^2 \\
& + \big(\left(m_{1,d}+m_2\right)c_{12} + \left(2K_d\zeta_r\omega_r + m_2\omega_r^2\right)m_{1,d}\big)2\tau_i\zeta_{LP}\omega_{LP} \\
& + \big(\left(m_{1,d}\omega_r^2 + c_{12}\right)K_d + \left(m_{1,d}+m_2\right)2c_{12}\zeta_r\omega_r\big)\tau_i \\
a_4 &= \big(\left(1+d_{U,x}\right)m_{1,d}m_2\omega_r^2 + 2m_{1,d}K_d\zeta_r\omega_r + \left(m_{1,d}+m_2\right)c_{12}\big)\tau_i\omega_{LP}^2 \\
& + \big(c_{12}K_d + \left(m_{1,d}+m_2\right)2c_{12}\zeta_r\omega_r + m_{1,d}K_d\omega_r^2\big)2\tau_i\zeta_{LP}\omega_{LP} \\
& + \big(\left(m_{1,d}+m_2\right)\omega_r^2 + K_p + 2K_d\zeta_r\omega_r\big)c_{12}\tau_i \\
a_3 &= \left(2m_2\zeta_r\omega_r + K_d\right)\tau_i c_{12}\omega_{LP}^2 \\
& + \big(\left(\tau_i K_d + m_2\right)d_{U,x}\omega_r^2 + \left(2c_{12}\zeta_r\omega_r + K_d\omega_r^2\right)\tau_i\big)m_{1,d}\omega_{LP}^2 \\
& + \big(\left(m_{1,d}+m_2\right)\omega_r^2 + 2K_d\zeta_r\omega_r + K_p\big)2c_{12}\tau_i\zeta_{LP}\omega_{LP} \\
& + \left(K_d\omega_r + 2K_p\zeta_r\right)c_{12}\omega_r\tau_i \\
a_2 &= \big(2K_d\zeta_r\omega_r + \left(m_{1,d}+m_2\right)\omega_r^2 + \left(m_{1,d}+m_2\right)d_{U,x}\omega_r^2 + K_p\big)\tau_i c_{12}\omega_{LP}^2 \\
& + d_{U,x}\omega_r^2 m_{1,d}K_d\omega_{LP}^2 + \left(K_d\omega_r^2 + K_p\zeta_r\omega_r\right)2\tau_i c_{12}\zeta_{LP}\omega_{LP} \\
& + K_p c_{12}\tau_i\omega_r^2 \\
a_1 &= \big(\left(1+d_{U,x}\right)\tau_i K_d\omega_r^2 + \left(m_{1,d}+m_2\right)d_{U,x}\omega_r^2 + 2K_p\tau_i\zeta_r\omega_r\big)c_{12}\omega_{LP}^2 \\
& + 2K_p c_{12}\tau_i\omega_r^2\zeta_{LP}\omega_{LP} \\
a_0 &= \left(K_p\tau_i + d_{U,x}K_d\right)c_{12}\omega_r^2\omega_{LP}^2
\end{aligned}
$$

D.2 Sensitivity function using parallel controller

The sensitivity function using the parallel control approach is determined under the assumption that $x_{ref} = 0$. In this case the sensitivity function S is defined as

$$S(s) = \frac{x_{out} + \delta}{\delta} = \frac{x_1 + x_3 + \delta}{\delta} \tag{D.7}$$

where δ is a positional output disturbance. The starting point of deriving $S(s)$ is defining the force F_{in} that is applied to the first actuator. This force can be calculated as

$$F_{in} = -K_p x_{out} - K_d s x_2 \tag{D.8}$$

Consequently, x_2 is solved from the force balance on m_2. This results in the following expression

$$x_2 = \frac{-K_p x_{out} + c_{12}x_1}{m_2 s^2 + sK_d + c_{12}} \tag{D.9}$$

The same approach is followed in order to obtain a relation for x_1 from the force balance on m_1

$$x_1 = \frac{-c_{12}K_p x_{out}}{m_{1,d}m_2 s^4 + m_{1,d}K_d s^3 + \left(m_{1,d}c_{12} + c_{12}m_2\right)s^2 + c_{12}K_d s} \tag{D.10}$$

Then, a relation for determining the position x_3 is derived. From the plant transfer function of the piezo-actuator can x_3 be determined as

$$x_3 = \frac{\omega_r^2}{s^2 + 2\zeta_r\omega_r s + \omega_r^2} x_{2^{nd}} \tag{D.11}$$

where $x_{2^{nd}}$ is given by

$$x_{2^{nd}} = -H_{PI,parallel} d_{U,x} x_{out} \tag{D.12}$$

where $H_{PI,parallel}$ is given by equation (4.7). Consequently, x_3 can be determined to be

$$x_3 = \frac{-\omega_{LP}^2 (\tau_i s + 1) d_{U,x} c_{13} x_{out}}{s\tau_i (s^2 + 2\zeta_{LP}\omega_{LP} s + \omega_{LP}^2)(m_3 s^2 + 2\zeta_r\omega_r m_3 s + c_{13})} \tag{D.13}$$

Finally, it is known that in this case $x_{out} = x_1 + x_3 + \delta$. A relation for x_{out} can be obtained by substituting the expressions for x_1 and x_3 in the previous expression and solve for x_{out}. From this relation the sensitivity function is directly calculated as

$$S(s) = \frac{x_{out}}{\delta} = \frac{b_8 s^8 + b_7 s^7 + b_6 s^6 + b_5 s^5 + b_4 s^4 + b_3 s^3 + b_2 s^2 + b_1 s + b_0}{a_8 s^8 + a_7 s^7 + a_6 s^6 + a_5 s^5 + a_4 s^4 + a_3 s^3 + a_2 s^2 + a_1 s + a_0} \tag{D.14}$$

where the coefficients are given as

$$\begin{aligned}
a_8 &= m_{1,d} m_2 m_3 \\
a_7 &= 2m_{1,d} m_2 m_3 \zeta_{LP}\omega_{LP} + m_{1,d} m_3 (2m_2\zeta_r\omega_r + K_d) \\
a_6 &= m_{1,d} m_2 m_3 \omega_{LP}^2 + (K_d + 2m_2\zeta_r\omega_r) 2m_{1,d} m_3 \zeta_{LP}\omega_{LP} \\
&\quad + (m_{1,d} + m_2) m_3 c_{12} + (m_2 c_{13} + 2m_3 K_d \zeta_r \omega_r) m_{1,d} \\
a_5 &= (2m_2\zeta_r\omega_r + K_d) m_{1,d} m_3 \omega_{LP}^2 \\
&\quad + \big((m_{1,d} + m_2) m_3 c_{12} + (m_2 c_{13} + 2m_3 K_d \zeta_r \omega_r) m_{1,d} \big) 2\zeta_{LP}\omega_{LP} \\
&\quad + (m_3 c_{12} + m_{1,d} c_{13}) K_d + (m_{1,d} + m_2) 2m_3 c_{12} \zeta_r \omega_r \\
a_4 &= \big((m_{1,d} + m_2) c_{12} m_3 + (1 + d_{U,x}) m_{1,d} m_2 c_{13} + 2m_{1,d} K_d \zeta_r \omega_r m_3 \big) \omega_{LP}^2 \\
&\quad + \big((m_{1,d} + m_2) 2m_3 c_{12} \zeta_r \omega_r + (m_3 c_{12} + m_{1,d} c_{13}) K_d \big) 2\zeta_{LP}\omega_{LP} \\
&\quad + (2K_d\zeta_r\omega_r + K_p) + (m_2 + m_{1,d}) c_{12} c_{13} \\
a_3 &= \Big(\left(m_2 \frac{1}{\tau_i} + K_d \right) c_{13} d_{U,x} + 2m_3 c_{12} \zeta_r \omega_r + c_{13} K_d \Big) \omega_{LP}^2 m_{1,d} \\
&\quad + (2m_2\zeta_r\omega_r + K_d) m_3 c_{12} \omega_{LP}^2 \\
&\quad + \big((m_{1,d} + m_2) c_{13} + (K_p + 2K_d\zeta_r\omega_r) m_3 \big) 2c_{12}\zeta_{LP}\omega_{LP} \\
&\quad + (c_{13} K_d + 2m_3 K_p \zeta_r \omega_r) c_{12} \\
a_2 &= \big((m_{1,d} + m_2) c_{13} + (m_{1,d} + m_2) c_{13} d_{U,x} + (K_p + 2K_d\zeta_r\omega_r) m_3 \big) c_{12} \omega_{LP}^2 \\
&\quad + m_{1,d} c_{13} d_{U,x} K_d \frac{1}{\tau_i} \omega_{LP}^2 \\
&\quad + (c_{13} K_d + 2m_3 K_p \zeta_r \omega_r) 2c_{12}\zeta_{LP}\omega_{LP} + c_{12} K_p c_{13} \\
a_1 &= \big((m_{1,d} + m_2) c_{13} d_{U,x} \frac{1}{\tau_i} + (1 + d_{U,x}) c_{13} K_d + 2K_p \zeta_r \omega_r m_3 \big) \omega_{LP}^2 c_{12} \\
&\quad + 2c_{12} c_{13} K_p \zeta_{LP} \omega_{LP} \\
a_0 &= \left(K_d d_{U,x} \frac{1}{\tau_i} + K_p \right) c_{12} c_{13} \omega_{LP}^2 \\
b_8 &= a_8 \\
b_7 &= a_7 \\
b_6 &= a_6
\end{aligned}$$

$$
\begin{aligned}
b_5 &= a_5 \\
b_4 &= \big((2m_3K_d\zeta_r\omega_r + m_2c_{13})\, m_{1,d} + (m_{1,d} + m_2)\, m_3c_{12} \big)\omega_{LP}^2 \\
&\quad + \big((m_{1,d}c_{13} + m_3c_{12})\, K_d + (m_{1,d} + m_2)\, 2m_3c_{12}\zeta_r\omega_r \big) 2\zeta_{LP}\omega_{LP} \\
&\quad + c_{12}\big((m_{1,d} + m_2)\, c_{13} + 2m_3K_d\zeta_r\omega_r \big) \\
b_3 &= \big((m_{1,d}c_{13} + m_3c_{12})\, K_d + (m_{1,d} + m_2)\, 2m_3c_{12}\zeta_r\omega_r \big)\omega_{LP}^2 \\
&\quad + \big((m_{1,d} + m_2)\, c_{13} + 2m_3K_d\zeta_r\omega_r \big) 2c_{12}\zeta_{LP}\omega_{LP} + c_{12}c_{13}K_d \\
b_2 &= \big(2m_3K_d\zeta_r\omega_r + (m_{1,d} + m_2)\, c_{13} \big)\omega_{LP}^2 c_{12} + 2c_{12}c_{13}K_d\zeta_{LP}\omega_{LP} \\
b_1 &= \omega_{LP}^2 c_{12}c_{13}K_d \\
b_0 &= 0
\end{aligned}
$$

Appendix E

Decoupled model: closed-loop transfer for decoupled controller

The starting point in deriving the closed-loop transfer of this measurement setup is in defining the force F_{in} that is applied to the first-stage as

$$F_{in} = K_p\left(x_{ref} - x_1\right) - sx_2K_d \tag{E.1}$$

Consequently, a relation for x_2 is determined by solving the force balance on m_2. This force balance is given by

$$m_2s^2x_2 = F_{in} + c_{12}(x_1 - x_2) \tag{E.2}$$

from this, x_2 is determined to be

$$x_2 = \frac{K_px_{ref} - K_px_1 + c_{12}x_1}{m_2s^2 + sK_d + c_{12}} \tag{E.3}$$

The same approach is followed for determining a relation for x_1. Hence, the force balance is given by

$$m_1s^2x_1 = -c_{12}(x_1 - x_2) \tag{E.4}$$

and x_1 is solved by substituting the relation for x_2 as

$$x_1 = \frac{c_{12}K_px_{ref}}{m_{1,d}m_2s^4 + m_{1,d}K_ds^3 + \left(m_{1,d}c_{12} + m_2c_{12}\right)s^2 + c_{12}K_ds + c_{12}K_p} \tag{E.5}$$

Finally, the position x_3 is determined. This is done by first defining the positional error e from the first-stage as

$$e = x_{ref} - x_1 \tag{E.6}$$

Furthermore, it can easily be seen that the transfer from e to x_3 with the feedback loop closed results in the desired relation for x_3. Thus

$$x_3 = \frac{H_{OL,MA}}{1 + H_{OL,MA}} \cdot e \tag{E.7}$$

where $H_{OL,MA}$ is the open-loop transfer of the micro-actuator controller and is given by

$$H_{OL,MA} = H_{PI,parallel}d_{U,x}\frac{\omega_r^2}{s^2 + 2\zeta_r\omega_rs + \omega_r^2} \tag{E.8}$$

where $H_{PI,parallel}$ is given by equation (4.7). Finally, the closed-loop transfer function from x_{ref} to $x_{out} = x_1 + x_3$ is given by

$$H(s) = \frac{c_5s^5 + c_4s^4 + c_3s^3 + c_2s^2 + c_1s + c_0}{(a_5s^5 + a_4s^4 + a_3s^3 + a_2s^2 + a_1s + a_0)(b_4s^4 + b_3s^3 + b_2s^2 + b_1s + b_0)} \tag{E.9}$$

where the coefficients are given by

$$
\begin{aligned}
a_5 &= \tau_i \\
a_4 &= \left(\zeta_{LP}\omega_{LP} + \zeta_r\omega_r\right) 2\tau_i \\
a_3 &= \left(\omega_{LP}^2 + 4\zeta_r\omega_r\zeta_{LP}\omega_{LP} + \omega_r^2\right) \tau_i \\
a_2 &= \left(\zeta_r\omega_r\omega_{LP}^2 + \omega_r^2\zeta_{LP}\omega_{LP}\right) 2\tau_i \\
a_1 &= \left(1 + d_{U,x}\right) \tau_i\omega_r^2\omega_{LP}^2 \\
a_0 &= \omega_r^2 d_{U,x}\omega_{LP}^2 \\
b_4 &= m_{1,d}m_2 \\
b_3 &= m_{1,d}K_d \\
b_2 &= \left(m_{1,d} + m_2\right) c_{12} \\
b_1 &= c_{12}K_d \\
b_0 &= c_{12}K_p \\
c_5 &= m_{1,d}m_2 d_{U,x}\tau_i\omega_r^2\omega_{LP}^2 + c_{12}K_p\tau_i \\
c_4 &= \left(K_d\tau_i + m_2\right) m_{1,d}\omega_r^2 d_{U,x}\omega_{LP}^2 + 2c_{12}K_p\tau_i \left(\zeta_{LP}\omega_{LP} + \zeta_r\omega_r\right) \\
c_3 &= \left(c_{12}K_p\tau_i + \left(m_{1,d} + m_2\right)\omega_r^2 d_{U,x}\tau_i c_{12} + \omega_r^2 d_{U,x}m_{1,d}K_d\right)\omega_{LP}^2 \\
&\quad + c_{12}K_p\tau_i \left(4\zeta_r\omega_r\zeta_{LP}\omega_{LP} + \omega_r^2\right) \\
c_2 &= c_{12}\omega_r \left(\omega_r d_{U,x}\tau_i K_d + \left(m_{1,d} + m_2\right)\omega_r d_{U,x} + 2K_p\tau_i\zeta_r\right)\omega_{LP}^2 \\
&\quad + 2c_{12}K_p\tau_i\omega_r^2\zeta_{LP}\omega_{LP} \\
c_1 &= c_{12}\omega_r^2\big(\left(1 + d_{U,x}\right) K_p\tau_i + d_{U,x}K_d\big)\omega_{LP}^2 \\
c_0 &= c_{12}K_p\omega_r^2 d_{U,x}\omega_{LP}^2
\end{aligned}
$$

Appendix F

Coupled model: transfer functions for end-effector position measurement

F.1 Closed-loop transfer using end-effector position measurement

Deriving the closed-loop transfer function from the reference position x_{ref} to the output position $x_{out} = x_3$ using a measurement of the end-effector position and the velocity of the first actuator starts with defining the error signal that is applied to both controllers.

The error signal that is fed to both controllers is denoted as e and is given by

$$e = x_{ref} - x_{out} = x_{ref} - x_3 \tag{F.1}$$

As before, relations that describe the positions x_1, x_2 and x_3 are derived by solving the force balances on each of the three masses. First the relation for the force of the first actuator F_{in} is given

$$F_{in} = K_p \left(x_{ref} - x_3\right) - K_d s x_2 \tag{F.2}$$

Consequently, the relation for x_2 is given by

$$x_2 = \frac{K_p x_{ref} - K_p x_3 + c_{12} x_1}{m_2 s^2 + K_d s + c_{12}} \tag{F.3}$$

The force balance on m_1 is in this case given by

$$m_{1,c} s^2 x_1 = -c_{12} \left(x_1 - \frac{K_p x_{ref} - K_p x_3 + c_{12} x_1}{m_2 s^2 + K_d s + c_{12}} \right) + c_{13} \left(x_3 - x_1 - x_{2^{nd}}\right) \tag{F.4}$$

and consequently, x_1 is solved as

$$x_1 = \frac{c_{12} K_p x_{ref} + \left(m_2 c_{13} s^2 + c_{13} K_d s + \left(c_{13} - K_p\right) c_{12} \right) x_3 - \left(m_2 s^2 + K_d s + c_{12}\right) c_{13} x_{2^{nd}}}{m_{1,c} m_2 s^4 + m_{1,c} K_d s^3 + \left(m_{1,c} c_{12} + m_2 c_{12} + m_2 c_{13}\right) s^2 + \left(c_{12} + c_{13}\right) K_d s + c_{12 c_{13}}} \tag{F.5}$$

In order to calculate a relation for x_3, first the output displacement of the position actuator is calculated:

$$x_{2^{nd}} = H_{PI,parallel} d_{U,x} \left(x_{ref} - x_3\right) \tag{F.6}$$

where $H_{PI,parallel}$ is given by equation (4.7). Consequently by substituting this relation for $x_{2^{nd}}$ in the force balance on m_3, x_3 can be solved. From this relation the closed-loop transfer function of this system can be determined to be

$$H(s) = \frac{b_4 s^4 + b_3 s^3 + b_2 s^2 + b_1 s + b_0}{a_8 s^8 + a_7 s^7 + a_6 s^6 + a_5 s^5 + a_4 s^4 + a_3 s^3 + a_2 s^2 + a_1 s + a_0} \tag{F.7}$$

where the coefficients are given by

$$
\begin{aligned}
b_4 &= m_{1,c}m_2 d_{U,x}\tau_i\omega_r^2\omega_{LP}^2 \\
b_3 &= (\tau_i K_d + m_2)\, d_{U,x}m_{1,c}\omega_r^2\omega_{LP}^2 \\
b_2 &= \big(\,(K_d + c_{12}\tau_i)\, m_{1,c} + m_2 c_{12}\tau_i\big) d_{U,x}\omega_r^2\omega_{LP}^2 + c_{12}\omega_r^2 K_p\tau_i \\
b_1 &= \big(m_{1,c} + m_2 + K_d\tau_i\big)c_{12}d_{U,x}\omega_r^2\omega_{LP}^2 + 2c_{12}\omega_r^2 K_p\tau_i\zeta_{LP}\omega_{LP} \\
b_0 &= (K_p\tau_i + d_{U,x}K_d)\, c_{12}\omega_r^2\omega_{LP}^2 \\
a_8 &= \tau_i m_{1,c}m_2 \\
a_7 &= 2m_{1,c}m_2\tau_i\zeta_{LP}\omega_{LP} + (2\zeta_r\omega_r m_2 + K_d)\, m_{1,c}\tau_i \\
a_6 &= \tau_i m_{1,c}m_2\omega_{LP}^2 + (2\zeta_r\omega_r m_2 + K_d)\, 2m_{1,c}\tau_i\zeta_{LP}\omega_{LP} \\
&\quad + \big(\,\big(2\zeta_r\omega_r K_d + \omega_r^2 m_2\big)\, m_{1,c} + m_2 c_{13} + (m_{1,c} + m_2)\, c_{12}\big)\tau_i \\
a_5 &= (2\zeta_r\omega_r m_2 + K_d)\, m_{1,c}\tau_i\omega_{LP}^2 \\
&\quad + \big(\,\big(2\zeta_r\omega_r K_d + \omega_r^2 m_2\big)\, m_{1,c} + m_2 c_{13} + (m_{1,c} + m_2)\, c_{12}\big)2\tau_i\zeta_{LP}\omega_{LP} \\
&\quad + \big(\,(m_2 c_{12} + m_2 c_{13} + m_{1,c}c_{12})\, 2\zeta_r\omega_r + \big(\omega_r^2 m_{1,c} + c_{13} + c_{12}\big)\, K_d\big)\tau_i \\
a_4 &= \big(\,(c_{12} + c_{13})\, m_2 + (2\zeta_r\omega_r K_d + c_{12})\, m_{1,c} + (1 + d_{U,x})\, \omega_r^2 m_{1,c}m_2\big)\tau_i\omega_{LP}^2 \\
&\quad + \big(\,\big(m_{1,c}\omega_r^2 + c_{12} + c_{13}\big)\, K_d + (m_2 c_{12} + m_{1,c}c_{12} + m_2 c_{13})\, 2\zeta_r\omega_r\big)2\tau_i\zeta_{LP}\omega_{LP} \\
&\quad + \big(\,(m_{1,c} + m_2)\, c_{12}\omega_r^2 + (c_{12} + c_{13})\, 2\zeta_r\omega_r K_d + c_{12}c_{13}\big)\tau_i \\
a_3 &= \big(\,(1 + d_{U,x})\, \tau_i K_d + d_{U,x}m_2\big)m_{1,c}\omega_r^2\omega_{LP}^2 \\
&\quad \big(\,(m_{1,c} + m_2)\, c_{12} + c_{13}m_2\big)2\tau_i\zeta_r\omega_r\omega_{LP}^2 + (c_{13} + c_{12})\, K_d\tau_i\omega_{LP}^2 \\
&\quad + \big(\,(c_{12} + c_{13})\, 2\zeta_r\omega_r K_d + (m_{1,c} + m_2)\, c_{12}\omega_r^2 + c_{13}c_{12}\big)\tau_i\zeta_{LP}\omega_{LP} \\
&\quad + \big(2\zeta_r\omega_r c_{13} + \omega_r^2 K_d\big)\, \tau_i c_{12} \\
a_2 &= \big(\,(m_{1,c} + m_2)\, \tau_i c_{12} + (\tau_i c_{12} + K_d)\, d_{U,x}m_{1,c} + d_{U,x}\tau_i c_{12}m_2\big)\omega_r^2\omega_{LP}^2 \\
&\quad \big(\,(c_{13} + c_{12})\, 2\zeta_r\omega_r K_d + c_{12}c_{13}\big)\tau_i\omega_{LP}^2 \\
&\quad + \big(2\zeta_r\omega_r c_{13} + \omega_r^2 K_d\big)\, 2c_{12}\tau_i\zeta_{LP}\omega_{LP} + c_{12}K_p\tau_i\omega_r^2 \\
a_1 &= \big(2\tau_i\zeta_r\omega_r c_{13} + (1 + d_{U,x})\, \omega_r^2\tau_i K_d + (m_{1,c} + m_2)\, \omega_r^2 d_{U,x}\big)c_{12}\omega_{LP}^2 \\
&\quad + 2c_{12}\omega_r^2 K_p\tau_i\zeta_{LP}\omega_{LP} \\
a_0 &= (d_{U,x}K_d + K_p\tau_i)\, \omega_r^2 c_{12}\omega_{LP}^2
\end{aligned}
$$

F.2 Sensitivity function using end-effector position measurement

The sensitivity function using the decoupled model and using end-effector position measurement is determined under the assumption that $x_{ref} = 0$. In this case the sensitivity function $S(s)$ is defined as

$$S(s) = \frac{x_3 + \delta}{\delta} \tag{F.8}$$

where δ is a positional output disturbance. The starting point of deriving $S(s)$ is defining the force F_{in} that is applied to the first actuator. This force can be calculated as

$$F_{in} = -K_p x_{out} - s x_2 K_d \tag{F.9}$$

Consequently, x_2 is solved from the force balance on m_2. This results in the following expression

$$x_2 = -\frac{K_p x_{out} - c_{12}x_1}{m_2 s^2 + K_d s + c_{12}} \tag{F.10}$$

The same approach is followed in order to obtain a relation for x_1. From the force balance on m_1, x_1 is solved as

$$x_1 = -\frac{\big(-c_{13}m_2 s^2 - c_{13}K_d s - c_{13}c_{12}\big)\, x_{2^{nd}} + \big(c_{13}m_2 s^2 + c_{13}K_d s - c_{12}c_{13}\big)\, x_3 - K_p c_{12}x_{out}}{m_{1,c}m_2 s^4 + m_{1,c}K_d s^3 + (c_{13}m_2 + m_{1,c}c_{12} + c_{12}m_2)\, s^2 + (c_{12}K_d + c_{13}K_d)\, s + c_{13}c_{12}} \tag{F.11}$$

Then, a relation for determining the output displacement of the position actuator is calculated as

$$x_{2^{nd}} = -H_{PI,parallel} d_{U,x} x_{out} \tag{F.12}$$

where $H_{PI,parallel}$ is given by equation (4.7). Consequently by substituting this relation for $x_{2^{nd}}$ in the force balance on m_3, x_3 can be solved. Consequently, this relation for x_3 is substituted in

$$-x_{out} + x_3 + \delta = 0 \tag{F.13}$$

The relation for x_{out} is obtained by solving x_{out} from the above relation. From the resulting relation for x_{out}, the sensitivity function is directly calculated as

$$S(s) = \frac{x_{out}}{\delta} = \frac{b_8 s^8 + b_7 s^7 + b_6 s^6 + b_5 s^5 + b_4 s^4 + b_3 s^3 + b_2 s^2 + b_1 s + b_0}{a_8 s^8 + a_7 s^7 + a_6 s^6 + a_5 s^5 + a_4 s^4 + a_3 s^3 + a_2 s^2 + a_1 s + a_0} \tag{F.14}$$

where the coefficients are given as

$$\begin{aligned}
b_8 &= m_{1,c} m_2 \tau_i \\
b_7 &= 2 m_{1,c} m_2 \tau_i \zeta_{LP} \omega_{LP} + \left(K_d + 2 m_2 \zeta_r \omega_r\right) m_{1,c} \tau_i \\
b_6 &= m_{1,c} m_2 \tau_i \omega_{LP}^2 + \left(K_d + 2 m_2 \zeta_r \omega_r\right) 2 m_{1,c} \tau_i \zeta_{LP} \omega_{LP} \\
&\quad + \big(\left(m_{1,c} + m_2\right) c_{12} + m_2 c_{13} + m_{1,c} \left(m_2 \omega_r^2 + 2 K_d \zeta_r \omega_r\right) \big) \tau_i \\
b_5 &= \left(K_d + 2 m_2 \zeta_r \omega_r\right) m_{1,c} \tau_i \omega_{LP}^2 \\
&\quad + \big(\left(m_{1,c} + m_2\right) c_{12} + m_2 c_{13} + m_{1,c} \left(m_2 \omega_r^2 + 2 K_d \zeta_r \omega_r\right) \big) 2 \tau_i \zeta_{LP} \omega_{LP} \\
&\quad + \big(\left(c_{13} + c_{12} + m_{1,c} \omega_r^2\right) K_d + \left(m_{1,c} c_{12} + m_2 c_{13} + m_2 c_{12}\right) 2 \zeta_r \omega_r \big) \tau_i \\
b_4 &= \big(\left(m_{1,c} + m_2\right) c_{12} + m_2 c_{13} + m_{1,c} \left(m_2 \omega_r^2 + 2 K_d \zeta_r \omega_r\right) \big) \tau_i \omega_{LP}^2 \\
&\quad + \left(c_{13} + c_{12} + m_{1,c} \omega_r^2\right) 2 \tau_i \zeta_{LP} \omega_{LP} K_d \\
&\quad + \left(m_2 c_{13} + m_2 c_{12} + m_{1,c} c_{12}\right) 4 \tau_i \zeta_r \omega_r \zeta_{LP} \omega_{LP} \\
&\quad + \big(\left(m_{1,c} + m_2\right) c_{12} \omega_r^2 + c_{12} c_{13} + \left(c_{12} + c_{13}\right) 2 \zeta_r \omega_r K_d \big) \tau_i \\
b_3 &= \left(c_{13} + c_{12} + m_{1,c} \omega_r^2\right) K_d \tau_i \omega_{LP}^2 \\
&\quad + \left(m_2 c_{13} + m_2 c_{12} + m_{1,c} c_{12}\right) 2 \tau_i \zeta_r \omega_r \omega_{LP}^2 \\
&\quad + \big(\left(m_{1,c} + m_2\right) c_{12} \omega_r^2 + c_{12} c_{13} + \left(c_{12} + c_{13}\right) 2 \zeta_r \omega_r K_d \big) 2 \tau_i \zeta_{LP} \omega_{LP} \\
&\quad + \left(\omega_r^2 K_d + 2 c_{13} \zeta_r \omega_r\right) c_{12} \tau_i \\
b_2 &= \big(\left(m_{1,c} + m_2\right) c_{12} \omega_r^2 + c_{12} c_{13} + \left(c_{12} + c_{13}\right) 2 \zeta_r \omega_r K_d \big) \tau_i \omega_{LP}^2 \\
&\quad + \left(\omega_r^2 K_d + 2 c_{13} \zeta_r \omega_r\right) 2 c_{12} \tau_i \zeta_{LP} \omega_{LP} \\
b_1 &= \left(\omega_r^2 K_d + 2 c_{13} \zeta_r \omega_r\right) c_{12} \tau_i \omega_{LP}^2 \\
b_0 &= 0 \\
a_8 &= b_8 \\
a_7 &= b_7 \\
a_6 &= b_6 \\
a_5 &= b_5 \\
a_4 &= \big(\left(m_{1,c} + m_2\right) c_{12} + \left(1 + d_{U,x}\right) m_{1,c} m_2 \omega_r^2 + 2 m_{1,c} \zeta_r \omega_r K_d + m_2 c_{13} \big) \tau_i \omega_{LP}^2 \\
&\quad + \left(m_2 c_{13} + m_2 c_{12} + m_{1,c} c_{12}\right) 4 \tau_i \zeta_r \omega_r \zeta_{LP} \omega_{LP} \\
&\quad + \left(c_{13} + c_{12} + m_{1,c} \omega_r^2\right) 2 K_d \tau_i \zeta_{LP} \omega_{LP} \\
&\quad + \big(\left(m_{1,c} + m_2\right) c_{12} \omega_r^2 + \left(c_{12} + c_{13}\right) 2 \zeta_r \omega_r K_d + c_{12} c_{13} \big) \tau_i \\
a_3 &= \left(c_{12} + c_{13}\right) \tau_i K_d \omega_{LP}^2 + \left(m_2 c_{12} + m_2 c_{13} + m_{1,c} c_{12}\right) 2 \tau_i \zeta_r \omega_r \omega_{LP}^2 \\
&\quad + \big(\left(1 + d_{U,x}\right) \tau_i K_d + m_2 d_{U,x} \big) m_{1,c} \omega_r^2 \omega_{LP}^2 \\
&\quad + \big(\left(c_{12} + c_{13}\right) 2 \zeta_r \omega_r K_d + c_{12} c_{13} + \left(m_{1,c} + m_2\right) c_{12} \omega_r^2 \big) 2 \tau_i \zeta_{LP} \omega_{LP}
\end{aligned}$$

$$
\begin{aligned}
& + \tau_i c_{12} \left(\omega_r^2 K_d + 2 c_{13} \zeta_r \omega_r \right) \\
a_2 &= \left(\left(m_{1,c} + m_2 \right) c_{12} \tau_i + \left(m_{1,c} c_{12} \tau_i + m_2 c_{12} \tau_i + m_{1,c} K_d \right) d_{U,x} \right) \omega_r^2 \omega_{LP}^2 \\
& + \left(c_{12} + c_{13} \right) 2 \tau_i \zeta_r \omega_r K_d \omega_{LP}^2 + \tau_i c_{12} c_{13} \omega_{LP}^2 \\
& + \left(\omega_r^2 K_d + 2 c_{13} \zeta_r \omega_r \right) 2 c_{12} \tau_i \zeta_{LP} \omega_{LP} + c_{12} \omega_r^2 K_p \tau_i \\
a_1 &= \left(\left(m_{1,c} + m_2 + \tau_i K_d \right) \omega_r^2 d_{U,x} + \left(2 c_{13} \zeta_r \omega_r + \omega_r^2 K_d \right) \tau_i \right) c_{12} \omega_{LP}^2 \\
& + 2 c_{12} \omega_r^2 K_p \tau_i \zeta_{LP} \omega_{LP} \\
a_0 &= \left(K_p \tau_i + d_{U,x} K_d \right) \omega_r^2 c_{12} \omega_{LP}^2
\end{aligned}
$$

Appendix G

Coupled model: transfer functions using carriage position measurement

G.1 Transfer function using carriage position measurement

Deriving the closed-loop transfer function from the reference position x_{ref} to the output position $x_{out} = x_3$ using measurements of the carriage position and the velocity of the first actuator starts with defining the error signal that is applied to both controllers.

The error signal that is fed to both controllers is denoted as e and is given by

$$e = x_{ref} - x_1 \tag{G.1}$$

As before, relations that describe the positions x_1, x_2 and x_3 are derived by solving the force balances on each of the three masses. First the relation for the force of the first actuator F_{in} is given

$$F_{in} = K_p \left(x_{ref} - x_1\right) - K_d s x_2 \tag{G.2}$$

Consequently, the relation for x_2 is given by

$$x_2 = \frac{K_p \left(x_{ref} - x_1\right) + c_{12} x_1}{m_2 s^2 + K_d s + c_{12}} \tag{G.3}$$

The force balance on m_1 is in this case given by

$$m_{1,c} s^2 x_1 = -c_{12} \left(x_1 - \frac{K_p \left(x_{ref} - x_1\right) + c_{12} x_1}{m_2 s^2 + K_d s + c_{12}} \right) + c_{13} \left(x_3 - x_{2^{nd}}\right) \tag{G.4}$$

and consequently, x_1 is solved as

$$x_1 = \frac{c_{12} K_p x_{ref} + \left(m_2 c_{13} s^2 + c_{13} K_d s + c_{12} c_{13}\right) x_3 - \left(m_2 c_{13} s^2 + c_{13} K_d s + c_{12} c_{13}\right) x_{2^{nd}}}{m_{1,c} m_2 s^4 + m_{1,c} K_d s^3 + \left(m_{1,c} + m_2\right) c_{12} s^2 + c_{12} K_d s + c_{12} K_p} \tag{G.5}$$

In order to calculate a relation for x_3, first the output displacement of the position actuator is calculated:

$$x_{2^{nd}} = H_{PI,parallel} d_{U,x} \left(x_{ref} - x_1 - x_3\right) \tag{G.6}$$

where $H_{PI,parallel}$ is given by equation (4.7). Consequently by substituting this relation for $x_{2^{nd}}$ in the force balance on m_3, x_3 can be solved. From this relation the closed-loop transfer function of this system can be determined to be

$$H(s) = \frac{b_5 s^5 + b_4 s^4 + b_3 s^3 + b_2 s^2 + b_1 s + b_0}{a_9 s^9 + a_8 s^8 + a_7 s^7 + a_6 s^6 + a_5 s^5 + a_4 s^4 + a_3 s^3 + a_2 s^2 + a_1 s + a_0} \tag{G.7}$$

where the coefficients are given by

$$
\begin{aligned}
b_5 &= m_{1,c} m_2 \omega_r^2 d_{U,x} \tau_i \omega_{LP}^2 \\
b_4 &= (m_2 + \tau_i K_d)\, m_{1,c} d_{U,x} \omega_r^2 \omega_{LP}^2 \\
b_3 &= \big((K_d + c_{12}\tau_i)\, m_{1,c} + (c_{12} - c_{13})\, m_2 \tau_i \big) d_{U,x} \omega_r^2 \omega_{LP}^2 \\
&\quad + c_{12} \omega_r^2 \tau_i K_p \\
b_2 &= \big(m_{1,c} c_{12} + (c_{12} - c_{13})\, m_2 + (c_{12} - c_{13})\, \tau_i K_d \big) d_{U,x} \omega_r^2 \omega_{LP}^2 \\
&\quad + 2 c_{12} \omega_r^2 K_p \tau_i \zeta_{LP} \omega_{LP} \\
b_1 &= (d_{U,x} K_d c_{12} - d_{U,x} c_{13} K_d + c_{12} K_p \tau_i - d_{U,x} c_{13} c_{12} \tau_i)\, \omega_r^2 \omega_{LP}^2 \\
b_0 &= -c_{12} c_{13} d_{U,x} \omega_r^2 \omega_{LP}^2 \\
a_9 &= m_{1,c} m_2 \tau_i \\
a_8 &= 2 m_{1,c} m_2 \tau_i \zeta_{LP} \omega_{LP} + m_{1,c} K_d \tau_i + 2 \zeta_r \omega_r m_{1,c} m_2 \tau_i \\
a_7 &= m_{1,c} m_2 \tau_i \omega_{LP}^2 + (2 \zeta_r \omega_r m_2 + K_d)\, 2 m_{1,c} \tau_i \zeta_{LP} \omega_{LP} \\
&\quad + \tau_i \big((m_{1,c} + m_2)\, c_{12} + \big(m_2 \omega_r^2 + 2 \zeta_r \omega_r K_d \big)\, m_{1,c} \big) \\
a_6 &= (K_d + 2 \zeta_r \omega_r m_2)\, m_{1,c} \tau_i \omega_{LP}^2 \\
&\quad + \big((m_{1,c} + m_2)\, c_{12} + \big(m_2 \omega_r^2 + 2 \zeta_r \omega_r K_d \big)\, m_{1,c} \big) 2 \tau_i \zeta_{LP} \omega_{LP} \\
&\quad + \tau_i \big(\big(c_{12} + \omega_r^2 m_{1,c} \big)\, K_d + (m_{1,c} + m_2)\, 2 \zeta_r \omega_r c_{12} \big) \\
a_5 &= \big(2 \zeta_r \omega_r m_{1,c} K_d + (m_{1,c} + m_2)\, c_{12} - d_{U,x} c_{13} m_2 + (1 + d_{U,x})\, m_{1,c} m_2 \omega_r^2 \big) \tau_i \omega_{LP}^2 \\
&\quad + \big(\big(\omega_r^2 m_{1,c} + c_{12} \big)\, K_d + (m_{1,c} + m_2)\, 2 \zeta_r \omega_r c_{12} \big) 2 \tau_i \zeta_{LP} \omega_{LP} \\
&\quad + \tau_i \big((K_p + 2 \zeta_r \omega_r K_d)\, c_{12} - m_2 \omega_r^2 c_{13} + (m_{1,c} + m_2)\, \omega_r^2 c_{12} \big) \\
a_4 &= \big((1 + d_{U,x})\, K_d \tau_i + m_2 d_{U,x} \big) m_{1,c} \omega_r^2 \omega_{LP}^2 \\
&\quad + \big((m_2 + m_{1,c})\, c_{12} - m_2 c_{13} d_{U,x} \big) 2 \tau_i \zeta_r \omega_r \omega_{LP}^2 \\
&\quad + \big((c_{12} - d_{U,x} c_{13})\, K_d \tau_i - m_2 c_{13} d_{U,x} \big) \omega_{LP}^2 \\
&\quad + \big(\omega_r^2 m_{1,c} c_{12} + \omega_r^2 c_{12} m_2 + 2 \zeta_r \omega_r c_{12} K_d + c_{12} K_p - m_2 \omega_r^2 c_{13} \big)\, 2 \tau_i \zeta_{LP} \omega_{LP} \\
&\quad + \tau_i \big((c_{12} - c_{13})\, \omega_r^2 K_d + 2 c_{12} \zeta_r \omega_r K_p \big) \\
a_3 &= \big((c_{12} - c_{13})\, d_{U,x} m_2 \tau_i + m_{1,c} d_{U,x}\, (\tau_i c_{12} + K_d) - m_2 c_{13} \tau_i + (m_{1,c} + m_2)\, c_{12} \tau_i \big) \omega_r^2 \omega_{LP}^2 \\
&\quad + \big(c_{12} K_d \tau_i - (m_2 - K_d \tau_i)\, c_{13} d_{U,x} \big) 2 \zeta_r \omega_r \omega_{LP}^2 \\
&\quad - \big((c_{12} \tau_i - K_d)\, d_{U,x} c_{13} + c_{12} K_p \tau_i \big) \omega_{LP}^2 \\
&\quad + \big((c_{12} - c_{13})\, \omega_r^2 K_d + c_{12} \zeta_r \omega_r K_p \big) 2 \tau_i \zeta_{LP} \omega_{LP} c_{12} \omega_r^2 \tau_i + (K_p - c_{13})\, c_{12} \omega_r^2 \tau_i \\
a_2 &= \Big((1 + d_{U,x})\, c_{12} K_d \tau_i - d_{U,x} c_{13} m_2 - (1 + d_{U,x})\, c_{13} K_d \tau_i + (m_{1,c} + m_2)\, c_{12} d_{U,x} \Big) \omega_r^2 \omega_{LP}^2 \\
&\quad \big(+ c_{12} K_p \tau_i - (K_d + c_{12} \tau_i)\, c_{13} d_{U,x} \big) 2 \zeta_r \omega_r \omega_{LP}^2 - c_{12} c_{13} d_{U,x} \omega_{LP}^2 \\
&\quad + (K_p - c_{13})\, 2 c_{12} \omega_r^2 \tau_i \zeta_{LP} \omega_{LP} \\
a_1 &= \big(c_{12} K_p \tau_i + (c_{12} - c_{13})\, d_{U,x} K_d - (1 - d_{U,x})\, c_{12} c_{13} \tau_i + d_{U,x} \tau_i c_{12} K_p \big) \omega_r^2 \omega_{LP}^2 \\
&\quad - 2 c_{12} c_{13} d_{U,x} \zeta_r \omega_r \omega_{LP}^2 \\
a_0 &= (K_p - c_{13})\, c_{12} \omega_r^2 d_{U,x} \omega_{LP}^2
\end{aligned}
$$

G.2 Sensitivity function using carriage position measurement

The sensitivity function using the decoupled model and carriage position measurement is determined under the assumption that $x_{ref} = 0$. Furthermore, only the sensitivity function $S(s)$ of the carriage position loop is derived.

This sensitivity function is defined as

$$S(s) = \frac{x_1 + \delta}{\delta} \tag{G.8}$$

where δ is a positional output disturbance. The starting point of deriving $S(s)$ is defining the force F_{in} that is applied to the first actuator. This force can be calculated as

$$F_{in} = -K_p x_{out} - s x_2 K_d \tag{G.9}$$

Consequently, x_2 is solved from the force balance on m_2. This results in the following expression

$$x_2 = \frac{c_{12} x_1 - x_{out} K_p}{m_2 s^2 + K_d s + c_{12}} \tag{G.10}$$

The same approach is followed in order to obtain a relation for x_1. From the force balance on m_1, x_1 is solved as

$$x_1 = -\frac{c_{12} x_{out} K_p - \left(m_2 c_{13} s^2 + c_{13} K_d s + c_{12} c_{13}\right) x_3 + \left(m_2 c_{13} s^2 + c_{13} K_d s + c_{12} c_{13}\right) x_{2^{nd}}}{m_{1,c} m_2 s^4 + m_{1,c} K_d s^3 + \left(m_{1,c} c_{12} + m_2 c_{12} + m_2 c_{13}\right) s^2 + \left(c_{12} + c_{13}\right) K_d s + c_{12} c_{13}} \tag{G.11}$$

Then, a relation for determining the output displacement of the position actuator is calculated as

$$x_{2^{nd}} = -H_{PI,parallel} d_{U,x} \left(x_{out} - x_3\right) \tag{G.12}$$

where $H_{PI,parallel}$ is given by equation (4.7). Subsequently by substituting this relation for $x_{2^{nd}}$ in the force balance on m_3, x_3 can be solved. This relation for x_3 is substituted in the relation for x_1, to obtain a relation for x_{out}. In this case,

$$-x_{out} + x_1 + \delta = 0 \tag{G.13}$$

The relation for x_{out} is obtained by solving x_{out} from the above relation. From the resulting relation for x_{out}, the sensitivity function is directly calculated as

$$S(s) = \frac{x_{out}}{\delta} = \frac{b_{15} s^{15} + b_{14} s^{14} + (..) + b_2 s^2 + b_1 s + b_0}{a_{15} s^{15} + a_{14} s^{14} + (..) + a_2 s^2 + a_1 s + a_0} \tag{G.14}$$

Since in this case, it can be directly seen that the sensitivity bandwidth of this loop does not increase after including the second-stage actuator, the coefficients of the above sensitivity function are not worked out.

Bibliography

Assembleon. Fcm multiflex. Online, http://www.assembleon.com, 2004.

K.J. Aström and T. Hägglund. *PID controllers*. Research Triangle Park, NC : Instrument Society of America, 2^{nd} edition, 1995. ISBN 1-556-17516-7.

H.J. Coelingh. *Design Support for Motion Control Systems*. PhD thesis, University of Twente, February 2000.

H. Fujita, K. Suzuki, M. Ataka, and S. Nakamura. A micro-actuator for head positioning system of hard disk drives. *IEEE Transactions on Magnetics*, 35(2):1006–1010, March 1999.

G. Guo., D. Wu, and T.C. Chong. Modified dual-stage controller for dealing with secondary-stage actuator saturation. *UEEE Transactions on magnetics*, 39(6):3587–3591, November 2003.

G. Herrmann and G. Guo. HDD dual-stage servo-controller design using μ-analysis tool. *Control engineering practice*, 12:241–251, 2004.

R. Horowitz, T.L. Chen, K. Oldham, and Y. Li. *Handbook of Nanotechnology*, chapter 32. Number ISBN 3-540-01218-4. Springer, 2004.

K-H. Kim and S-H. Lee. An approach to dual-stage servo design in computer disk drives. *IEEE Transactions on control systems technology*, 12(1):12–20, January 2004.

M. Kobayashi and R. Horowitz. Track seek control for hard disk dual-stage servo systems. *IEEE Transactions on Magnetics*, 37(2):949–954, March 2001.

S.-H. Lee, S.-E. Baek, and Y.-H. Kim. Design of a dual-stage actuator control system with discrete-time sliding mode for hard disk drives. In *Proc. IEEE Conf. Decision and Control*, pages 3120–3125, 2000.

Y. Li and R. Horowitz. Mechatronics of electrostatic microactuators for computer disk drive dual-stage servo systems. *IEEE/ASME transactions on Mechatronics*, 6(2):111–121, June 2001.

K. Mori, H. Munemoto, H. Otsuki, Y. Yamaguchi, and K. Akagi. A dual-stage magnetic disk drive actuator using a piezoelectric device for a high track density. *IEEE Transactions on Magnetics*, 27:5298–5300, 1991.

Y. Niu, W. Guo, G. Guo, K. Ong E-H. Sivadasan, and T. Huang. A pzt micro-actuated suspension for high tpi hard disk servo systems. *IEEE Transactions on Magnetics*, 36(5):2241–2243, September 2000.

H. Numasato and M. Tomizuka. Settling control and performance of a dual-actuator system for hard-disk drives. *IEEE/ASME transactions on mechatronics*, 8(4):431–438, December 2003.

PI-datasheets. Picma high-performance monolithic multilayer piezo actuators. Online, http://www.physikinstrumente.de/pdf/Picma_Datasheet.pdf, 2004.

PI-Tutorial. Theory and applications of piezo actuators and pzt nanopositioning systems. Online Tutorial: http://www.physikinstrumente.de/products/section4/content.php, 2004.

S. Salapaka, A. Sebastian, J.P. Cleveland, and M.V. Salapaka. High bandwidth nano-positioner: A robust control approach. *Review of scientific instruments*, 73(9):3232–3241, September 2002.

M. Sasaki, T. Suzuki, E. Ida, F. Fujisawa, M. Kobayashi, and H. Hirai. Track-following control of a dual-stage hard disk drive using a neuro-control system. *Eng. Applications of Artificial Intelligence*, 11:707–716, 1998.

S.J. Schroeck, W.C. Messner, and R.J. McNab. On compensator design for linear time-invariant dual-input single-output systems. *IEEE/ASME Transactions on Mechatronics*, 6(1):50–57, March 2001.

T. Semba, T. Hirano, J. Hong, and L. Fan. Dual-stage servo controller for HDD using MEM microactuator. *IEEE Transactions on Magnetics*, 35(5):2271–2273, September 1999.

S. Skogestad and I. Postlethwaite. *Multivariable feedback control, analysis and design*. John Wiley and Sons, 1996. ISBN 0-471-94277-4, 0-471-94330-4.

Y. Soeno, S. Ichikawa, T. Tsuna, Y. Sato, and I. Sato. Piezo-electric piggy-back micro-actuator for hard disk drive. *IEEE Transactions on Magnetics*, 35(2):983–987, March 1999.

S-H. Suh, C.C. Chung, and S-H Lee. Discrete-time LQG/LTR dual-stage controller design in magnetic disk drives. *IEEE transactions on magnetics*, 37(4):1891–1895, July 2001.

T. Suthasun, I. Mareels, and A. Al-Mamun. System identification and controller design for dual actuated hard disk drive. *Control engineering practice*, 12:665–676, 2004.

J. Van Dijk. Piezo actuated mechanisms. Lecture notes of the course ”Mechatronics”, 2003.

P.B.A. Van Lochem. Towards automated mechatronic system design. Master’s thesis, University of Twente, 1997.

D. Wu, G. Gua, and T.C. Chong. Comparative analysis on resonance compensation in HDD dual-stage actuation systems. *IEEE Transactions on industrial electronics*, 50(6):1179–1186, December 2003.